NAME OF AUTHOR...... KOLES   ZOLY JOSEPH

TITLE OF THESIS..... A...STUDY..OF...THE..SENSORY ..DYNAMICS...OF..A..MUSCLE.... ...SPINDLE...........................

UNIVERSITY...OF...ALBERTA........................

DEGREE FOR WHICH THESIS WAS PRESENTED.....PH..D...........

YEAR THIS DEGREE GRANTED........1970...................

Permission is hereby granted to THE NATIONAL LIBRARY OF CANADA to microfilm this thesis and to lend or sell copies of the film.

The author reserves other publication rights, and neither the thesis nor extensive extracts from it may be printed or otherwise reproduced without the author's written permission.

(Signed)....Zoly J. Koles

PERMANENT ADDRESS:

PARENTS:...MR..J.S..KOLES ......10018.-113.ST. ......EDMONTON......

DATED..Sept..25...1970   Z.J. KOLES WILL BE IN LONDON, ENGLAND FOR 1 YEAR.

THE UNIVERSITY OF ALBERTA

A STUDY OF THE SENSORY DYNAMICS OF A MUSCLE SPINDLE

by

(C) Zoly Joseph Koles

A THESIS

SUBMITTED TO THE FACULTY OF GRADUATE STUDIES

IN PARTIAL FULFILMENT OF THE REQUIREMENTS FOR THE DEGREE

OF DOCTOR OF PHILOSOPHY

DEPARTMENT OF ELECTRICAL ENGINEERING

EDMONTON, ALBERTA

FALL, 1970

UNIVERSITY OF ALBERTA

FACULTY OF GRADUATE STUDIES

The undersigned certify that they have read,
and recommend to the Faculty of Graduate Studies for acceptance,
a thesis entitled A Study of the Sensory Dynamics of a Muscle Spindle
submitted by Zoly J. Koles in partial fulfilment of the requirements
for the degree of Doctor of Philosophy.

_____
Supervisor

_____

_____

_____

_____
External Examiner

Date _____   _____

ACKNOWLEDGEMENTS .

ABSTRACT

The sensory dynamics of muscle spindles in the toad <u>Xenopus</u> <u>laevis</u> have been studied using methods of consistent spectral estimation. The receptor discharges at both a constant muscle length, and with small random variations superimposed on the steady length, were recorded and analysed. Spectral estimates involving the discrete discharges were obtained by low-pass filtering the process and applying the Fast Fourier Transform to the resulting waveform. Estimates of the power spectrum of the receptor discharges at a steady length were used to show that the discharges could be adequately described as a renewal process. In addition, evidence was obtained which suggests that the power spectrum of the receptor discharges at a constant muscle length was acting as the carrier for the information related to the superimposed length variations. Estimates of the cross spectrum between the applied length variations and the spindle discharges were used to obtain estimates of the 'best' linear transfer function for the dynamic behavior of the receptor. The technique used is extremely well suited to the transfer function analysis of simultaneous neuronal spike trains.

The results show that the variability in the intervals between the receptor discharges was such that low-noise recovery of low frequency dynamic information was possible by low-pass filtering. Also, the receptor was shown to be only slightly sensitive to different levels of static stretch. However, in the band of frequencies studied, the sensitivity of the spindle to superimposed length variations was strongly dependent upon the steady length.

TABLE OF CONTENTS

LIST OF FIGURES AND TABLES

TABLES

CHAPTER 1

INTRODUCTION

In biology, the quantitative analysis of sensory sytems usually involves the interpretation of neuronal spike activity resulting from the controlled application of an effective physical stimulus. This procedure resembles the so-called 'black box' problem of electrical engineering. Here, the investigator tries, while impressing a known voltage or current upon an undescribed system, to relate these, through a set of parameters, to the observed fluctuations of these variables at a set of responding terminals. The parameters may be nonlinear, as for example the dynamic resistance of a junction diode, or frequency dependent, as is the transconductance of a triode vacuum tube. The biologist may also attempt to describe his systems with a set of parameters. Usually though, he must first deal with a number of additional problems. In the case of sensory systems he must decide not only what constitutes an effective and appropriate input, but also, how to characterize and control it. He must also decide how the activity in the sensory nerves is related if at all to the applied stimulus. The problem of sensory coding has in general not been solved and its interpretation, therefore, must be clearly defined in any model which is developed to characterize the system.

Sensory systems usually respond to adequate physical stimuli with long trains of nerve impulses or action potentials. Each impulse is distinguishable from its neighbors only by its location in time. The time course of each is usually short when compared to the interpulse interval and each has a characteristic 'all-or-none' nature. The intervals between impulses usually exhibit the properties of random variables and as a result, many ideas originating from the theory of stochastic point processes have become associated with the analysis of neuronal impulse activity (1-3).

Although some of the methods reviewed in (1-3) are extremely powerful techniques for characterizing either single or simultaneous

spike trains, they can become inadequate when either or both of the
processes are not stationary in time. In many sensory systems the
result of the application of a stimulus is to introduce nonstationarities
or trends into a previously stationary process. In such cases a
representation of the nonstationarity in the frequency domain becomes
one of the few practical means of characterization. Normalized with
respect to input these frequency domain representations or transfer
functions are now common in the biological literature (4-9).

Procedures that establish the existence or nonexistence of
correlation between pairs of simultaneous point processes are clearly
defined (3). However, the investigator of sensory dynamics is usually
confronted with the situation where one of the two processes is
continuous. Here, correlation techniques are not as clearly defined.
As a result, a number of nonequivalent representations of neuronal
activity have been used (7, 10-12). Of these, the two most often
considered are those related to impulse frequency: the number of
spikes in a unit of time; and those related to interval: the time elapsed
between a pair of adjacent spikes. Recently McKean et al. (13) have
obtained evidence indicating that impulse frequency is probably bio-
logically more relevent. They have also shown that both measurements
are equivalent at very low frequencies with the interval method intro-
ducing spurious gain and phase fluctuations into the transfer relation
as the stimulus frequency approaches and passes the mean discharge
frequency. A smoothed version of either of these measurements can be
obtained by applying the stimulus repetitively and averaging the results
from each application (8-9). Smoothing the impulse frequency measure-
ment this way results in the production of a function that is propor-
tional to the probability density of a nerve spike occurring at a
specific time after the onset of the stimulus. Smoothing the intervals
results in an estimate for the average interval, or equivalently, the
average frequency of spike activity following the stimulus onset.
Matthews and Stein (8) use both of these methods to obtain their transfer
function. The average frequency, because of its lower variability,
was used at low frequencies while the probability density method was
used at higher frequencies. Groen et al. (14) have also used both

methods in their analysis, however at opposite ends of the frequency spectrum to that of Matthews and Stein.

This thesis is a quantitative study of the dynamics of a sensory receptor, specifically, the amphibian muscle spindle. The dynamics of a single spindle, isolated with only its sensory nerve intact, are described, using broad-bandwidth stimuli, in terms of the power spectrum of the point sensory discharge. The results show directly what information can be recovered from the receptor output by various filtering operations. The potential usefulness of this kind of analysis has been discussed by Bayly (15) with reference to the usually low pass filter characteristic shown by the synaptic response to a nerve impulse. That demodulation of neuronal output resembles a low pass filter has been demonstrated in the transfer properties of both nerve-muscle preparations (13,16), and nerve-nerve preparations (17). The recordings of Fatt and Katz (18), obtained near the end plate region of a muscle cell responding to single spikes in the motor nerve, show a strong resemblance to the impulse response of a low pass filter. Indeed, Stevens (19), in his model-oriented review of synaptic physiology has approximated the postynaptic potential as a single exponential. A description of neuronal 'integration' in the central nervous system has been given by Katz (20), chapter 10.

The power spectrum of a point process contains information related to both the serial dependence between, and the distribution of, interspike intervals and is applicable over all frequencies. These properties are not shared by any of the measurements discussed in the preceding paragraphs. In addition to the power spectrum, estimates of various related spectra, such as the coherency function, have shown approximately how 'noisy' stimulus recovery would be from this particular sensory receptor under linear filter demodulation. Gain and phase function estimates have uncovered the best linear model, in a least squares sense, for the spindle dynamics.

In 1931 Matthews (21) showed that in the frog, stretch applied to a muscle, constitutes an effective stimulus to the spindle receptors. It was also noted that these organs were not only sensitive to changes in length but also to the rate of change of length. As a matter of

speculation, Matthews suggested that perhaps structures with viscous properties underlying the sensory nerve endings could be responsible for this rate sensitivity. Some evidence does exist that supports this speculation in the mammalian muscle spindle (24) but recent observations, relating to the amphibian spindle, are completely contradictory to the idea (22-23).

Although it was originally intended that a study of the role of muscle fiber mechanics in the overall spindle response would be included in this thesis, the results of Ottoson and Shepherd (22-23) have made this unnecessary. There is agreement that the gross mechanical properties of the muscle fibers innervated by the sensory nerves do not contribute to the dynamic behavior of the receptor. There are however purely elastic differences along the fiber which are involved in spindle sensitivity. These observations are somewhat contrary to those of Ottoson and Shepherd and will be published under a separate cover (25).

The following two chapters are reviews. Chapter 2 is a brief account of amphibian muscle spindle physiology along with a description of some of the models proposed for its behavior. Chapter 3 is a review of power spectrum estimation and describes the impact of the Fast Fourier Transform (26) on spectral estimation. Chapter 3 also consolidates some of the more recent ideas concerning spectral estimation that are relevant to the methods of this work.

CHAPTER 2

AMPHIBIAN MUSCLE SPINDLE PHYSIOLOGY

2.1 Morphology

Muscle, like all living tissue, consists of the orderly
arrangement of a large number of individual cells. The structure of
each of the cells and the way they are collectively organized is
specialized to perform a specific function. Skeletal muscle cells are
elongated forms which usually extend from tendon to tendon in the
muscle. When excited by activity in their motor nerves, they develope
tension between the tendons which may result, depending on the load,
in an overall shortening of the cell. Skeletal muscle cells are organized
into motor units; a motor unit is a group of muscle cells that receive
their excitation along branches of the same nerve axon. Motor units
are also specialized in their function: some are suited for slow
precise movements, others are better suited for quick-withdrawal or
reflex-type activity.

The specialized nature of motor units implies that not all
muscle cells are identical. Studies on single muscle cells have
revealed that some cells, when stimulated by activity in their motor
nerves, contract very quickly but are able to maintain tension for
only short periods. Other cells contract much more slowly but are
able to maintain this state over much longer periods.

Amphibian skeletal muscle has been broadly classified into
two groups, 'fast' and 'slow'. The division has been shown both
functionally, by motor units (27-28), and structurally (29-30). Recent
investigations have shown that functional and structural subgroups are
present in each of the two major groups (31-32). However, the essential
distinction between 'fast' and 'slow' cells remains. The membrane of
the 'fast' muscle cells is capable of actively spreading contractile
activity along its entire length via an 'all-or-none' action potential.
This action potential is initiated in the region of contact between the
motor nerve and the muscle cell by a neuromuscular transmitter (33). By
contrast, 'slow' muscle cells are unable to produce action potentials

and contraction occurs only in regions of local depolarization around motor nerve end plates (34). The larger motor nerves innervate the 'fast' motor units and form well-localized contacts on the muscle cells; the smaller motor nerves end in more diffuse end plates on the slightly smaller 'slow' muscle cells (35-36). There is evidence that only one region of contact exists between a 'fast' muscle cell and an innervating motor nerve, while the 'slow' cell may receive end plates from one or several motor nerves along its entire length (35). The 'fast' motor units respond to a single impulse in their motor nerve with a characteristic tension twitch. Repetitive stimulation results in the fusion of the twitches into a smooth contraction in which the tension generated can be graded by the frequency of the stimulation (cf 32). On the other hand the 'slow' motor units develop appreciable tension only when stimulated repetitively (37). This tension develops relatively slowly and can also be graded by altering the stimulus frequency. All mammalian skeletal muscle cells appear to be of the 'fast' type in as much as all are capable of producing action potentials (24,38-39).

In addition to motor nerves, skeletal muscle is also innervated by sensory nerves. In the frog these axons have terminations inside spindle-shaped capsules which, over lengths of about 1 mm, enclose a number of small muscle cells in a fluid-filled compartment. In the extracapsular regions these so-called intrafusal muscle fibers also receive terminations from motor nerves. That the axons innervating the capsular regions are sensory has been verified both by histological examination (40) and by electrophysiological experiment (41). Contractions of the intrafusal fibers have been observed, by light microscopy, to occur on stimulation of motor nerves (42). The existence of sensory endings on extrafusal muscle cells have been reported in some amphibian muscles (42), although these are apparently rare. In the mammal, in addition to spindles, the existence of sensory receptors in the tendon region of most muscles is well established (43).

According to Gray (35), in the frog toe muscle extensor digitorum longus IV, there are two or three spindle systems. Each consists of a bundle of intrafusal muscle fibers with two, three or

four discrete encapsulated sensory regions. Only one sensory axon
enters each capsule; after entering the capsule it divides into a
number of unmyelinated varicose threads which lie along the intrafusal
fibers over most of the intracapsular region. A parent axon may
innervate more than one sensory region. In his more detailed study of
this region Katz(45) describes a series of nerve bulbs of up to 2-3 μm
in diameter connected by cylindrical tubes about .15μm thick. The
muscle fiber contains numerous sockets in which these bulbs are seated
in close-fitting contact. The gap between the respective membranes is
much narrower than that found at the motor end plates. Katz also describes
the presence of fine filaments bridging the gap between the membranes.
In a few cases the bulbs were seen not to be in contact with the muscle
membrane at all, but floating freely in the intracapsular fluid. In
the center of the sensory region most of the intrafusal fibers seemed to
lose their characteristic striated structure and instead appeared
reticulate. These 'reticular zones' were approximately 50-100μm long
and devoid of some 85% of the contractile material present in adjacent
regions. A few of the smaller intrafusal fibers showed little
differentiation in the 'reticular zone' losing less than 30% of the
contractile materials. Katz called the regions immediately adjacent to
the 'reticular zone' the 'compact zones'. These areas, each about 250μm
long, were the site of the majority of nerve bulbs, although significant
numbers were also present on the 'reticular zone'.

Gray's observations (35) provided histological evidence that
the motor terminations on the extracapsular region of the intrafusal
fibers were characteristic of motor end plates on the extrafusal fibers.
He showed that the motor innervation of intrafusal fibers was in fact
branches of the same nerve axon that innervated the extrafusal fibers.
Branches of motor nerves that innervated intrafusal fibers formed
the same type of end plate on the intrafusal fibers that they did
on the extrafusals. Earler, Katz (46) had also obtained evidence that
intrafusal and extrafusal fibers were co-innervated. He found that,
under isometric conditions, stimulation of a single, either 'large' or
'small', motor nerve, increased the afferent discharge from a single
spindle while at the same time causing a contraction in the muscle.

Sometime later, Eyzaguirre (42,47) demonstrated the difference in the time course of the afferent discharge resulting from stimulation of the individual motor nerves. On beginning repetitive stimulation of the larger fibers there was an immediate acceleration of the discharge of the sensory ending. Repetitive stimulation of the 'small' motor fiber resulted in the frequency of afferent discharges rising very slowly. These observations led him to conclude that intrafusal fibers were also of the 'fast' and the 'slow' variety. He was however, able to directly detect the presence of action potentials in only the intrafusal fibers innervated by the 'large' motor nerves. More recently Smith (48-49) has shown that both intrafusal muscle fibers are able to produce and propagate action potentials. The fibers supplied by small diameter motor nerves however, respond to single stimuli with much slower and longer lasting contractions. There is evidence indicating that the non-reticulating fibers observed by Katz (45) are members of this group of slowly contracting fibers.

The motor innervation of mammalian muscle spindles appears to be separate from extrafusal fibers (50). Sensory innervation is more complex in that two sensory nerves originate from the capsule of the mammalian spindle (51).

2.2 Physiological Behavior

The behavior of single amphibian muscle spindles in response to stretching the muscle was first studied in detail by B.H.C. Matthews (21). In these experiments the muscle was stretched by loading it with weights. During application of the load the frequency of sensory discharges increased dramatically after which, under maintained load, it gradually declined toward a steady level. When small loads were applied rapidly, the frequency of discharge adapted much more quickly than when the loads were large. This led Matthews to speculate that perhaps the rapid adaptation might be due to differences in viscosity between the center and the poles of the intrafusal fiber. On the other hand, he speculated, the much slower adaptation to larger loads may be dependent on the depletion of some substance from the sensory ending. The peak

frequency reached during application of the load was proportional to the
rate at which it was applied. The adapted discharge rate was approximately
proportional to the logarithm of the maintained load. Matthews later
showed (52) that the afferent discharge ceased when the whole muscle
contracted, suggesting that the sensory ending was in parallel with the
fibers that produce the bulk of the tension. Sometime later, Katz (41),
using controlled stretches of constant velocity, showed that the response
of the spindle to applied stretch depends on two main factors: the
velocity and the amplitude of the imposed increase in muscle length.
He divided the response to these variables into a 'dynamic' and 'static'
component respectively. Recently, Shepherd and Ottoson (53) have more
quantitatively related the response pattern to the parameters of the
ramp stretches.

The variability of amphibian muscle spindle discharges has
been examined by Buller et al. (54). Their results indicate that at
very low discharge frequencies the standard deviation in the frequency
approaches the mean. Hence, in the statistical sense, the discharges
of the spindle at very short lengths resemble a completely random
process. As the mean frequency is increased, by stretching the muscle,
the standard deviation increases to about 3.5 impulses per second at a mean
rate of 8 impulses per second. Further increases in mean discharge
rate do not result in significant changes in the standard deviation.
The speculation is that this behavior may be due to a constant noise
voltage due to thermal agitations in the fine sensory terminals.

Stimulation of the motor nerves which innervate a spindle can
result, as has already been pointed out, in the acceleration of the
sensory discharge (42,46,47). Matthews and Westbury (55) have shown that
repetitive stimulation of 'fast' motor fibers markedly excited the
spindle when the muscle was at a constant length. The dynamic response
to stretching however, was left almost unaffected. On the other hand,
repetitive stimulation of the 'slow' motor fibers only weakly excited
the sensory ending when the muscle was at a constant length, while
stretching the muscle resulted in an augmented dynamic response. As
Matthews and Westbury point out, this is in direct contrast to the effect

of the large and small fusimotor fibers on the mammalian spindle.

2.3 Mechanisms Underlying Receptor Behavior

In 1950, Katz (41) showed that when the recording electrodes
were placed very close to the spindle capsule, the afferent discharges
were superimposed upon a local potential which re-developed after each
discharge. By applying a local anesthetic to the preparation he was
able to abolish the spike activity and record undistorted the potential
charges near the sensory ending. The frog spindle thus became the first
mechanoreceptor from which a receptor potential was recorded. Katz
observed that the size of the receptor potential varied continuously
with the amplitude and the rate of stretching. He therefore considered
the receptor potential to be the immediate cause of the sensory spikes
present in the unanesthetized condition. He also suggested that the
conversion from the mechanical stimulus to electrical energy in this
receptor does not involve an 'active response' of the nerve endings, at
least not the kind that is associated with the action potential.
Sometime later Edwards (56) showed that the potential change produced by
an external current applied to the sensory axon near the capsule would
sum with the receptor potential. He was able to show that the discharge
frequency resulting from stretching the spindle could either be raised
or lowered depending on the direction of the applied current. This
was direct evidence supporting the view that the generator potential
was the underlying cause of the sensory spikes.

Katz (41) was also able to make measurements relating the
magnitude of the receptor potential to the frequency of afferent spikes.
His data showed a linear correlation coefficient of .97 and was thus
significant evidence that the two were linearly related. Edwards (56)
using external currents also obtained a linear relationship between the
applied current and the frequency of discharges. He also noted that the
spike producing mechanism showed no adaption to step applications of
current. When the direction of the applied current was reversed, the
relationship between the current and the discharges showed a markedly
different slope. This was attributed to the rectification properties

of the nerve membrane. Ottoson and Shepherd (57) have shown an
approximately linear relationship between the following: rate of stretch
and rate of rise of the receptor potential, rate of stretch and the
dynamic peak attained by the receptor potential, the amplitude of the
stretch and the magnitude of the partially adapted receptor potential.
These results were obtained by applying ramp stretches directly to the
encapsulated region of the spindle. A linear and instantaneous relation
between applied current and discharge frequency has also been shown in
the mammalian muscle spindle (58), although adaptation to constant
currents seems to be present in some crustacean stretch receptors (6).

In a paper which preceded his study of the receptor potential,
Katz (59) described the presence of small 'all-or-nothing' spikes which
were quite distinct from both the receptor potential and the full sized
action potentials. These were present in greatest numbers when the
muscle was under low tension and tended to disappear as the muscle was
stretched. They were observed to occur in a number of different sizes
and also formed the prepotentials on the main spikes. Katz suggested
that these small spikes were formed in the terminal branches of the
sensory axon and sometimes failed to initiate active propagation past
the branch points. Those that failed to initiate propagation were
observed as abortive spikes. The maintained receptor potential at
greater muscle tensions probably facilitated the passage of the active
potentials through the branch points. Recently Ito (60) has produced
a quantitative report which describes the effect of muscle length upon
the pattern and frequency of the abortive spikes. The ideas here generally
support the speculations of Katz(59).

2.4 Models

Until recently, most evidence related to the mechanisms of
muscle spindle dynamics, both in the amphibian and the mammal, pointed
to muscle fiber mechanics as the main underlying factor. Matthews' (21)
original suggestion that the form of the afferent discharge in response
to stretch is a reflection of the differences in viscosity between the
center and the poles of the intrafusal fiber, has received much

speculative attention. In a theoretical treatment Katz (41) related
the possibility that changes of electrical capacity in the terminal
nerve membrane, as a result of stretch, could contribute to the phasic
response of the spindle. He showed however, that this mechanism could
not provide a phasic receptor potential of the observed magnitude unless
there was a substantial mechanical amplification of the stretch. In
introducing his later histological work (45) he said "it is natural
to suppose that a mechano-receptor such as the spindle owes its high and
specific sensitivity, at least in part, to the way in which the mechanical
stimulus is bought to bear on the membrane of the sensory nerve terminal."
The results of this work showed that most intrafusal fibers showed a
'reticular zone' in which there were few contractile filaments.
Excitation of the motor nerves would therefore stretch this zone and thus
explain the observed increase in afferent discharge (42,46,47). Also,
the polar region, with its mass of interdigitating contractile filaments,
will probably be much more viscous than the 'reticular zone' where these
filaments are largely absent. Therefore, it might be expected that
changes in muscle length would first appear across the 'reticular zones',
followed by a gradual and partial shift to the polar regions after the
muscle length is fixed. In addition, the works of Edwards (56) and
Lippold et al.(58) suggest, because of the failure of the encoding
mechanism to adapt to constant currents, that mechanical factors are
very prominent in overall spindle dynamics. Indeed, there is direct
evidence that mechanical factors are involved in the adaptation of
mammalian muscle spindles (24), in the mammalian Pacinian corpuscle (61),
and receptors in the skin of the frog (62).

In light of the evidence, a number of models have been developed
for both the amphibian (63-66) and the mammalian (66-69) muscle spindle.
Of these, the model by Houk et al. (65) seems most typical and will be
briefly described. This model assumes that the 'reticular zone' of
the intrafusal muscle fiber is less viscous but stiffer than the
adjacent polar regions. Also, the viscosity of the 'reticular zone' and
the stiffness of the polar regions are assumed negligible. The intra-
fusal muscle fibers are therefore represented as a spring in series with
the parallel combination of a force generator and viscous dash pot.

The spring represents the lumped stiffness of the 'reticular zone' while
the dash pot and force generator depict the lumped viscous and contractile
properties of both polar regions. The effect of stretching the model
is to produce strain in the elements representing each of the regions.
The resulting generator potential is considered proportional to the
strain in each of the passive elements weighted by the number of nerve
terminations present on each of the regions in the actual muscle. Katz
(45) reported that on average, 3.5 times as many nerve bulbs were located
on the 'compact zones' than there were on the 'reticular zone'. Strain
of the polar regions will therefore be more prominent in the generator
potential when the model is passively stretched; while strain of the
'reticular zone' will be the sole contributor to the generator potential
during motor nerve input under isometric conditions. The encoder in
the model produces a train of impulses whose frequency is directly
proportional to the instantaneous magnitude of the generator potential.
The parameters of this model have been adjusted so that the theoretical
responses resemble those of the amphibian spindle (66).

In 1965 Buller (70) published a model designed to test the
suppositions of the earlier work of Buller et al. (54) concerning the
events occurring at the sensory nerve terminals of the frog muscle
spindle. These experiments had shown that, above a certain minimum
mean frequency, the standard deviation in the frequency about the mean
was approximately 3.5 impulses per second. Below this critical
frequency, the standard deviation tended toward the mean as the mean
decreased. It was suggested that the critical frequency corresponds to
threshold depolarization of the nerve terminals with further depolariz-
ation resulting in directly proportional increases in the discharge
frequency. Variations in the frequency are introduced by a source of
random potential variations due possibly to molecular agitation in the
mechanical receptor substance or to ionic noise in the terminal nerve
membrane. Discharge below the critical frequency would therefore be
the result of noise transients on the subthreshold depolarization.
Buller's model was based on these assumptions and its responses show a
remarkable similarity to the results obtained earlier from the actual

-13-

spindle. In addition, the results show that the variability which exists
in the discharges of the model above the critical frequency are not
particularily sensitive to changes in the rms value of the disturbing
noise used to represent the nerve terminal fluctuations. Changes in the
shape and the bandwidth of the noise spectrum have even less effect upon
the variability. It was therefore concluded, that, in spite of the
probable changes in the terminal membrane electrical time constant brought
on by the different levels of depolarization, the disturbing noise may
be considered as remaining constant over the physiological operating range
of the receptor.

More recently, Stein (71) has pointed out that the distribution
of intervals collected by Buller et al. (54) from the single frog
spindle is extremely well described by the well known Gamma density
function. Hagiwara (72) has shown that adjacent intervals from muscle
spindles in the sartorius muscle of the toad are statistically independent.
Apparently then, the discharges from the amphibian muscle spindle can
be considered as realizations of a renewal process and therefore, under
steady state conditions the Gamma density would be a complete description
of the process. The Gamma density has also been used to describe
empirically the maintained discharge originating from the retina of the
cat (73) and the responses of primary auditory neurons to acoustic
stimuli (74).

CHAPTER 3

SPECTRAL ESTIMATION

3.1 Introduction

The power spectrum $S_{xx}(t,f)$ of a random process as a function of time t and frequency f is defined by

$$S_{xx}(t,f) = \int_{-\infty}^{\infty} R_{xx}(t,\tau) \; e^{-j2\pi f\tau} \; d\tau \qquad (3.1)$$

where $R_{xx}(t,\tau)$ is the autocovariance function of the process. The autocovariance function is the mathematical expectation of the product of two values which the random process x(t) assumes for two instants of time. That is,

$$R_{xx}(t,\tau) = E\{x(t)x(t+\tau)\} \qquad (3.2)$$

defines the autocovariance between the value of the process at time t and its value at another time t+τ. For a stationary random process $R_{xx}(t,\tau)$ can be shown to be (75)

$$R_{xx}(t,\tau) = R_{xx}(\tau) = \lim_{T\to\infty} \frac{1}{2T} \int_{-T}^{T} x(t)x(t+\tau) \; dt \qquad (3.3)$$

The cross spectrum between two processes x(t) and y(t) is defined as

$$S_{xy}(t,f) = \int_{-\infty}^{\infty} R_{xy}(t,\tau)e^{-j2\pi f\tau} \; d\tau \qquad (3.4)$$

For a stationary random process $R_{xy}(t,\tau)$ is given by

$$R_{xy}(t,\tau) = R_{xy}(\tau) = \lim_{T\to\infty} \frac{1}{2T} \int_{-T}^{T} x(t)y(t+\tau) \; dt \qquad (3.5)$$

$S_{xx}(t,f)$ and $S_{xy}(t,f)$, for a stationary random process, become simply $S_{xx}(f)$ and $S_{xy}(f)$ respectively. By manipulation of the expressions which define these spectra it is possible to show that, among other

-15-

things, $S_{xx}(f)$ is a real function of frequency while $S_{xy}(f)$ is usually a complex function of frequency (75-76).

   If the process $y(t)$ is derived from $x(t)$ by passing $x(t)$ through a linear system, it can be shown that

$$S_{xy}(f) = H(f) \ S_{xx}(f) \tag{3.6}$$

and

$$S_{yy}(f) = |H(f)|^2 \ S_{xx}(f) \tag{3.7}$$

where

$$H(f) = \int_0^\infty h(t) \ e^{-j2\pi ft} \ dt \tag{3.8}$$

$h(t)$ being the response of the system to a unit impulse. $H(f)$ is the frequency response of the system.

   The squared coherency spectrum between two stationary processes $x(t)$ and $y(t)$ is defined as

$$\gamma^2_{xy}(f) = \frac{|S_{xy}(f)|^2}{S_{xx}(f) \ S_{yy}(f)} \tag{3.9}$$

It can be shown that

$$0 \leq \gamma^2_{xy}(f) \leq 1 \tag{3.10}$$

   The coherency spectrum is a measure of the linear correlation between the processes $x(t)$ and $y(t)$ as a function of frequency. For the linear system described by equations 3.6 - 3.8 $\gamma^2_{xy}(f) = 1$ for all f. Bendat and Piersol (76) describe the situation of a squared coherency greater than zero but less than one as indicating one or more of three possibilities:

   a)   extraneous noise is present in the measurements;

   b)   the system relating $x(t)$ and $y(t)$ is not linear;

c) y(t) is an output due to an input x(t) as well as to other inputs. A coherency of zero at all frequencies implies that the processes x(t) and y(t) are completely uncorrelated. Goodman (77) describes the squared coherency spectrum for a nonlinear system as a measure of the degree to which the output y(t) at a particular frequency is related by a linear time invariant operator to the input x(t). The quantity $S_{xy}(f)/S_{xx}(f)$ is the linear operator that best approximates y(t), in a least squares sense, by acting on x(t).

The squared coherency spectrum has the interesting property that makes it invariant under linear filtering operations. For example, if $\gamma^2_{xy}(f)$ is the squared coherency spectrum between the processes x(t) and y(t) and $\gamma^2_{uv}(f)$ is the same function between u(t) and v(t) then $\gamma^2_{xy}(f) = \gamma^2_{uv}(f)$ if u(t) is derived from x(t) by passing x(t) through some linear filter and v(t) from y(t) by passing y(t) through some other linear filter.

The most serious problems associated with obtaining reliable spectral estimates are those which result from the application of the previous formulas to finite pieces of data. Today, two practical approaches, each with distinct advantages, are available and can result in good estimates of the various spectra from finite lengths of data. Neither of the methods, however, is entirely clear cut and usually must be applied several times with systematic modifications to produce the final estimate. A rough idea of the shape of the spectrum before estimation is extremely helpful in reducing the labor involved.

The oldest of the two approaches to power spectrum estimation is that formalized by Blackman and Tukey (78). Until 1965 this approach was used almost exclusively and offered the additional advantage that an estimate of the covariance function was a byproduct of the operation. In 1968 Jenkins and Watts (79) extended these ideas to the estimation of the cross spectrum between several processes. The subsequent role of the cross spectrum in the estimation of the squared coherency spectrum and the gain and the phase functions was also developed.

In 1965 a highly efficient algorithm for the digital evaluation of complex Fourier coefficients was discovered by Cooley and Tukey (26).

The Fast Fourier Transform has, in the minds of some (80), revolutionized the processes of spectral estimation. The so-called direct route to spectral estimates is computationally several orders of magnitude faster than the older Blackman-Tukey approach. On the other hand, the direct method suffers from the disadvantage that the covariance function is not a byproduct of the operation. The role of the Fast Fourier Transform will be discussed further in the last section of this chapter after the ideas underlying each of the approaches to spectral estimation have been described and compared.

3.2 The Sample Spectrum

Estimates of the power spectrum of a stochastic process are derived from the so-called sample spectrum defined as

$$\hat{S}_{xx}(f) = \int_{-T}^{T} \hat{R}_{xx}(\tau) e^{-j2\pi f\tau} d\tau \qquad (3.11)$$

where $\hat{R}_{xx}(\tau)$ is the estimator for the autocovariance function $R_{xx}(\tau)$. Two widely used estimators for the autocovariance function are

$$\hat{R}_{xx}(\tau) = \begin{cases} \hat{R}_{xx1}(\tau) = \begin{cases} \dfrac{1}{T} \int_{0}^{T-|\tau|} x_T(t) x_T(t+|\tau|)\ dt & 0 \le |\tau| \le T \\ 0 & |\tau| > T \end{cases} \\[2em] \hat{R}_{xx2}(\tau) = \begin{cases} \dfrac{1}{T-|\tau|} \int_{0}^{T-|\tau|} x_T(t) x_T(t+|\tau|)\ dt & 0 \le |\tau| \le T \\ 0 & |\tau| > T \end{cases} \end{cases} \qquad (3.12)$$

where

$$x_T(t) = \begin{cases} x(t) & 0 \le t \le T \\ 0 & T < 0,\ t > T \end{cases} \qquad (3.13)$$

The $\hat{R}_{xx}(\tau)$ given above are each functions of the random variable

$x_T(t)$. Therefore $\hat{R}_{xx}(\tau)$ is also a random variable. This means that $\hat{R}_{xx}(\tau)$ at all τ will be subject to some probability density function. This density function is called the sampling distribution of the random variable $\hat{R}_{xx}(\tau)$.

It is useful to compare the estimators $\hat{R}_{xx1}(\tau)$ and $\hat{R}_{xx2}(\tau)$ by calculating what are usually called the sampling moments of their respective distributions. It has been shown (79) that the expected values (means) for the estimators are given by

$$E\{\hat{R}_{xx1}(\tau)\} = \begin{cases} R_{xx}(\tau) \; 1-\dfrac{|\tau|}{T} & |\tau| \le T \\[3mm] 0 & |\tau| > T \end{cases} \qquad (3.14)$$

and

$$E\{\hat{R}_{xx2}(\tau)\} = \begin{cases} R_{xx}(\tau) & |\tau| \le T \\[3mm] 0 & |\tau| \ge T \end{cases} \qquad (3.15)$$

Thus $\hat{R}_{xx2}(\tau)$ is what is called an unbiased estimator of $R_{xx}(\tau)$ whereas $\hat{R}_{xx1}(\tau)$ is only asymptotically unbiased as the record length T tends to infinity. The variances of each of the estimators are

$$\text{Var}\{\hat{R}_{xx1}(\tau)\} = \frac{1}{T^2} \int_{-(t-\tau)}^{T-\tau} (T-\tau-|r|)[R_{xx}^2(r)+R_{xx}(r+\tau)R_{xx}(r-\tau)] \, dr$$

$$|\tau| \le T \qquad (3.16)$$

$$\text{Var}\{\hat{R}_{xx2}(\tau)\} = \frac{1}{(T-|\tau|)^2} \int_{-(T-\tau)}^{T-\tau} (T-\tau-|r|)[R_{xx}^2(r)+R_{xx}(r+\tau)R_{xx}(r-\tau)] \, dr$$

$$|\tau| \le T \qquad (3.17)$$

It is seen that these expressions are identical with the exception of the multiplying factors preceding the integrals. The variance of $\hat{R}_{xx2}(\tau)$ grows without bound as $|\tau| \to T$. The mean square errors in each of

-19-

the estimators are

$$E \{[\hat{R}_{xx1}(\tau) - R_{xx}(\tau)]^2\} = \text{Var} \{\hat{R}_{xx1}(\tau)\} + [\frac{\tau}{T} R_{xx}(\tau)]^2 \qquad (3.18)$$

$$E \{[\hat{R}_{xx2}(\tau) - R_{xx}(\tau)]^2\} = \text{Var} \{\hat{R}_{xx2}(\tau)\} \qquad (3.19)$$

It is usually true that the mean square error in $\hat{R}_{xx1}(\tau)$ is less than that in $\hat{R}_{xx2}(\tau)$. Therefore, $\hat{R}_{xx1}(\tau)$ is preferred to $R_{xx2}(\tau)$ for auto-covariance estimates. In the remainder of this chapter $R_{xx}(\tau) = \hat{R}_{xx1}(\tau)$ is assumed.

By using the definition of the sample spectrum given by equation 3.11 it is possible to show that

$$\hat{S}_{xx}(f) = \frac{1}{T} \int_0^T x_T(t) e^{-j2\pi ft} dt \int_0^T x_T(t_1) e^{j2\pi ft_1} dt_1$$

$$= \frac{1}{T} X_T(f) X_T^*(f)$$

$$= \frac{1}{T} |X_T(f)|^2 \qquad (3.20)$$

where $X_T(f)$ is the Fourier transform of $x_T(t)$ and $X_T^*(f)$ is its complex conjugate. $X_T(f)$ can be expressed as the sum of real and imaginary components

$$X_T(f) = A_T(f) + jB_T(f) \qquad (3.21)$$

where $j=\sqrt{-1}$. It can be shown that

$$A_T(f) = \int_0^T x_T(t) \cos 2\pi ft \, dt \qquad (3.22)$$

and

$$B_T(f) = \int_0^T x_T(t) \sin 2\pi ft \, dt \qquad (3.23)$$

Therefore

$$\hat{S}_{xx}(f) = \frac{1}{T} [A_T^2(f) + B_T^2(f)] \tag{3.24}$$

It has been shown (79) that if $x_T(t)$ is a sample from a Normal process then, since the Fourier transform is a linear operation, $A_T(f)$ and $B_T(f)$ are also Normally distributed. Therefore $\hat{S}_{xx}(f)$ is distributed as a chi-squared random variable with two degrees of freedom since it is the sum of the squares of two Normal random variables. If the sample $x_T(t)$ is not Normal, $A_T(f)$ and $B_T(f)$ tend to Normality as T becomes large as a consequence of the Central Limit Theorem. Hence the distribution of $\hat{S}_{xx}(f)$ will be very nearly as chi-squared with two degrees of freedom irrespective of the distribution of $x(t)$.

The expected value of the sample spectrum estimator is

$$E\{\hat{S}_{xx}(f)\} = E\{\int_{-T}^{T} \hat{R}_{xx}(\tau)\, e^{-j2\pi f\tau}\, d\tau\}$$

$$= \int_{-T}^{T} R_{xx}(\tau)\, 1-\frac{|\tau|}{T}\, e^{-j2\pi f\tau}\, d\tau \tag{3.25}$$

Hence, using the convolution theorem

$$E\{\hat{S}_{xx}(f)\} = \int_{-\infty}^{\infty} T \left[\frac{\sin\pi Tg}{\pi Tg}\right]^2 S_{xx}(f-g)\, dg$$

$$= \int_{-\infty}^{\infty} W(g)\, S_{xx}(f-g)\, dg \tag{3.26}$$

The function $W(f)$ is a slit whose width is of the order of $1/T$ so that for large T it is reasonable to assume that $S_{xx}(f)$ is approximately constant over the slit. Hence

$$E\{\hat{S}_{xx}(f)\} \simeq S_{xx}(f) \int_{-\infty}^{\infty} T \left[\frac{\sin\pi Tg}{\pi Tg}\right]^2 dg$$

$$= S_{xx}(f) \tag{3.27}$$

The bias in $\hat{S}_{xx}(f)$ can always be made arbitrarily small by choosing T

-21-

sufficiently large.

As the length of the available record becomes large, it can be shown (79) that the variance of the spectral estimator tends to

$$\text{Var } \{\hat{S}_{xx}(f)\} \simeq S^2_{xx}(f) \qquad\qquad (3.28)$$

For a white Normal process this result is exact. Thus the variance of $\hat{S}_{xx}(f)$ is dominated by a term which remains finite as the length of the record tends to infinity. This indicates that $\hat{S}_{xx}(f)$ is not a consistent estimator of $S_{xx}(f)$ in the sense that its distribution does not tend to cluster more closely about the true spectrum as the sample size increases. It is almost equally probable for $\hat{S}_{xx}(f)$ to lie anywhere from 0 to $2S_{xx}(f)$. The reason for the inconsistency of $\hat{S}_{xx}(f)$ can be described simply as follows. The estimate of the spectrum at frequency f is actually drawn from a band of frequencies W(f) whose width is about 1/T. As T is increased the power at f is estimated over narrower and narrower frequency bands. However, the efficiency of the estimate of the power in the narrowing band does not improve.

3.3   Consistent Power Spectrum Estimation

The inconsistency of the sample spectrum has forced investigators to seek other means of estimating power spectra. The technique universally adopted is to trade the 1/T resolution afforded by $\hat{S}_{xx}(f)$ for the lower variances provided by an estimator with a coarser resolution. However, not all techniques that result in a loss of the 1/T resolution produce a corresponding decrease in variance (81).

The Blackman-Tukey or indirect approach to obtaining consistent power spectrum estimates is to consider only that part of the auto-covariance function to lag $\tau=M$ where M<<T. This procedure can be thought of as looking at the estimator of the autocovariance $\hat{R}_{xx}(\tau)$ through a rectangular window of width 2M, or more simply, as a multiplication of the autocovariance estimator by a function $w_R(\tau)$ where

$$w_R(\tau) = \begin{cases} 1 & |\tau| \leq M \ll T \\ \\ 0 & |\tau| > M \end{cases} \tag{3.29}$$

Blackman and Tukey (78) refer to $w_R(\tau)$ as a rectangular lag window.

The smoothed power spectrum estimator is defined, using the convolution theorem, to be

$$\hat{\hat{S}}_{xx}(f) = \int_{-\infty}^{\infty} W_R(g)\hat{S}_{xx}(f-g)\,dg \tag{3.30}$$

$W_R(f)$ is the Fourier transform of $w_R(\tau)$ and

$$W_R(f) = 2M \left[\frac{\sin 2\pi fM}{2\pi fM} \right] \quad -\infty < f < \infty \tag{3.31}$$

and is referred to as a spectral window. The expected value of the smoothed estimator is (79)

$$E\{\hat{\hat{S}}_{xx}(f)\} = \int_{-\infty}^{\infty} W_R(g)S_{xx}(f-g)\,dg \tag{3.32}$$

This expression is very similar to that derived for the expected value of the sample spectrum with the important difference that $W_R(f)$ now has a major base width of $1/M$. This means that estimates at a particular frequency will be influenced by power at least $1/2M$ away. On the other hand, if $S_{xx}(f)$ is slowly varying in $W_R(f)$, $\hat{S}_{xx}(f)$ tends to be an unbiased estimator of the true spectrum. The variance of $\hat{S}_{xx}(f)$ can be shown to be (79)

$$\begin{aligned} \text{Var}\{\hat{\hat{S}}_{xx}(f)\} &\approx \frac{S_{xx}^2(f)}{T} \int_{-\infty}^{\infty} w_R(\tau)\,d\tau \\ \\ &= \frac{2M}{T} S_{xx}^2(f) \end{aligned} \tag{3.33}$$

The variance of the smoothed estimator is reduced by a factor $2M/T$ from that of the sample spectrum. Also, the variance tends to zero as T becomes large. $\hat{S}_{xx}(f)$ is therefore a consistent estimator of $S_{xx}(f)$.

The direct approach to consistent power spectrum estimation
is to break up the data record of length T into subrecords of length
L with L<<T. The sample spectrum is computed for each segment via the
relation

$$\hat{S}_{xx_k}(f) = \frac{1}{L} \left| X_{L_k}(f) \right|^2 \qquad\qquad (3.34)$$

where k refers to the kth segment. The smoothed power spectrum
estimator becomes

$$\hat{\hat{S}}_{xx}(f) = \frac{L}{T} \sum_{k=1}^{k=\frac{T}{L}} \hat{S}_{xx_k}(f) \qquad\qquad (3.35)$$

It can be shown (82) that the expected value of this estimator is

$$E\{\hat{\hat{S}}_{xx}(f)\} \simeq \int_{-\infty}^{\infty} W_B(g) S_{xx}(f-g)\, dg \qquad\qquad (3.36)$$

with

$$W_B(f) = L \left[\frac{\sin \pi L f}{\pi L f} \right]^2 \qquad\qquad (3.37)$$

$W_B(f)$ is known as the Bartlett spectral window. The variance of $\hat{\hat{S}}_{xx}(f)$
can be derived heuristically. From the previous discussions, it is
known that the variance of each of the $\hat{S}_{xx_k}(f)$ is approximately equal
to $S_{xx}^2(f)$ regardless of the length of the subrecord. Since the $\hat{S}_{xx_k}(f)$
are T/L independent estimates of $S_{xx}(f)$ it follows that the variance of
$\hat{\hat{S}}_{xx}(f)$ is reduced to L/T that of $\hat{S}_{xx}(f)$. That is

$$\text{Var}\{\hat{\hat{S}}_{xx}(f)\} \simeq \frac{L}{T} S_{xx}^2(f) \qquad\qquad (3.38)$$

It is seen that if L=2M the direct and the indirect approaches both
result in smoothed consistent estimates with approximately the same
variance.

The bias in the smoothed estimates can be compared by looking

-24-

at $W_R(f)$, the spectral window corresponding to the rectangular lag window, and $W_B(f)$, the Bartlett spectral window. To make the comparison, the variances of the two smoothed estimators were set equal, that is with L=2M. When using the Blackman-Tukey approach, any bias in $\hat{S}_{xx}(f)$ is due to leakage from neighboring frequencies through $W_R(f)$; while with the directly approach, leakage is through $W_B(f)$. Half of each of these windows, centered at zero frequency, is shown in figure 3.1. Both estimators then, result in good estimates of the power in the band about some frequency f. Both approaches allow, by a simple choice of L or M, the possibility of exchanging spectral resolution for a corresponding decrease in variance. As far as bias considerations are concerned, if the true spectrum is reasonably smooth there is little to choose between the two approaches. If however, $S_{xx}(f)$ contains large fluctuations, the large and slowly declining side lobes of $W_R(f)$ can result in widespread leakage between regions of different power concentration. Large bias in spectral estimates is often not acceptable and a process called quadratic modification is used to reduce its effects.

Quadratic modification is the process of viewing the auto-covariance function through lag windows other than the rectangular window. The windows are chosen such that their spectral equivalents have lower side lobes and die away faster than those of the rectangular lag window. There are many lag windows that have these properties (78,79). One of the most popular means of reducing side lobe leakage is via the Hanning lag window

$$
w_H(\tau) = \begin{cases} 1/2 (1 + \cos \frac{\pi\tau}{M}) & |\tau| \leq M \\\\ 0 & |\tau| > M \end{cases}
$$

(3.39)

The Hanning spectral window is shown compared to the spectral equivalent of the rectangular lag window in figure 3.2. In addition to increasing the rate of side lobe decay, the Hanning window has a considerably wider
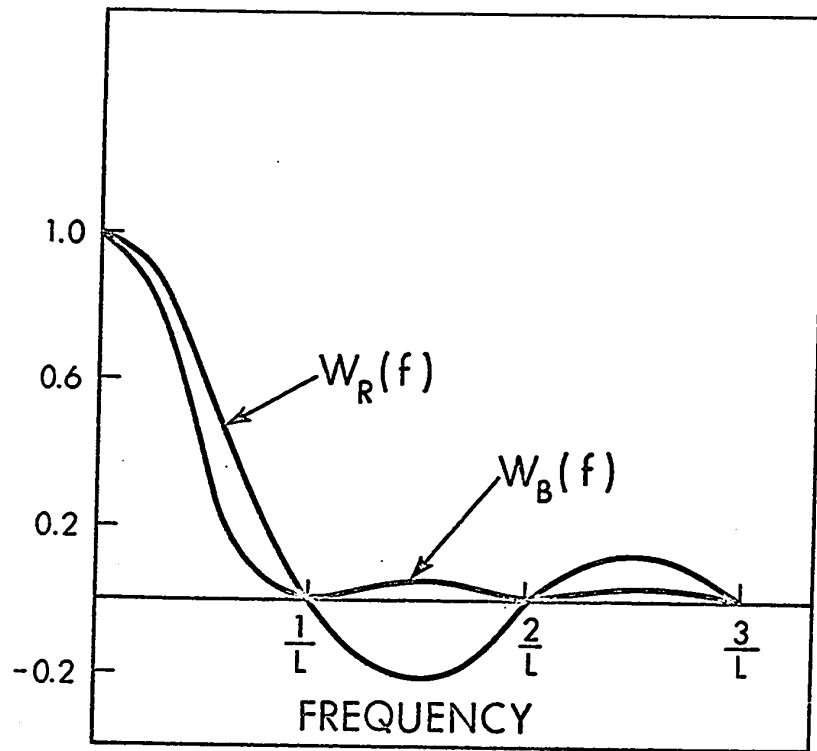
Figure 3.1

SPECTRAL EQUIVALENT OF THE RECTANGULAR LAG WINDOW, $W_R(f)$,
AND THE BARTLETT SPECTRAL WINDOW, $W_B(f)$.
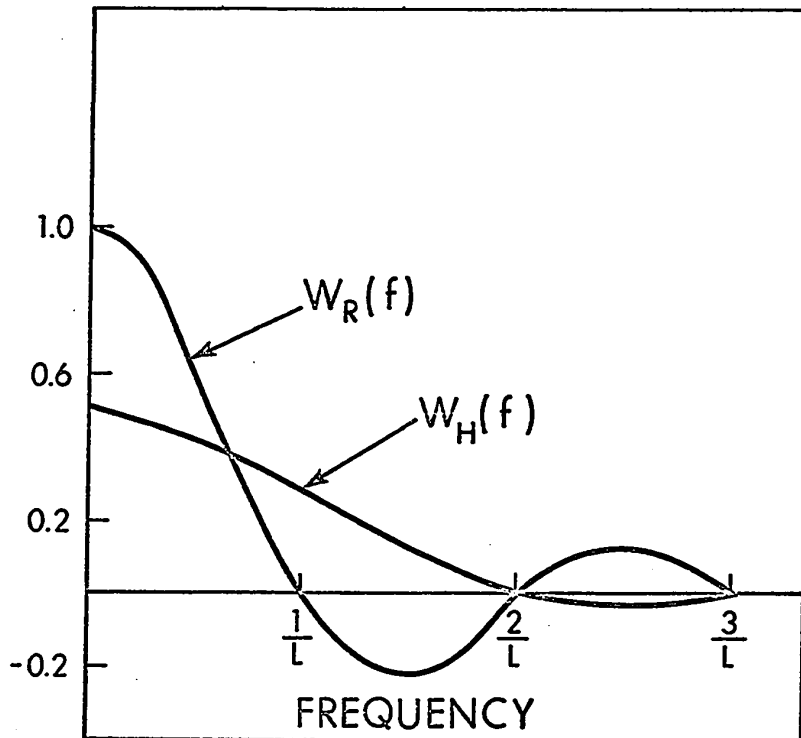
Figure 3.2

SPECTRAL EQUIVALENT OF THE RECTANGULAR LAG WINDOW, $W_R(f)$,
AND THE HANNING SPECTRAL WINDOW, $W_H(f)$.

major lobe width. This increased loss in spectral resolution is of course accompanied by a decrease in the variance of the estimator. It can be shown that (79)

$$\text{Var } \{\hat{S}_{xx}(f)\} \simeq \frac{S_{xx}(f)}{T} \int_{-\infty}^{\infty} w_H(\tau) \, d\tau$$

$$= \frac{.75M}{T} S_{xx}^2(f)$$

(3.40)

as opposed to a multiplying factor of 2M/T with the rectangular lag window. Reductions in variance from $L/T \ S_{xx}^2(f)$ can also be obtained for a fixed L and T with the direct approach. This is achieved by averaging in the frequency domain (84) or by overlapping the subrecords (83).

The process of linear modification which has arisen with the increasing popularity of the direct approach has been shown to result in a loss of spectral resolution without a compensating decrease in variance (81). Linear modification is the process of looking at the raw data through windows other than the rectangular data window. All lag windows can, with minor modifications, be used as data windows. Some authors (80,85) feel that some minor linear modification is desirable as this process is extremely effective in reducing the leakage of power between adjacent frequency bands.

The distribution of $\hat{S}_{xx}(f)$ was described earlier as being approximately that of chi-squared with two degrees of freedom. The two degrees of freedom arise from the condition that $\hat{S}_{xx}(f)$ is the sum of the squares of two Normally distributed random variables. Strictly speaking, chi-squared with k degrees of freedom is the sum of k Normally distributed random variables each with zero means and variances of one. Therefore, some normalization of $\hat{S}_{xx}(f)$ is required since the random variables $A_T(f)$ and $B_T(f)$ do not necessarily satisfy these requirements. It can be shown (79) that if the mean of $x_T(t)$ is removed and if f is somewhat removed from zero then, $2\hat{S}_{xx}(f)/S_{xx}(f)$ is approximately distributed as chi-squared with two degrees of freedom. It can also be shown that $\hat{S}_{xx}(f)$ is also a chi-squared random variable but with greater than two degrees of freedom. A chi-squared random variable

becomes relatively less variable as its degrees of freedom increase. As before, because of the required normalizations, it can be shown that $k\hat{S}_{xx}(f)/S_{xx}(f)$ is distributed as chi-squared with k degrees of freedom. k is calculated (78) from

$$k = \frac{2[E\{\hat{S}_{xx}(f)\}]^2}{\text{Var}\{\hat{\hat{S}}_{xx}(f)\}} \qquad (3.41)$$

It is worth noting that if $\hat{S}_{xx}(f)$ is substituted for $\hat{\hat{S}}_{xx}(f)$ in equation 3.41 then k=2 since $[E\{\hat{S}_{xx}(f)\}]^2 = \text{Var}\{\hat{S}_{xx}(f)\} \simeq S^2_{xx}(f)$. This is consistent with the previous discussion.

Knowledge of the approximate sampling distribution for $\hat{\hat{S}}_{xx}(f)$ is invaluable in that it enables one to make probabilistic statements concerning the accuracy of the estimates. That is, it is possible to construct intervals of confidence around the estimate $\hat{S}_{xx}(f)$ which will enclose the true value $S_{xx}(f)$ on 100(1-α)% of occasions on average. As a consequence of the chi-squared distribution of $k\hat{S}_{xx}(f)/S_{xx}(f)$ it can be shown (79) that the 100(1-α)% confidence interval for $S_{xx}(f)$ is given by

$$\frac{k\hat{\hat{S}}_{xx}(f)}{z_k\{1-\frac{\alpha}{2}\}} \leq S_{xx}(f) < \frac{k\hat{\hat{S}}_{xx}(f)}{z_k\{\frac{\alpha}{2}\}} \qquad (3.42)$$

where $z_k\{\frac{\alpha}{2}\}$ and $z_k\{1-\frac{\alpha}{2}\}$ are the α/2 and 1-α/2 points on the cumulative chi-squared distribution with k degrees of freedom.

3.4 Consistent Cross Spectrum Estimation

The sample cross spectrum is given by

$$\hat{S}_{xy}(f) = \int_{-T}^{T} \hat{R}_{xy}(\tau)\, e^{-j2\pi f\tau}\, d\tau$$

$$= \frac{1}{T}\, X_T^*(f)\, Y_T(f) \qquad (3.43)$$

$\hat{R}_{xy}(\tau)$ is the sample cross covariance function and $X_T(f)$ and $Y_T(f)$ are

the Fourier transforms of $x_T(t)$ and $y_T(t)$ respectively. Unlike $\hat{S}_{xx}(f)$, which is always real, $\hat{S}_{xy}(f)$ is usually a complex function of frequency.

The sample cross spectrum is statistically similar to the sample power spectrum. The values of $\hat{S}_{xy}(f)$ do not tend to a limiting value in any statistical sense as the record length T tends to infinity. Hence, $\hat{S}_{xy}(f)$ like $\hat{S}_{xx}(f)$, is an inconsistent estimator. Smoothing techniques are therefore again required.

The indirect approach to consistent cross spectral estimation involves calculating the cross covariance function between the processes out to lag M, where M<<T. The result is quadratically modified and Fourier transformed. The direct approach requires that the data records be segmented into subrecords of length L, with L<<T. Each subrecord is Fourier transformed and the products $X_{L_k}^*(f)Y_{L_k}(f)$ formed. $\hat{\hat{S}}_{xy}(f)$ is then obtained by averaging the contribution of $X_{L_k}^*Y_{L_k}(f)/L$ from all of the subrecords. The $\hat{\hat{S}}_{xy}(f)$ obtained by either of these routes are consistent estimates of $S_{xy}(f)$.

The expected value of the smoothed spectral estimator can be shown to be (79)

$$E\{\hat{\hat{S}}_{xy}(f)\} \approx \int_{-\infty}^{\infty} W(g)S_{xy}(f-g)\, dg \qquad (3.44)$$

The bias in $\hat{\hat{S}}_{xy}(f)$ will be small if $S_{xy}(f)$ is slowly varying over the spectral window $W(f)$.

In complex notation $\hat{\hat{S}}_{xy}(f)$ can be written as

$$\hat{\hat{S}}_{xy}(f) = \hat{\hat{M}}_{xy}(f)\, e^{j\hat{\hat{P}}_{xy}(f)} \qquad (3.45)$$

where

$$\hat{\hat{M}}_{xy}(f) = |\hat{\hat{S}}_{xy}(f)| \qquad (3.46)$$

and

$$\hat{\hat{P}}_{xy}(f) = \tan^{-1} \frac{\text{IM } \hat{\hat{S}}_{xy}(f)}{\text{RE } \hat{\hat{S}}_{xy}(f)} \qquad (3.47)$$

with IM and RE representing the imaginary and real parts of their arguments respectively. If L=2M and there is no linear or quadratic modification then it can be shown (82) that

$$\text{Var} \{ \hat{\hat{M}}_{xy}(f) \} \simeq \frac{L}{2T} S_{xx}(f) S_{yy}(f) \left[1 + \gamma^2_{xy}(f) \right] \tag{3.48}$$

and

$$\text{Var} \{ \hat{\hat{P}}_{xy}(f) \} \simeq \frac{L}{2T} \left[\frac{1}{\gamma^2_{xy}(f)} - 1 \right] \tag{3.49}$$

These variances can of course be reduced by, for example, using the Hanning lag window or overlapping the subrecords depending on which approach is used. It is worth while noting that the variability of $\hat{\hat{M}}_{xy}(f)$ and $\hat{\hat{P}}_{xy}(f)$ is a function of the true squared coherency between the two processes. Therefore, although the variances can be controlled to some extent by smoothing they may be dominated by the uncontrollable influence of the coherency spectrum.

A more useful function than the magnitude of the cross spectrum $M_{xy}(f)$ is the gain function $G_{xy}(f)$. A consistent estimator for this function can be obtained from

$$\hat{\hat{G}}_{xy}(f) = \frac{\hat{M}_{xy}(f)}{\hat{S}_{xx}(f)} \tag{3.50}$$

It can be shown (79) that approximate confidence intervals for $G_{xy}(f)$ and $P_{xy}(f)$ are given by

$$\hat{\hat{G}}_{xy}(f) \left[1 \overset{+}{} \left(\frac{2}{k-2} f_{2,k-2} \{1-\alpha\} \frac{1 - \hat{\hat{\gamma}}^2_{xy}(f)}{\hat{\hat{\gamma}}^2_{xy}(f)} \right)^{1/2} \right] \tag{3.51}$$

and

$$P_{xy}(f) \overset{+}{} \sin^{-1} \left(\frac{2}{k-2} f_{2,k-2} \{1-\alpha\} \frac{1 - \hat{\hat{\gamma}}^2_{xy}}{\hat{\hat{\gamma}}^2_{xy}} \right)^{1/2} \tag{3.52}$$

$f_{2,k-2}$ $\{1-\alpha\}$ is the $1-\alpha$ point on the cumulative Fisher's F distribution with 2 and $k-2$ degrees of freedom. $\overset{\ast}{\gamma}{}^2_{xy}$ is the smoothed coherency spectrum estimator.

3.5 Consistent Coherency Spectrum Estimation

The sample squared coherency spectrum is defined as

$$\hat{\gamma}^2_{xy}(f) = \frac{|\hat{S}_{xy}(f)|^2}{\hat{S}_{xx}(f)\hat{S}_{yy}(f)}$$

$$= \frac{\dfrac{|X_T^*(f)\ Y_T(f)|^2}{T}}{\dfrac{|X_T(f)|^2}{T}\ \dfrac{|Y_T(f)|^2}{T}}$$

$$= 1 \tag{3.53}$$

regardless of the relationship between the underlying processes. The sample coherency spectrum is therefore useless as an estimator of the true coherency between two processes. The smoothed squared coherency estimator

$$\hat{\overset{\ast}{\gamma}}{}^2_{xy}(f) = \frac{|\hat{\overset{\ast}{S}}_{xy}(f)|^2}{\hat{\overset{\ast}{S}}_{xx}(f)\ \hat{\overset{\ast}{S}}_{yy}(f)} \tag{3.54}$$

is a considerably better estimator of $\gamma^2_{xy}(f)$, the true squared coherency, and is the estimator most commonly used for this purpose.

Using Monte Carlo methods, Foster and Guinzy (86) and later Benignus (87-88) have shown that $\hat{\overset{\ast}{\gamma}}{}^2_{xy}$ is actually a biased estimator of γ^2_{xy}. This bias increases as the true coherency tends toward zero and can be considerable if the number of degrees of freedom associated with the estimates $\hat{\overset{\ast}{S}}_{xy}(f)$, $\hat{\overset{\ast}{S}}_{xx}(f)$ and $\hat{\overset{\ast}{S}}_{yy}(f)$ are low. Using the distribution function developed by Goodman (89) for $\hat{\overset{\ast}{\gamma}}{}^2_{xy}(f)$ between two Gaussian

processes, Foster and Guinzy have shown that their maximum likelihood estimator for $\gamma^2_{xy}(f)$ produces consistently lower estimates of γ^2_{xy} than $\hat{\gamma}^2_{xy}$. This is especially true at low γ^2_{xy} when the number of degrees of freedom associated with the estimates is less than 50. Benignus (87-88), on the other hand, has published a set of curves which describe the bias in $\hat{\gamma}^2_{xy}(f)$ as a function of $\gamma^2_{xy}(f)$ and k, the number of degrees of freedom. These curves show that as $\gamma^2_{xy}(f)$ approaches zero the bias in $\hat{\gamma}^2_{xy}(f)$ increases monotonically. For k=4,8,16,32 and 64 the bias in $\hat{\gamma}^2_{xy}(f)$ approaches .25, .11, .05, .025 and .01 respectively. It is also shown that these curves are not sensitive to the amplitude distributions of the underlying processes. Jenkins and Watts (79) have shown that the bias in $\hat{\gamma}^2_{xy}(f)$ depends largely on the sum of two terms. The first of these becomes small as the number of degrees of freedom associated with the estimates increases. The second term contains the true phase function between the processes. If there is a considerable delay or phase lag between the two processes this second term can contribute significant bias to $\hat{\gamma}^2_{xy}(f)$.

The variance of the smoothed squared coherency estimator can be shown to be (79)

$$\text{Var}\,\{\hat{\gamma}^2_{xy}(f)\} \simeq \frac{L}{2T}\,4\gamma^2_{xy}(f)\;[1-\gamma^2_{xy}(f)]^2 \tag{3.55}$$

and (82)

$$\text{Var}\,\{\hat{\gamma}_{xy}(f)\} \simeq \frac{L}{2T}\,[1-\gamma^2_{xy}(f)]^2 \tag{3.56}$$

An approximate confidence interval for $\gamma^2_{xy}(f)$ can be constructed by assuming that (76,79)

$$\hat{U}_{xy}(f) = \tanh^{-1}\hat{\gamma}_{xy}(f) \tag{3.57}$$

is Normally distributed. Hence, confidence intervals for $U_{xy}(f)$ are given by

$$\frac{\hat{U}_{xy}(f) \pm m \{1-\frac{\alpha}{2}\}}{\sqrt{k}} \qquad (3.58)$$

where $m \{1-\frac{\alpha}{2}\}$ is the $1-\frac{\alpha}{2}$ point on the cumulative unit normal distribution.

In section 3.1, the invariance property of $\gamma^2_{xy}(f)$ under linear filtering operations was discussed. Foster and Guinzy (86) have shown that $\hat{\gamma}^2_{xy}(f)$ does not necessarily share this property. If u(t) and v(t) are derived from x(t) and y(t) by passing the latter processes through the same linear filter then the invariance property extends to the smoothed estimators. If they are not passed through the same filter the invariance property only holds if the characteristics of the respective filters are slowly varying over the equivalent spectral window. If this is not the case, $\hat{\gamma}^2_{xy}(f)$ will tend to be on the low side of $\gamma^2_{xy}(f)$.

3.6 The Fast Fourier Transform

Today, the most practical route by far to spectral estimation is with a digital computer. Continuous data is therefore replaced by discrete or sampled data and the continuous Fourier transform gives way to the discrete Fourier transform. The discrete Fourier transform can be written as

$$X(i) = \frac{1}{N} \sum_{q=0}^{N-1} x(q) \, e^{-j2\pi i q/N} \qquad (3.59)$$

where x(q) is the discrete time series and X(i) is the discrete frequency series. N is the number of data points, $j=\sqrt{-1}$, $i=0,1,...n-1$. In general both x(q) and X(i) are complex series. To calculate all N Fourier coefficients the obvious way, approximately N^2 arithmetic operations are required. In 1965 Cooley and Tukey (26) showed that if equation 3.59 was judiciously factored, the number of operations could be reduced to $2N\log_2 N$. However, N must be chosen to be an integral power of 2. For N=1024 this represents a computational reduction of more than 200 to 1.

A more striking example is given by Cochran et al. (90) who report that when conventional procedures are used with N=8192, the computations on an IBM 7094 computer require about half-an-hour. With the Fast Fourier Transform about five seconds are required. On the IBM 360/67 used for the computations in this thesis, the calculation of all 8192 Fourier coefficients is reported to require about 2.9 seconds (91). Many descriptions of the Cooley-Tukey algorithm are now in the literature (85,90).

When the Fast Fourier Transform is applied directly to obtain estimates of the power spectrum of a process, the autocovariance function is not a byproduct of the operation as it is with the Blackman-Tukey method. Jenkins and Watts(79) have pointed out that the covariance function can sometimes be used to advantage in reducing the bias especially in cross spectral estimates. Bingham et al. (80) have shown that to obtain the first 500 terms of the discrete covariance function based on 4096-500 data points, it is computationally 12 times faster to first go the direct route to the power spectrum with the Fast Fourier Transform. This frequency series is then Fast Fourier re-Transformed to arrive at the covariance. The 3596 original data points are padded with 500 zeros to avoid circular convolutions. Before the Fast Fourier Transform, the most efficient route to the power spectrum was via the covariance function; since the Fast Fourier Transform, the most efficient route to the covariance function is via the power spectrum.

CHAPTER 4

PROCEDURE

4.1 The Preparation

In all experiments, muscle spindles from the extensor digitorum
longus IV muscle of the male toad Xenopus laevis were used. Often more
simply referred to as the long toe extensor, this muscle is located in
the hind limbs of the animal and is supplied by branches of nervus
peronus lateralis. In the adult, the relaxed in situ length of the muscle
(L_o) is between 19 and 25 mm. The muscle contains about 50 muscle fibers
with diameters varying from 5 to 100µ. The muscle was removed from the
limb with about 1 1/2 inches of the innervating nerve intact and placed
in a bath containing Ringer's solution. The composition of the Ringer
has been given elsewhere (48). The capsular portion of a muscle spindle
was located with a microscope by shining a light through the isolated
muscle. This region was then denuded by cutting and removing all other
fibers from the area. All nerve fibers, except the single afferent axon
which innervated the denuded capsule, were cut. The isolated preparation
is illustrated diagrammatically near the top of figure 4.1. In the bath,
the muscle was held taut by two wires each hooked into one of its tendons.
Sensory discharges were obtained by measuring the potential changes
produced by longitudinal action currents across a petroleum jelly seal
placed around the nerve trunk. The time course of the action current is
approximately proportional to the rate of change of the nerve action
potential. Recordings were obtained from a total of 17 apparently
normally functioning receptors. The temperature of the bathing Ringer's
solution was maintained at 20°C ± .5°C throughout by continuous perfusion
from a temperature controlled reservoir.

4.2 Data Collection

The afferent discharges of the spindle were recorded in response
to two classes of stimuli. The first of these could be called static
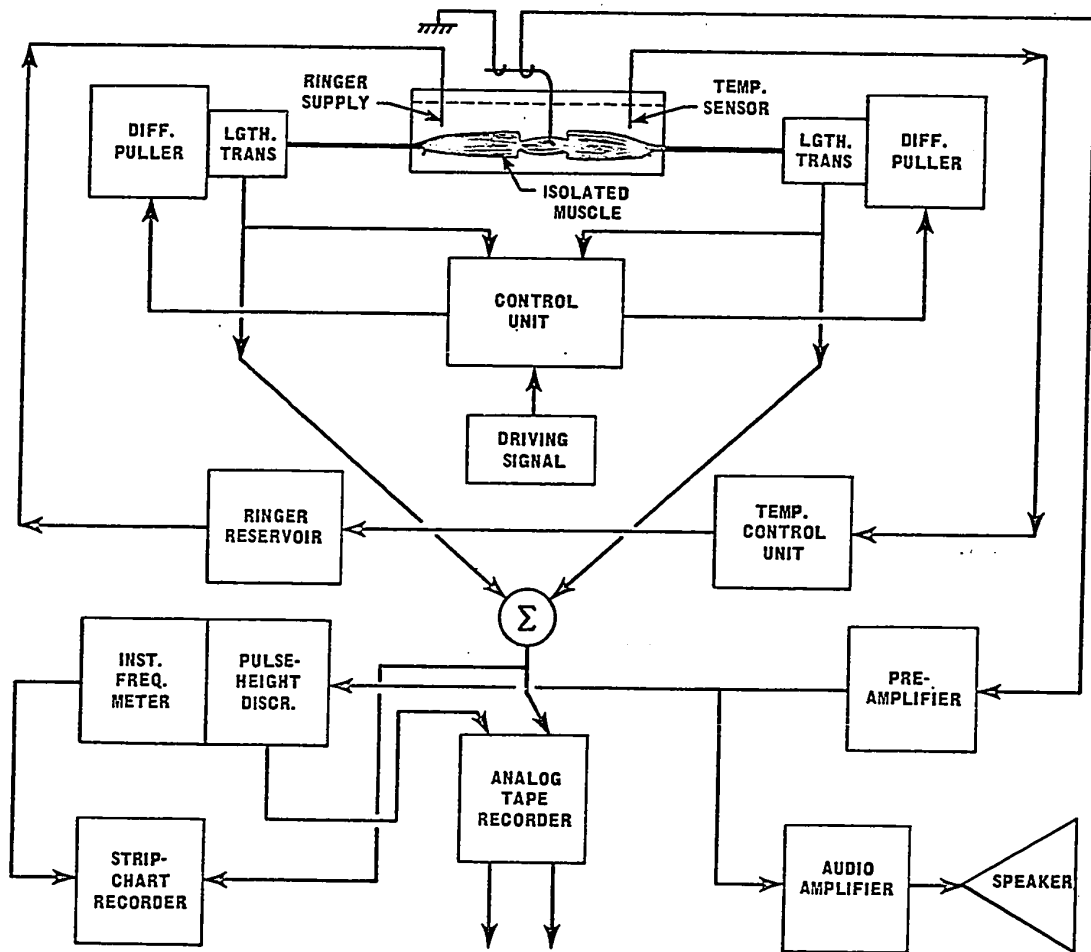stimuli and consisted of maintaining the muscle at various constant

Figure 4.1

THE EXPERIMENTAL AND DATA COLLECTION PROCEDURES.

lengths ranging from well below L_o up to the point of fracture. The
other class of stimuli was of the dynamic type; upon each static stimulus
was superimposed a small and usually random perturbation the course of
which was recorded simultaneously with the sensory discharges.

The wire rods hooked to each muscle tendon were securely
fastened to the shafts of a differential puller. The puller was
designed so that the displacements of each of the shafts accurately
followed the voltage level at the input of the control unit. The control
unit contained a continuously-variable signal-splitting circuit. This
allowed adjustment of the magnitude of the displacement at each of the
puller shafts while keeping the overall magnitude of the displacement
between the shafts constant. It was therefore possible to keep any point
along the length of the muscle stationary while the overall length was
changed. The splitter control was always adjusted so that the spindle
capsule remained stationary during the application of a stimulus. The
length changes of the reticular zone could therefore be observed with
a microscope while applying controlled length changes to the ends of the
muscle. Stationarity of the capsular region also ensured that no strain
would be placed on the nerve-capsule junction during stimulation. The
component and circuit diagram of the differential puller along with some
performance curves are given in appendix 1.

During all phases of the experiments, the receptor discharges
were continuously monitored using both visual and auditory means. As
a consequence, and through experience, a normal preparation could be
immediately recognized. During an experiment, the audio system seemed
to provide the first noticable sign of forthcoming abnormalities. This
occurred as either a change in the tone of the individual discharges or
as a general change in the pattern in which they occurred. The output
of the preamplifier was also fed into a pulse-height discriminator-
instantaneous frequency meter combination. The pulse-height discriminator
is a device that is electronically capable of selecting both the lowest
and the highest amplitude spike at its input that will be processed. It
responds to a spike of the selected amplitude by outputting a pulse
200 μsec long and 10 volts high coincident with the fall of the input

spike. Responses of the spindle were recorded by first passing the preamplified signals through the pulse-height discriminator. This procedure removed the base-line noise present on the raw signal and resulted in clean homogeneous recordings from all experiments. The circuit diagram of the pulse-height discriminator is shown in appendix 2. The instantaneous frequency meter is an analog device which computes the reciprocal of the time that has elapsed between successive pulses at the output of the pulse-height discriminator. During the interval between pulses, the output of the instantaneous frequency meter is constant and directly proportional to the reciprocal of the time interval between the last two pulses. The output of this device, displayed on a strip-chart recorder, was invaluable in, for example, determining when the spindle response to a change in static stimulus had reached a steady state. A description of the instantaneous frequency meter has been published elsewhere (92).

The dynamic input-output properties of the muscle spindle were examined by applying random changes in length to the isolated muscle. The signals used as input to the control unit were obtained from a General Radio Company type 1390-B random noise generator. The output of this unit was passed through a Krohn-Hite Model 330M band-pass filter and recorded on an fm channel of a Precision Instrument PI-6200 tape recorder at 37.5 inches per second. The lower cut-off frequency of the band-pass filter was set at the .2 cps minimum while the upper cut off was set at either 200, 800 or 1500 cps. The signals recorded on the tape were played back at .375 inches per second resulting in random signals with approximately 2, 8 and 15 cps upper frequency limits. The power spectrum of each of the signals was estimated using the methods in Chapter 5. Using these results, filters were constructed to produce from these signals another set of signals with approximately flat power spectra in the range from .04 cps to the upper cutoff frequency.

There were primarily two reasons for the choice of a random dynamic stimulus. The first was that the techniques of spectral analysis, especially cross spectrum analysis, are most reliable if the processes involved have relatively flat spectra. The shape of the power

spectrum of the sensory point discharges will be considered in Chapter 5. Second, a random stimulus is probably physiologically more real than other commonly used stimuli. However, since high frequency stimuli can also be unphysiological, the effect of changing the upper frequency limit of the stimulus had to be investigated. Problems which resemble the phase-locking phenomenon sometimes present with sinusoidal stimuli, were not encountered in any of the experiments. The time course of the length changes applied to the muscle were recorded by a Precision Instrument PI-6200 simultaneously with the muscle spindle discharges. The stimulus was recorded on an fm channel while the discharges were recorded on a direct channel.

4.3 Data Manipulation

The data on the analog tape was analyzed as illustrated in figure 4.2. The role of the Hewlett Packard 2116B computer was to digitize the analog data and convert the resulting binary records into a format that could be easily and quickly read into the memory of the IBM 360/67 computer. The '360 was in turn programmed to perform the required computations and to produce the instructions for the Calcomp plotter unit.

The spindle discharges recorded on the direct channel of the analog tape recorder were preprocessed in one of two ways prior to analog-to-digital conversion. This, in both cases, consisted of reshaping the spikes into narrow square pulses of about 200 μsec in duration and 10 volts in amplitude. These in turn were either used to trigger a bistable multivibrator (flip-flop) or passed through a low-pass electrical filter. The waveform presented to the analog to digital converter was then either a square wave whose state changed with the occurrence of each action potential or a waveform resembling electronic shot noise (93). Preprocessing of the signal representing the changes in the muscle length was confined to a gain adjustment of the waveform so that maximum resolution over the ±1 volt range of the analog to digital converter could be obtained.
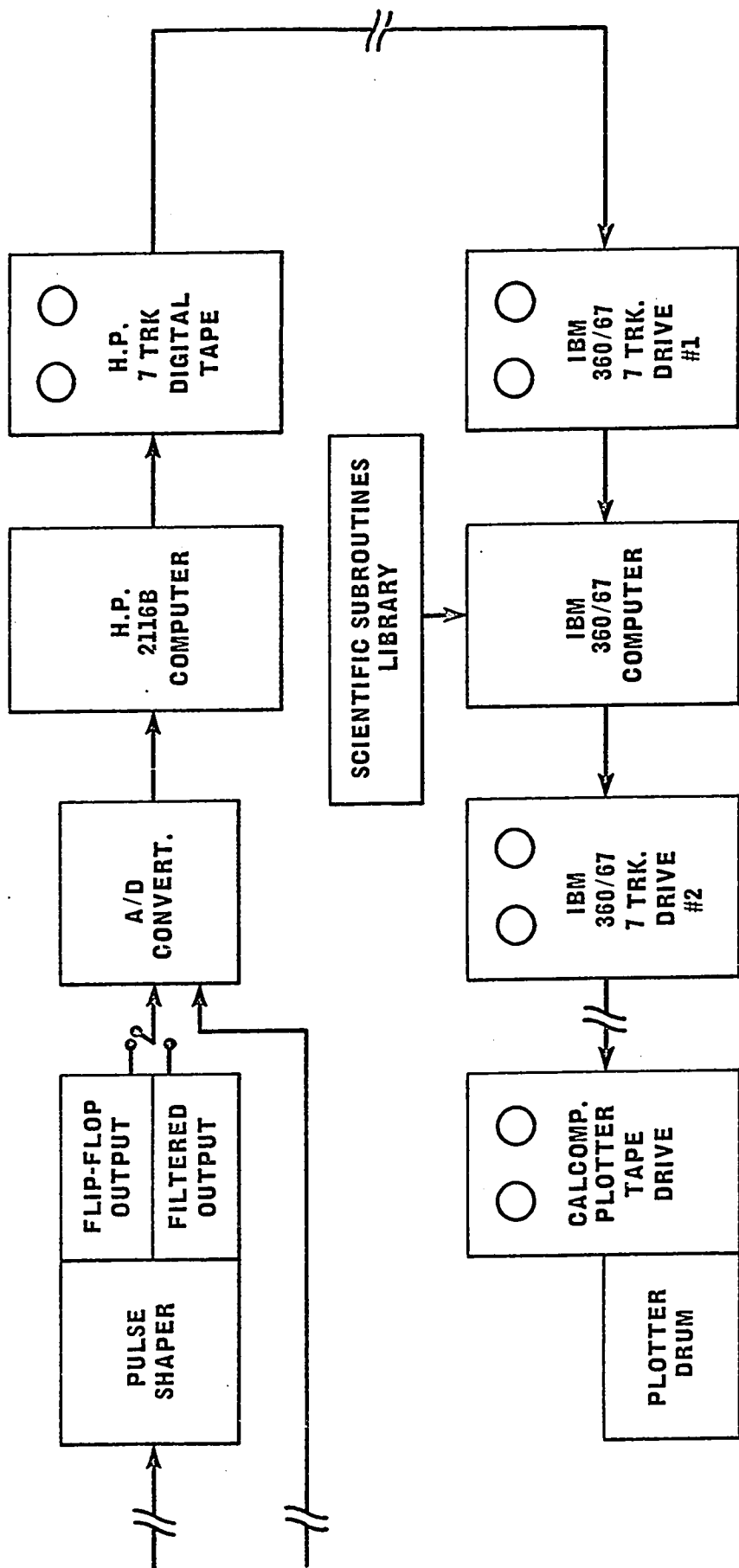
Figure 4.2

DATA ANALYSIS PROCEDURE.

Each analog to digital conversion resulted in the production of a 10 bit binary number. The ±1 volt input range of the converter is therefore quantized into 1024 equal increments. According to Bendat and Piersol (76) the effect of quantization upon the continuous waveform can be considered as an additive rms noise on the original waveform. The results of these authors can be used to show that the additive rms noise due to the 10 bit quantization of the ±1 volt range of the converter amounts to about .3 millivolts rms.

The 2116B computer was programmed to accept binary numbers from the converter at regular intervals until a total of 8192 numbers had been collected. Each number was then converted into 6-level binary coded decimal (BCD) characters and written on a 7-track digital tape. All translations from BCD to the internal code of the '360 were performed by the '360 during the execution of the 'READ' command in the Fortran IV source language.

CHAPTER 5

ANALYTICAL METHODS

5.1 Statistical Techniques

If the flip-flop output of the pulse shaper is sampled regularly, the occurrence of an action potential can be detected by testing for the condition where two consecutive samples are not equal. This procedure was used to obtain the information needed to construct pulse-interval histograms of the spindle responses to static stimulation. The instantaneous frequency meter indicated that under all conditions of static stimulation, the discharge rate of a normal preparation seldom if ever exceeded 50 pulses per second (pps) and always averaged less than 20 pps. The sampling rate for the analysis of interval statistics was chosen to be 200 samples per second. The resultant bin width for the interval histograms was therefore 5 msec which divided the average interpulse interval into at least 10 units and resulted in histograms of useful stability.

The histogram of intervals between successive events (histogram of first-order intervals) was used to estimate the two parameters of the Gamma density

$$p(t) = \frac{\beta^g t^{g-1}}{\Gamma(g)} \, e^{-\beta t} \qquad (5.1)$$

where g and β are the required parameters. $\Gamma(g)$ is the gamma function of g. g is often called the order of the Gamma density. $p(t)$ is the probability density of an interval t. The mean and variance of this density are

$$E\{t\} = \bar{t} = \frac{g}{\beta} \qquad (5.2)$$

and

$$E\{(t-\bar{t})^2\} = \text{Var}\{t\} = \sigma_t^2 = \frac{g}{\beta^2} \qquad (5.3)$$

respectively.

Estimates of β and g can therefore be obtained by using the mean and variance of the intervals. However, Cox and Lewis (94) have shown that only poor estimates of these parameters are obtainable by using the sample mean and variance. This is especially true for low values of g (g<10). Estimates of β and g using the sample mean and variance are called inefficient estimates. Bendat and Piersol (76) define an efficient estimator as that which produces the least mean square error between the parameter itself and its estimator.

The class of maximum likelihood estimates is known to exhibit the minimum variance that can be achieved by any unbiased estimator (79). For large data samples this estimator is approximately unbiased and Normally distributed. The maximum likelihood estimates for β and g are obtained by maximizing the likelihood function for the N observed times between the events with respect to these parameters. The likelihood function is

$$L(t,g,\beta) = \frac{\beta^{Ng} \left(\prod_{i=1}^{N} t_i^{g-1} \right) e^{-\beta \sum_{i=1}^{N} t_i}}{[\Gamma(g)]^n} \tag{5.4}$$

where t_i refers to the ith interval. The results of such an analysis (94) indicate that the maximum likelihood estimator for g is the solution of

$$\log_e(\hat{g}) - \Psi(\hat{g}) = \log_e \hat{\bar{t}} - \frac{\sum_{i=1}^{N} \log_e t_i}{N} \tag{5.5}$$

where $\hat{\bar{t}}$ is the sample mean given by

$$\hat{\bar{t}} = \frac{\sum_{i=1}^{N} t_i}{N} \tag{5.6}$$

$\Psi(\hat{g})$ is the so-called digamma function and is defined as

$$\Psi(\hat{g}) = \frac{d \, \log_e \Gamma(\hat{g})}{d\hat{g}} \tag{5.7}$$

The quantities $\hat{\bar{t}}$ and $\sum\limits_{i=1}^{N} \log_e t_i$ are therefore sufficient statistics for maximum likelihood estimates of β and g. Using these, equation 5.5 was solved iteratively. The initial estimate for $\hat{g}$ was obtained from the sample mean and variance. To evaluate equation 5.7 subroutine DLGAM which calculates $\log_e \Gamma(\hat{g})$ to 16 significant figures was used. The digamma function was obtained by replacing the differential operator $d/d\hat{g}$ in equation 5.7 by the finite difference operator δ where

$$\delta \log_e \Gamma(\hat{g}) = \log_e \Gamma(\hat{g} + \frac{\Delta\hat{g}}{2}) - \log_e \Gamma(\hat{g} - \frac{\Delta\hat{g}}{2}) \tag{5.8}$$

It can be shown (95) that the relationship between the differential operator and the finite difference operator is given by

$$\frac{d}{d\hat{g}} = \frac{2}{\Delta\hat{g}} \sinh^{-1} \frac{\delta}{2} \tag{5.9}$$

where $\Delta\hat{g}$ is an increment in $\hat{g}$. The first few terms of a Taylor's series expansion of the right hand side of equation 5.9 were used for equation 5.7. The maximum likelihood estimate for β was then obtained from

$$\hat{\beta} = \frac{\hat{g}}{\hat{\bar{t}}} \tag{5.10}$$

The Gamma density with the maximum likelihood parameters was scaled to the same area as the first-order interval histogram from which it was estimated and drawn on the same axis.

The characteristic function of a random variable t is defined as

$$\Phi_t(f) = E\{e^{j2\pi ft}\}$$

$$= \int_{-\infty}^{\infty} e^{j2\pi ft} \, p(t) \, dt \qquad\qquad (5.11)$$

If t_1 and t_2 are two independent random variables with a common distribution function then the characteristic function of their sum is by definition (94)

$$\Phi_{t_1+t_2}(f) = \Phi_t^2(f) \qquad\qquad (5.12)$$

The characteristic function of the sum of three or more independent random variables with common distributions follows from equation 5.12. The characteristic function of a Gamma density can be shown to be (94)

$$\Phi_t(f) = \frac{1}{(1-j\frac{2\pi f}{\beta})^g} \qquad\qquad (5.13)$$

The sum of two independent random variables each distributed with identical Gamma densities is therefore also distributed with a Gamma density. It follows from equation 5.12 that the parameters of the sum distribution are β and $2g$. Parameters of the sum of three random variables would be β and $3g$ and so on.

As a test for the independence of successive interpulse intervals, the parameters of the maximum likelihood Gamma function of the first-order spike intervals were modified as required to obtain the density functions which describe the sum of two and three successive intervals (second and third-order intervals) assuming all intervals are independent. These curves, properly scaled as to area, were drawn on the same axis as the second and third-order interval histograms obtained from the data.

It can be shown (96), that the power spectrum of a point process whose intervals exhibit the properties of a random variable, is

given by

$$S_{pp}(f) = \frac{A^2}{\bar{t}} \left[1 + 2\mathrm{Re} \left(\sum_{i=1}^{\infty} \Phi_{\Sigma t_i}(f) \right) \right]$$ (5.14)

where $\Phi_{\Sigma t_i}(f)$ is the characteristic function of the ith order interval.

A is the area or strength of the points in the process. If successive intervals are independent then as a consequence of equation 5.12 (see (96))

$$S_{pp}(f) = \frac{A^2}{\bar{t}} \left[1 + 2\mathrm{Re} \left(\frac{\Phi_t(f)}{1 - \Phi_t(f)} \right) \right]$$ (5.15)

Re represents the real part of the complex quantity in the brackets which follow it. The power spectrum of an independent Gamma process is then

$$S_{pp}(f) = \frac{A^2 \beta}{g} \left[1 + 2\mathrm{Re} \left(\frac{1}{\left[1 - \frac{j 2\pi f}{\beta} \right]^g - 1} \right) \right]$$ (5.16)

This equation was programmed on the computer and values of $S_{pp}(f)$ were calculated at various frequencies for a number of different g. To test the sensitivity of $S_{pp}(f)$ to small changes in the shape and the form of the underlying density function, the power spectrum of a high order Gamma density was compared to that of a Gaussian density both with the same peak and variance. The characteristic function of a Gaussian density is

$$\Phi_t(f) = e^{-\frac{1}{2}\sigma_t(2\pi f)^2 + j\bar{t} 2\pi f}$$ (5.17)

where $\bar{t}$ and σ_t^2 are the mean and variance of the intervals respectively.

The power spectrum of the independent point process with this distribution of intervals is

$$S_{pp}(f) = \frac{A^2}{t}\left[1-\text{Re}\left(\frac{e^{\frac{d}{2}}(\cos\frac{b}{2}+j\sin\frac{b}{2})}{\sinh\frac{d}{2}\cos\frac{b}{2}+j\cosh\frac{d}{2}\sin\frac{b}{2}}\right)\right] \qquad (5.18)$$

where $d = -\frac{1}{2}\sigma_t^2(2\pi f)^2$ and $b = \bar{t}2\pi f$.

The serial correlation coefficient between successive intervals is defined as

$$\rho_h = \frac{E\{(t_i-\bar{t})(t_{i+h}-\bar{t})\}}{\sigma_t^2} \qquad (5.19)$$

where ρ_h, $h=0,1,2,\ldots$ is the serial correlation between intervals separated by h events. If the intervals are drawn independently from a common distribution then the expected value of all the coefficients is zero. Since serial correlation coefficients are one of the most powerful tests for the serial independence of intervals and also one of the easiest to implement, the results of such an analysis on the spindle discharges have been included. Estimation of ρ_h requires that $\bar{t}$ and σ_t^2 be estimated from the sample data. To avoid the bias introduced by the use of the sample mean and variance, the formulas suggested by Cox and Lewis (94) were used. These formulas are repeated here. The estimator of ρ_h is given by

$$\hat{\rho}_h = \frac{\hat{C}_h}{(\hat{C}'_h \hat{C}''_h)^{\frac{1}{2}}} \qquad (5.20)$$

where

$$\hat{C}_h = \frac{1}{N-h}\sum_{i=1}^{n-h} t_i t_{i+h} \quad - \hat{T}'_h \hat{T}''_h \qquad (5.21)$$

where

$$\hat{T}'_h = \frac{1}{N-h} \sum_{i=1}^{N-h} t_i \qquad \hat{T}''_h = \frac{1}{N-h} \sum_{i=1}^{N-h} t_{i+h} \qquad (5.22)$$

and

$$\hat{C}'_h = \frac{1}{N-h} \sum_{i=1}^{N-h} (t_i - \hat{T}'_h)^2 \qquad \hat{C}''_h = \frac{1}{N-h} \sum_{i=1}^{N-h} (t_{i+h} - \hat{T}''_j)^2 \qquad (5.23)$$

For N large and $\rho_h = 0$, $\hat{\rho}_h / (N-1)^{\frac{1}{2}}$ has an approximately unit Normal distribution. Therefore, the hypothesis of independence can be rejected at the α level if

$$|\hat{\rho}_h| > \frac{m\{1-\frac{\alpha}{2}\}}{(N-1)^{\frac{1}{2}}} \qquad (5.24)$$

where $m\{1-\frac{\alpha}{2}\}$ is the 1-α/2 point on the cumulative normal distribution. To reduce the possibilities of obtaining false positive serial correlations that result from long-term trends or nonstationarities in the process (2), the data was always divided into a number of segments. The first twenty serial correlation coefficients were calculated using equations 5.20 to 5.23 for each segment. The final estimate for the twenty coefficients was obtained by averaging the contributions from each segment.

5.2 Sampling the Point Process

If the spindle discharges are treated as a series of point events (Dirac delta functions) the sample Fourier transform of the data is given by

$$X_T(f) = \int_0^T \sum_{i=1}^N \delta(t-t_i) \, e^{-j2\pi ft} \, dt$$

$$= \sum_{i=1}^N \left(\cos 2\pi ft_i - j \sin 2\pi ft_i \right) \qquad (5.25)$$

where $\delta(t-t_i)$ is a Dirac delta function at $t=t_i$. When treated this way the estimation of the power spectrum of nerve spikes is extremely well suited to digital computer evaluation since only the summation of cosine and sine terms at the instants in time at which the spikes occur is required. Knox (97) has used this method to obtain estimates of the power spectrum of the discharges from receptors in the statocyst organ of the lobster. A serious shortcoming of this method is apparent from the behavior of $X_T(f)$ at $f=0$. $X_T(f)$ at this point is a spike of amplitude N, the number of action potentials in the sample data. Since $X_T(0)$ stands far above $X_T(f)$ for $f \neq 0$, leakage through the spectral window will introduce considerable bias into the estimates of the power spectrum near zero frequency.

If the method used to detect the occurrence of events is by regularly sampling the flip-flop output of the pulse shaper in figure 4.2, it is necessary that the sampling rate be much higher than the maximum frequency component of interest. The errors resulting in a sampling rate that is too low would probably be somewhat similar to the quantization error which results when a continuous waveform is sampled with too few bits available for the conversion.

It is a well known result, that if a continuous waveform is sampled regularily at a rate which is at least twice as fast as the highest frequency component in that waveform, then the sampled version of the continuous waveform contains an undistorted copy of the power spectrum of the original waveform (75,98). If the signal contains components higher than half the sampling frequency a so-called aliasing of frequencies occurs. In this case, the signal must be sampled at a higher rate or, the undesirable components removed before sampling by filtering. Half the sampling frequency is called the Nyquist or folding frequency. Aliasing of frequencies refers to the phenomenon whereby power in a

waveform above the folding frequency masquerades as power at frequencies
below the folding frequency. The general rule for the aliasing of
frequencies has been given by Bendat and Piersol (76). For any frequency
f in the range $0 \leq f \leq f_c$, where f_c is the Nyquist frequency, the higher
frequencies which are aliased with f are defined by the infinite series

$$(2f_c \pm f), \quad (4f_c \pm f), \quad (6f_c \pm f), \quad \dots \qquad (5.26)$$

Once a signal is sampled, nothing short of resampling after either
filtering the signal or increasing the sampling rate can possibly remove
any aliasing which may have occurred.

The estimates of the various spectra which involved the point
discharges of the spindle were obtained, with one exception, by filtering
the shaped discharges. Equation 5.25 was applied in one instance by
sampling the flip-flop output of the pulse shaper at a rate much higher
than the highest frequency of interest. In all other cases, the shaped
pulses were passed through a low-pass filter. The filter was designed
so that after estimating the spectrum of the filtered pulses, the effect
of the filter could be removed from the estimates up to 80% of the folding
frequency with negligible error due to aliasing. Filtering the pulses
has the effect of converting the point process into a continuous waveform
so that all the ideas of chapter 3 are directly applicable. Nelsen (96)
has shown that if the interevent intervals of a point process are drawn
independently from a common density function, then, if this density function
is bounded, the power spectrum of the process tends to a constant value
with increasing frequency. There is evidence that interspike intervals
from amphibian muscle spindles are independent (54,72) and that the
underlying density function is bounded (54,71). Work with equations
5.16 and 5.18 (see chapter 5) which are based on these assumptions, has
shown that the power spectrum of a point process with about as much
variability as the discharges from an amphibian muscle spindle is flat in
the region of the spectrum above the mean discharge frequency. The sampling
rate for spectral estimates was chosen at 100 samples per second. The
power spectrum of the sensory discharges was assumed to be flat in the

region above the folding frequency of 50 cps since the average discharge
rate was always well below this. Also, no stimulus was applied to the
spindle which contained any significant power above 30 cps. Therefore,
because of the filter, reliable estimates of the various spectra could
be obtained to about 40 cps. The band of frequencies topped by 40 cps
seemed a physiologically relevant choice.

Consideration of the bias in the estimates of the various
spectra seemed to indicate that the filter characteristic in the passband
should be reasonably flat and should not introduce excessive phase lags
between the input to, and the measured output from, the spindle. The
filter used had the following magnitude and phase characteristics
respectively.

$$M(f) = \frac{1}{1+\left(\frac{f}{21}\right)^4} \qquad (5.27)$$

and

$$P(f) = -\tan^{-1}\left[\frac{\frac{\sqrt{2}f}{21}}{1-\left(\frac{f}{21}\right)^2}\right] \qquad (5.28)$$

The circuit diagram of this filter is given in appendix 3. If the power
spectrum of the unfiltered spikes is $S_{pp}(f)$ then the power present in
the signal after filtering will be given by

$$S_{xx}(f) = \left[\frac{1}{1+\left(\frac{f}{21}\right)^4}\right]^2 S_{pp}(f) \qquad (5.29)$$

using equation 3.7. If the power in $S_{pp}(f)$ at 40 and 60 cps was approxi-
mately the same, then the power in $S_{xx}(f)$ at 60 cps would be down to
less than 2.5% of that at 40 cps. At 70 cps it would be down to less
than .2% of that at 30 cps. Since 50 cps is the folding frequency, the
aliased power in $S_{xx}(f)$ at 40 cps from 60 cps and higher frequencies

would be about 2.5%. At 30 cps aliased power would be less than .2%. Therefore, assuming that $S_{pp}(f)$ is reasonably constant above 50 cps, and this can be established by plotting $S_{xx}(f)$, estimates of $S_{pp}(f)$ can be obtained up to at least 40 cps with little error due to aliasing. Estimates of $S_{pp}(f)$ from $S_{xx}(f)$ are obtained using equation 5.29.

5.3 Methods of Spectral Estimation

Spectral estimates were obtained using the direct approach and the Fast Fourier Transform subroutine PS301A (91). The method was that suggested by Welch (83), slightly modified. The data, both single and double channel (spindle under static and dynamic stimulus respectively), was sampled 100 times per second. Exactly 163.84 seconds of data were used for each analysis. Since the HP2116B, as programmed, had capacity for 8192 data points, power spectrum data was stored on the digital tape in two blocks of 81.92 seconds each. Data for cross-spectral estimates was stored in four blocks of 40.96 seconds each. Welch (83) suggests that in order to obtain a near maximum reduction in the variance of spectral estimates from a fixed amount of data, the data segments from which the sample spectra are obtained should be overlapped to about one-half their length. This suggestion was followed. The data was divided into segments of 1024 data points. Sample spectra were obtained from points 1 to 1024, points 512 to 1536, 1024 to 2048 and so on until all points in the data block were exhausted. The procedure was repeated for all blocks and the spectral estimator obtained by averaging the contributions from all the sample spectra (See equations 3.34, 3.35 and 3.43). The power-spectrum estimator was therefore the result of averaging 30 sample power spectra while the cross-spectrum estimator was the result of averaging 28 sample cross-spectra.

Welch (83) has shown that the variance of the power-spectrum estimator described in the preceding paragraph is

$$\text{Var}\{\hat{S}_{xx}(f)\} = \frac{S_{xx}^2(f)}{K} \left[1+2 \sum_{i=1}^{K-1} \frac{K-i}{K} \xi(i) \right] \qquad (5.30)$$

where

$$\xi(i) = \frac{\left[\sum_{h=1}^{L} w(h) \, w(h+iD)\right]^2}{\left[\sum_{h=1}^{L} w^2(h)\right]^2}$$

(5.31)

K is the number of data segments in the estimate, L is the number of points in each segment and D is the number of points between the starting points of the segments. For the power spectrum estimator used in this thesis K=30, L=1024 and D=512. $w(h)$ is the data window. It is of interest to note that if $D \geq L$, $\xi(i)=0$ for all i and hence $\text{Var}\{\hat{S}_{xx}(f)\}$ does not depend upon the shape of the data window. Sloane (81) has shown however, that windowing the data does result in a loss of spectral resolution.

If the data segments are overlapped, the shape of the data window does effect the variance of the estimator. It can be shown, using equations 5.30 and 5.31, that overlapping the data segments by half their length with a rectangular data window results in a variance reduction to 75% of that if the segments are not overlapped. If the Hanning data window is used then 50% overlap of the data segments results in a reduction in variance to about 55% of that when the segments are not overlapped and the rectangular data window is used. All spectral estimates in this work were obtained using the Hanning data window. Therefore, using equations 3.41, 5.30 and 5.31 it can be shown that the power-spectrum estimator had 56 degrees of freedom while the cross-spectrum estimator had 52 degrees of freedom. Confidence bands for estimates of the power spectrum, gain and phase functions and the squared coherency spectrum were thus obtained using equations 3.42, 3.51, 3.52 and 3.58 respectively. The statistical tables given by Bendat and Piersol (76) were used. Gain and phase estimators were corrected for the presence of the spike filter by using equation 3.6.

It can be shown (81) that the spectral window resulting from the Hanning data window is given by

$$W(f) = \left[\frac{\sin \frac{\pi f L}{2} \; \cos \frac{\pi f L}{2}}{\frac{\pi f L}{2}} \cdot \frac{\left(\frac{2\pi}{L}\right)^2}{\left(\frac{2\pi}{L}\right)^2 - (2\pi f)^2} \right]^2 \tag{5.32}$$

This equation is shown plotted in figure 5.1 with a normalized amplitude of one. Leakage problems were all but eliminated from the estimates by this spectral window.

5.4 Plotting the Results

The Fast Fourier Transform of 1024 data points results in 1024 Fourier coefficients. These coefficients sample the frequency space from zero frequency up to the sampling frequency in steps of 1/10.24 cps. All estimators were plotted on a logarithmic frequency scale. This transformation of the frequency scale resulted in points that were widely separated at the low frequency end and highly clustered toward the high frequency end. To improve the low frequency resolution all plots shown in the results were obtained by padding the data segments out to 2048 points with 1024 zeros before Fourier transformation. This procedure, suggested by Bergland (85), increased spectral resolution to 1/20.48 cps or to about .05 cps and improved considerably the appearance of the estimators at low frequencies. Power spectrum and gain function estimates were plotted in decibels (db) while phase function estimates were plotted in degrees.

Of the 2048 points which resulted from each analysis for each estimator, only the first 800 were required to span the region of interest from .05 to 40 cps. The plotting function as written required three arguments: the abscissa dimension, the ordinate dimension and the minimum distance between the plotted points. A fourth argument required for cross-spectrum analysis was the maximum frequency of interest. This was necessary since, for example, coherency studies are meaningless at frequencies outside the bandwidth of the applied input. Before plotting points, all data was scaled to the abscissa and ordinate dimensions supplied. Points were plotted starting from the low frequency end. No point was plotted which fell closer to the previously plotted point
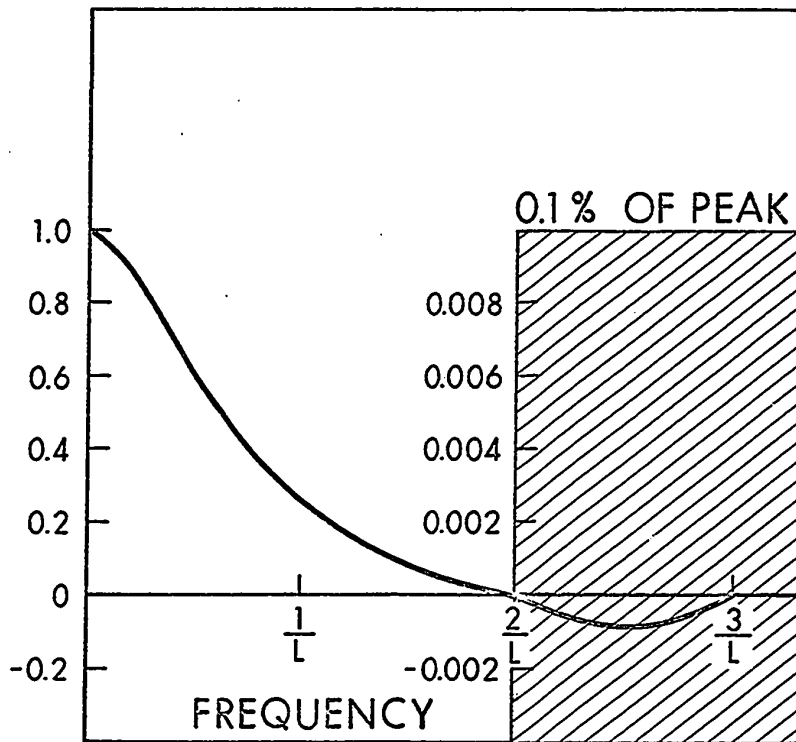
Figure 5.1

SPECTRAL EQUIVALENT OF THE HANNING DATA WINDOW.

than the minimum distance parameter. This point was instead averaged with succeeding points until the logarithmic mean of the abscissae of the first and last point averaged exceeded the minimum distance parameter. All 800 points were used in this way. Because of the logarithmic frequency scale, averaging became more and more prevalent as the plotting progressed. The result of this was that the statistical confidence in the plotted points was increased as more and more averaging was required.

The width of the spectral window shown in figure 5.1 is not changed by padding the data segments with zeros (85). Therefore averaging two adjacent points does not halve the variance of the new estimator since the average was formed using nonindependent constituents. It is not until 5 adjacent points are averaged that two independent points are combined. Therefore, when plotting confidence bands around the various estimators, the number of degrees of freedom associated with a particular plotted point was increased by the base value (56 for power spectra, 52 for cross spectra) each time the number of averaged points reached a multiple of 5.

Appendix 4 contains a copy of the Fortran IV source program used to perform the cross-spectral analysis. The program instructed the computer to read two channel data from the 7 track tape, to calculate estimates of the squared coherency spectrum and the gain and phase functions together with their respective confidence bands, and to plot the results.

CHAPTER 6

RESULTS

6.1 Static Behavior

The results reported in this chapter were obtained from three separate muscle spindles. The responses of these however, were representative of all the normally functioning preparations examined. The instantaneous frequency of the discharges from a single muscle spindle under conditions of static stimulus is shown in figure 6.1A. Recordings of the discharges from this particular spindle were obtained at various steady lengths which ranged from about 1.5 mm less than the resting length of the muscle _in vivo_ (L_o) to the point of fracture about 1.3 mm greater than L_o. L_o for this muscle was 23 mm. After changing the static stimulus, data was recorded only when the instantaneous frequency of the discharges had apparently reached a steady state. The occurrence of an action potential was detected by sampling the flip-flop output of the pulse shaper 200 times per second. Some results from the subsequent analysis are shown in table 6.1. The sample means calculated in table 6.1 were not biased by the spike detection technique. On the other hand, the sample variances were biased positively by about 8 $msec^2$. This bias has been removed from the sample standard deviations and the sample coefficients of variation given in table 6.1.

Muscle Length	No. of Intervals	Mean Interval	Interval Variance	Standard Deviation	Coef. of Variation
L_o-1.5mm	2473	66 msec	420 $msec^2$	20.3 msec	.31
L_o	2529	65	357	18.7	.29
L_o+0.2mm	2326	70	538	23.0	.33
L_o+0.4mm	2370	69	443	20.8	.30
L_o+0.6mm	2376	69	464	21.3	.31
L_o+1.0mm	2686	60	313	17.5	.29
L_o+1.1mm	2796	58	285	16.6	.29

Table 6.1. Some Statistics of the Static Response

A   C

300 μm

60
40
20
0

60
40
20
0

B   D

300 μm

60
40
20
0

60
40
20
0
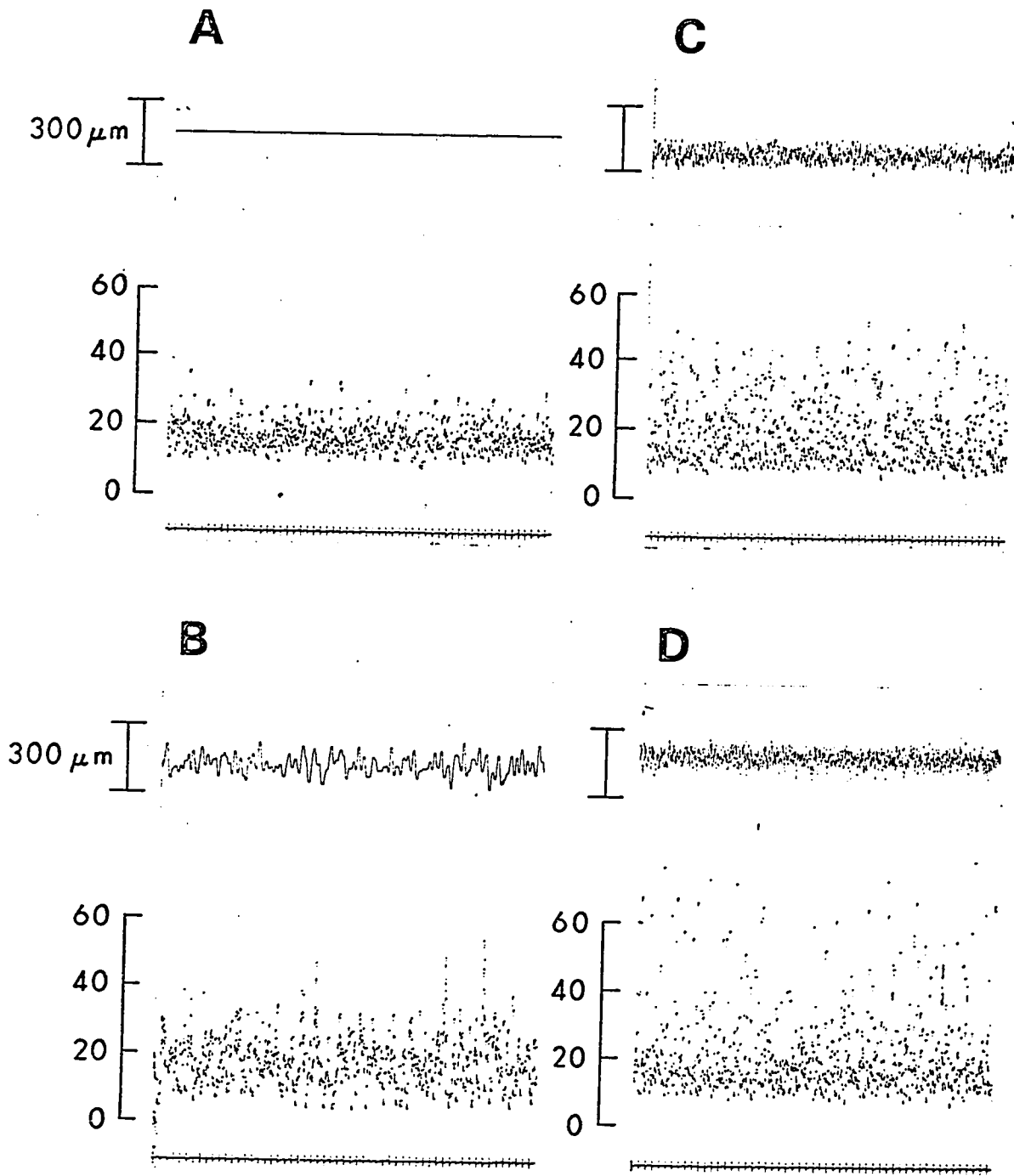
1 sec/mm

Figure 6.1

INSTANTANEOUS FREQUENCY OF THE DISCHARGES FROM A DE-EFFERENTED AMPHIBIAN

MUSCLE SPINDLE IN RESPONSE TO STATIC AND RANDOM DYNAMIC LENGTH STIMULI.

Table 6.1 shows that the spindle responded to a static stimulus only slightly. It is not until the muscle was stretched to near the point of fracture that any significant changes are noticable in the response. The variability in the intervals, defined as the ratio of the standard deviation to the mean (coefficient of variation),was largely indifferent to the static stimulus. These results are in agreement with those of Buller et al. (54) in as much as for a 70 msec mean interval from the frog muscle spindle they obtained a standard deviation of 19 msec.

First, second, and third order spike interval histograms at a muscle length of $L_o+0.2$mm (table 6.1) are shown in figure 6.2. The first order interval histogram was fitted with the maximum likelihood Gamma density curve estimated from the data. The second and third order histograms were fitted with Gamma density curves whose parameters were obtained from the first order curve by assuming that all intervals were statistically independent. The data was fitted extremely well by the Gamma curves and therefore supports earlier findings related to both the distribution of, and the dependence between, spindle interspike intervals (54,71,72). The maximum likelihood estimates for the parameters of a number of Gamma densities obtained from the spindle intervals under different static stimuli are compared in table 6.2 with the estimates of these parameters obtained from the sample mean and variance. The bias was removed from the sample variance before calculating the parameters.

No. of Intervals	Maximum Likelihood $\hat{g}$	$\hat{\beta}$	Sample $\bar{\hat{t}}$ and $\hat{\sigma}_t^2$ $\hat{g}$	$\hat{\beta}$
733	3.2	.014	2.5	.011
2472	10.4	.16	10.6	.16
2326	9.5	.14	9.2	.13
2787	12.5	.22	12.2	.21

Table 6.2. Estimates of g and β.

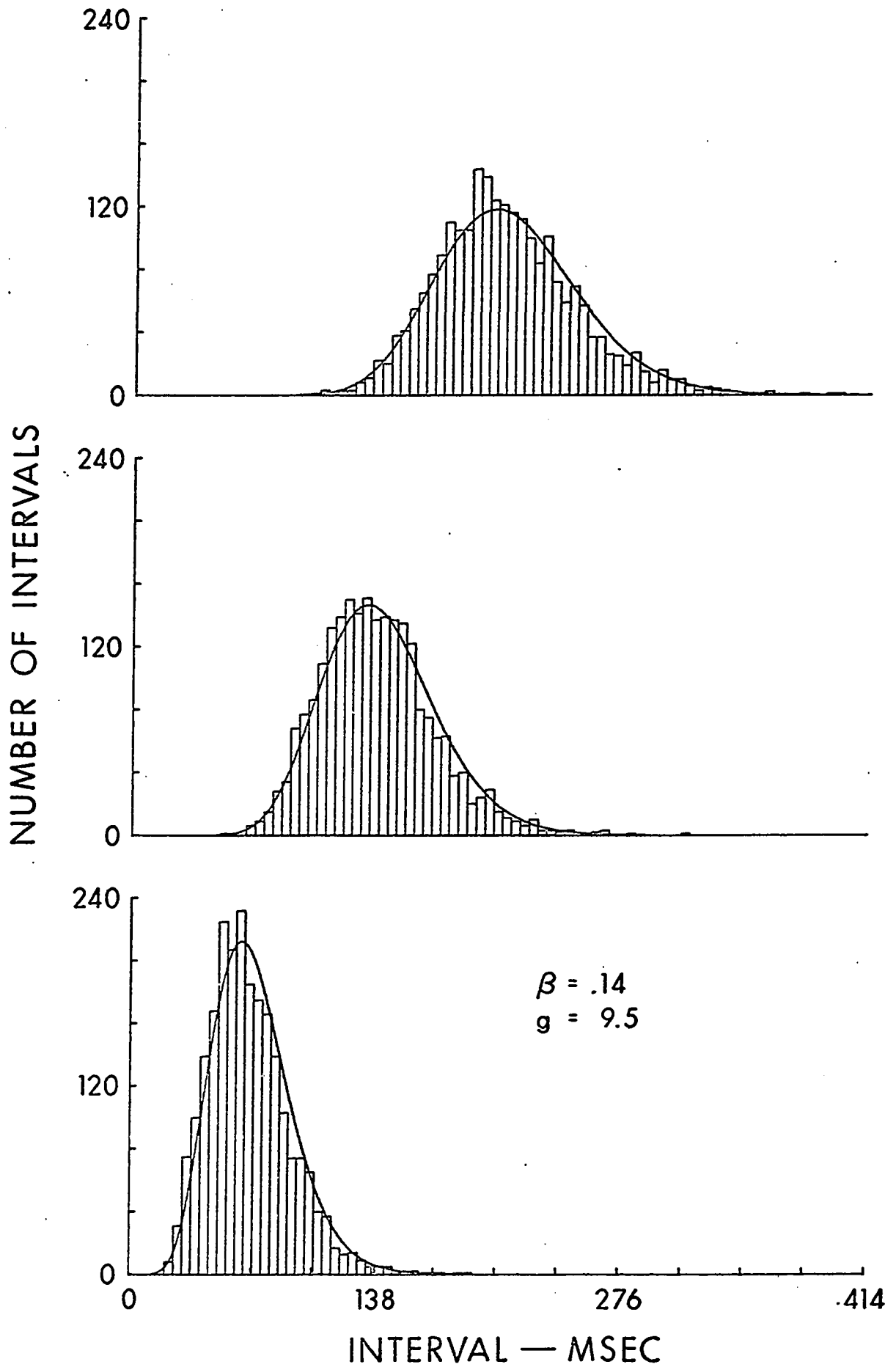If the premise that interspike intervals were independent

Figure 6.2

DISTRIBUTION OF INTERVALS DURING STATIC LENGTH STIMULATION.

and distributed with a Gamma density is accepted, then the power spectrum of the point sensory process can be calculated by using equation 5.16. The results of such a calculation are shown in figure 6.3 for Gamma densities of various orders. In this figure $\omega = 2\pi f$. All of the curves are normalized to the same high frequency value to enable comparison. The Poisson process, with its exponential distribution of intervals, corresponds to a Gamma density of order 1 and has a flat power spectrum at all frequencies. As the order of the Gamma density is increased from 1, the spectrum contains less and less power at low frequencies. The transition between the very low frequency power and the high frequency power is much more abrupt and tends to occur at lower frequencies as the order of the density is increased.

Estimates of the power spectrum of the spindle discharges were obtained initially in two ways. The first was as described in section 5.3, that is by filtering the shaped pulses, applying a Hanning data window to the data segments from which the mean had been removed, and finally, averaging the sample spectra obtained from the modified segments. The results of such an analysis on a statically-stimulated spindle are shown in figure 6.4A. The 95% confidence band for the estimate is also shown. Figure 6.4B shows an estimate of the power spectrum of the same data obtained by sampling the flip-flop output of the pulse shaper 200 times per second. The continuous Fourier transform of each data segment was obtained using equation 5.25. Figure 6.4B is an excellent demonstration of distortion at the low frequency end of the spectrum due to leakage from the spike in the spectrum at zero frequency. If the distortion due to leakage is temporarily ignored, both figures 6.4A and 6.4B indicate a relatively flat low frequency spectrum with an increase of about 5db occurring in the power between 1 and 10 cps. This similarity is considered token proof of the validity of the impulse filtering method of spectral estimation outlined in section 5.2.

Figure 6.5 shows the estimate of the power spectrum of the data used in figure 6.2. The estimated spectrum is fairly flat in the region less than about 2 cps but increases by between 10 and 15 db from there to 10 cps. The maximum likelihood Gamma parameters for the first
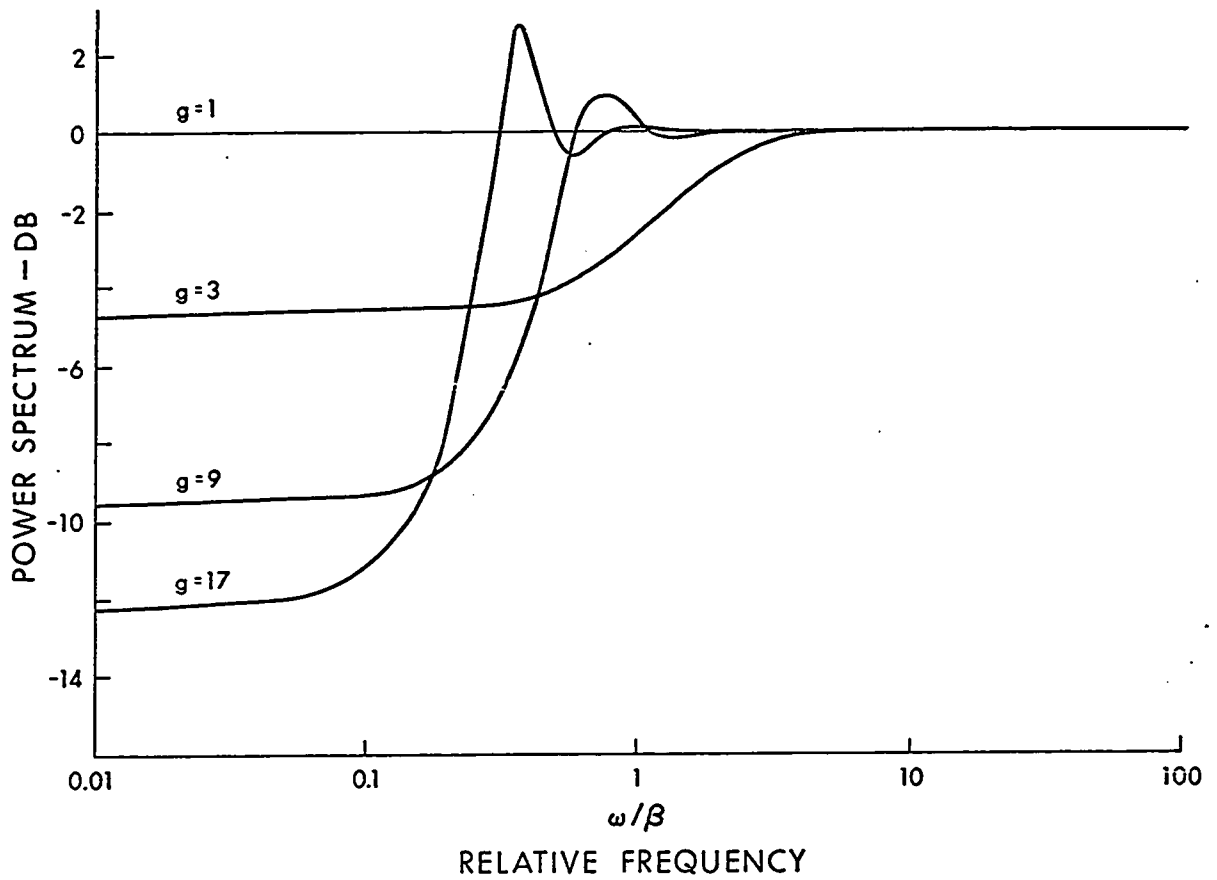
Figure 6.3

THEORETICAL POWER SPECTRA OF POINT PROCESSES WITH INTERVALS

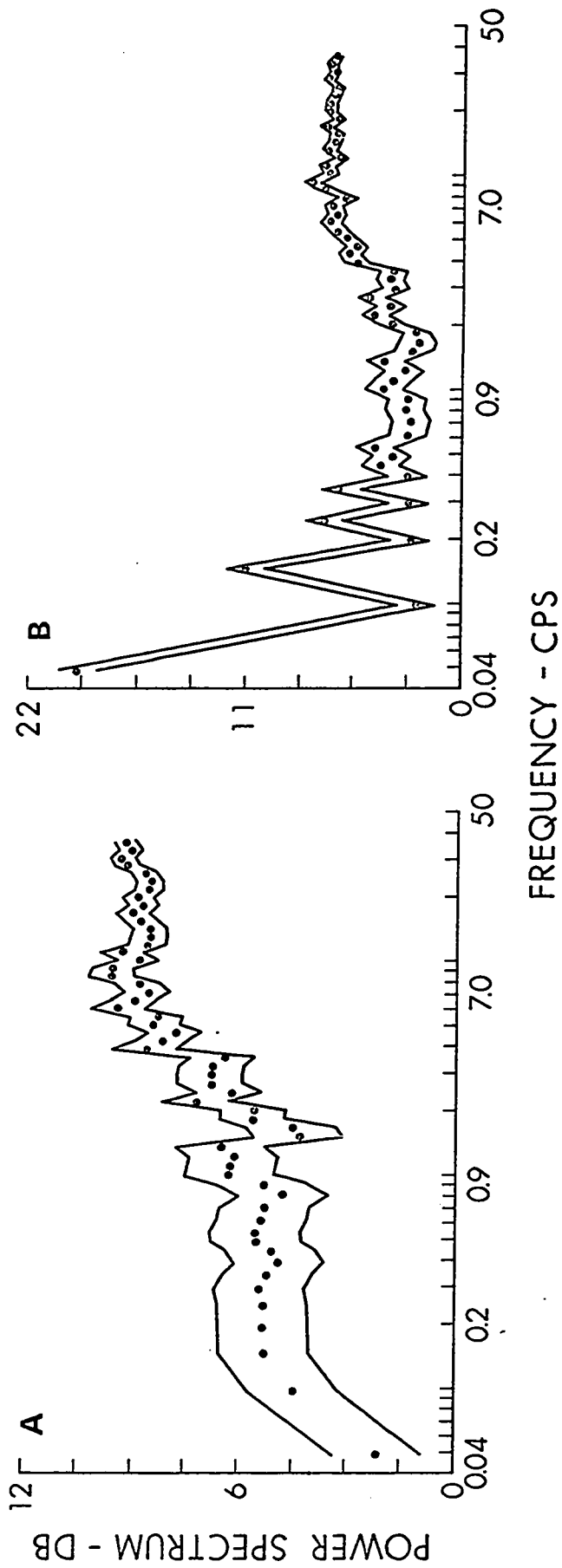DESCRIBED BY GAMMA DENSITIES OF VARIOUS ORDERS.

Figure 6.4

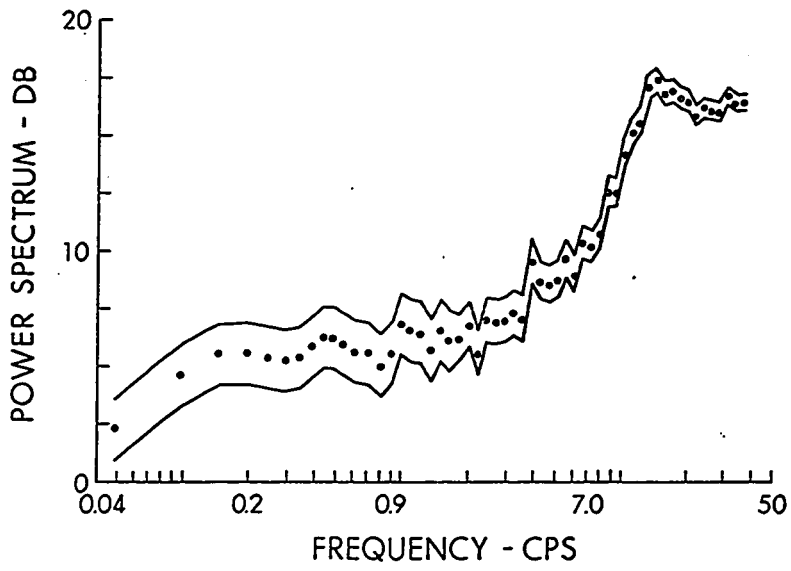ESTIMATES OF THE POWER SPECTRUM OF A POINT PROCESS.

Figure 6.5

ESTIMATE OF THE POWER SPECTRUM OF THE POINT PROCESS

IN FIGURE 6.2.

order intervals in figure 6.2 are $\hat{g}$ = 9.5 and $\hat{\beta}$ = .14 (msec)$^{-1}$. Figure
6.3 indicates that the power spectrum of a Gamma density of order 9
undergoes a change of slightly less than 10 db. In this respect, the
theoretical and experimental results agree. Also, figure 6.3 shows that
the transition from low-frequency power to high-frequency power for
g = 9 is all but complete at ω = β. This means that the experimental
spectrum should have reached its high frequency value by about 22 cps.
This is in agreement with figure 6.5

Equation 5.15 shows that the power spectrum of an independent
point process is related only to the distribution function which describes
the first-order intervals. To test the sensitivity of the power spectrum
of an independent point process to slight changes in the form of the
underlying density function, the theoretical spectrum of a point process
whose intervals are distributed as a Gaussian random variable was compared
with the spectrum of the Gamma density of figure 6.2 The Gaussian
density function was chosen to have the same peak and variance as the
Gamma density. The two density functions are shown in figure 6.6. Figure
6.7 shows the respective spectra each normalized to the same high frequency
value. This figure shows that the power spectrum of an independent
point process is not particularly sensitive to slight variations in the
shape and the form of the underlying density function. Therefore, the
agreement between the theoretical and the estimated spectra is apparently
not heavily dependent upon the choice of density function.

Figure 6.8 shows the first nine serial correlation coefficients
between interspike intervals from the spindle in table 6.1. The left
side of figure 6.8 was obtained from the intervals in figure 6.2 (L_o+0.2mm)
while the right side was obtained at a longer muscle length (L_o+1.1mm).
Formulas 5.20 to 5.23 were used with segmented data to obtain the results
in figure 6.8. It can be shown that the spike detection technique will
result in a slight negative serial correlation between adjacent intervals
even if the interspike intervals are statistically independent. This
bias in the first serial correlation coefficient amounts to about .004
in the left side of figure 6.8 and about .007 in the right side. To
test the independence hypothesis, 75, 95, and 99% confidence bands for
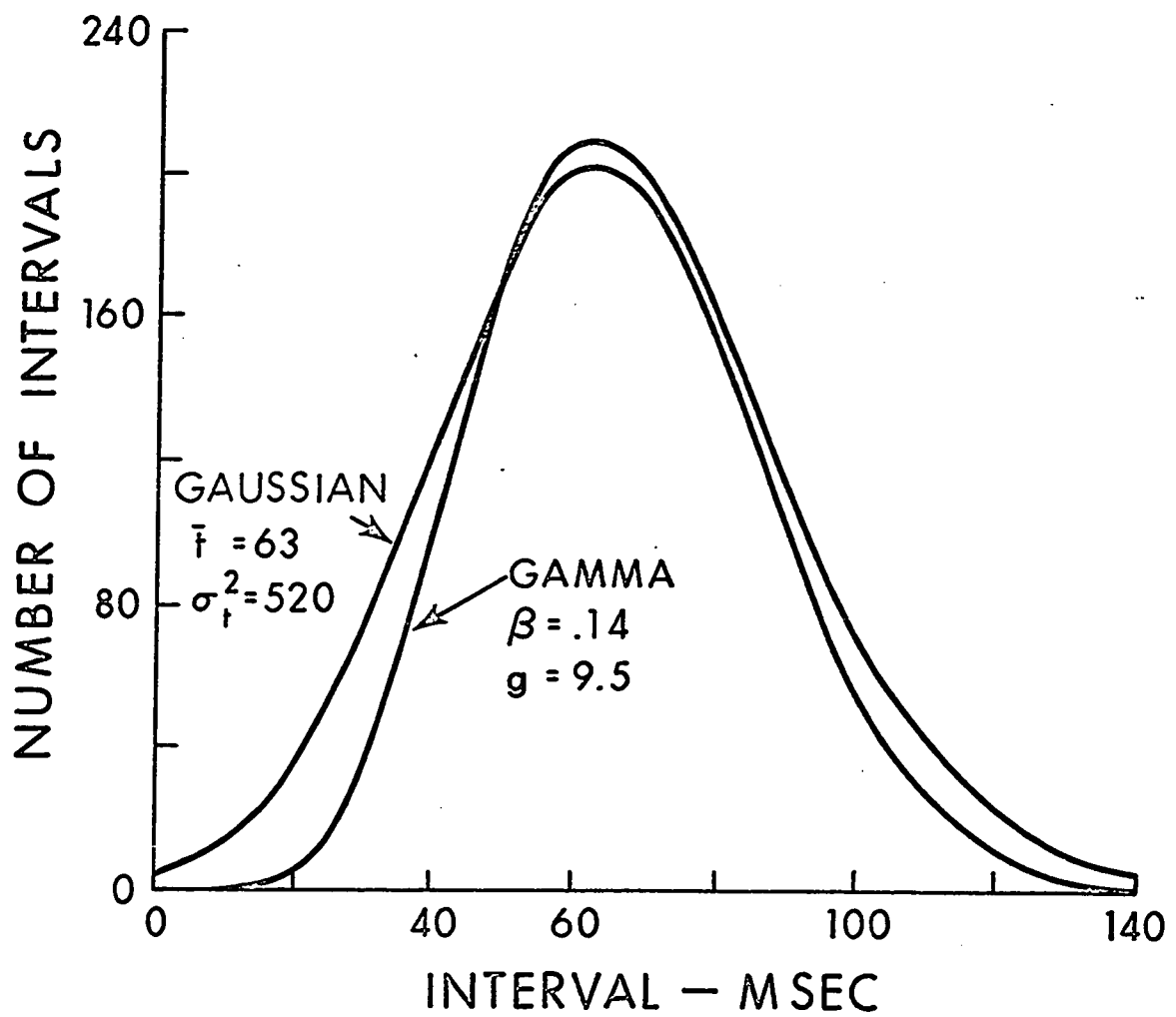
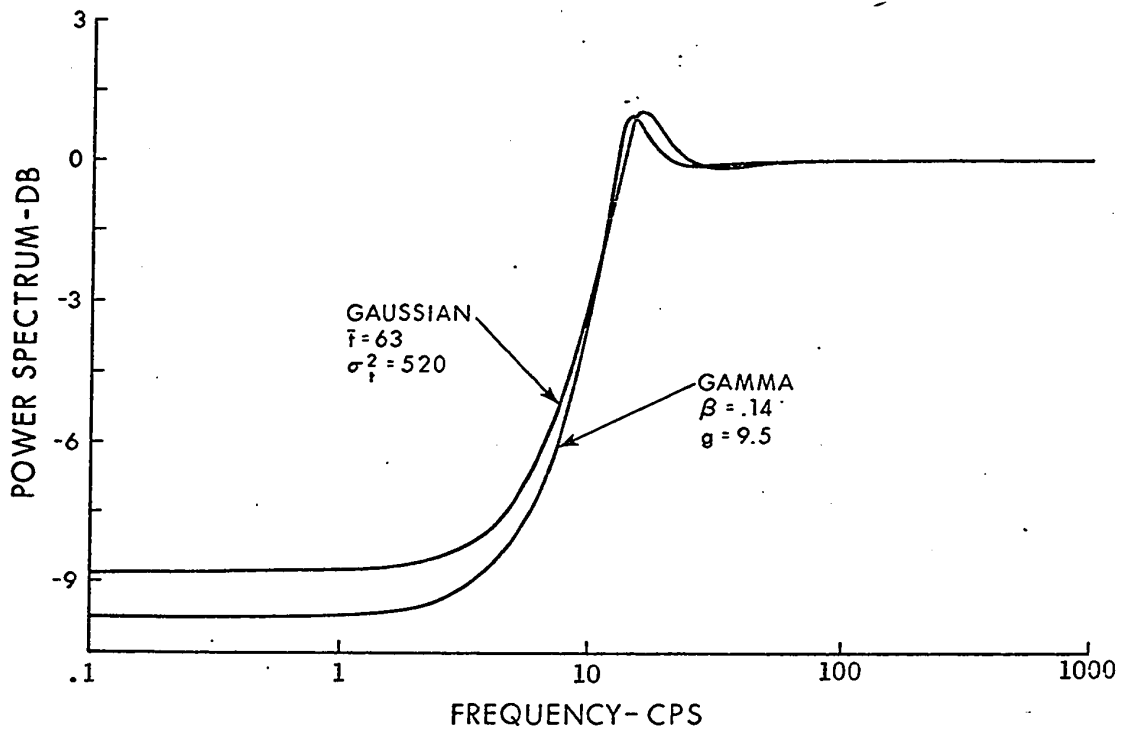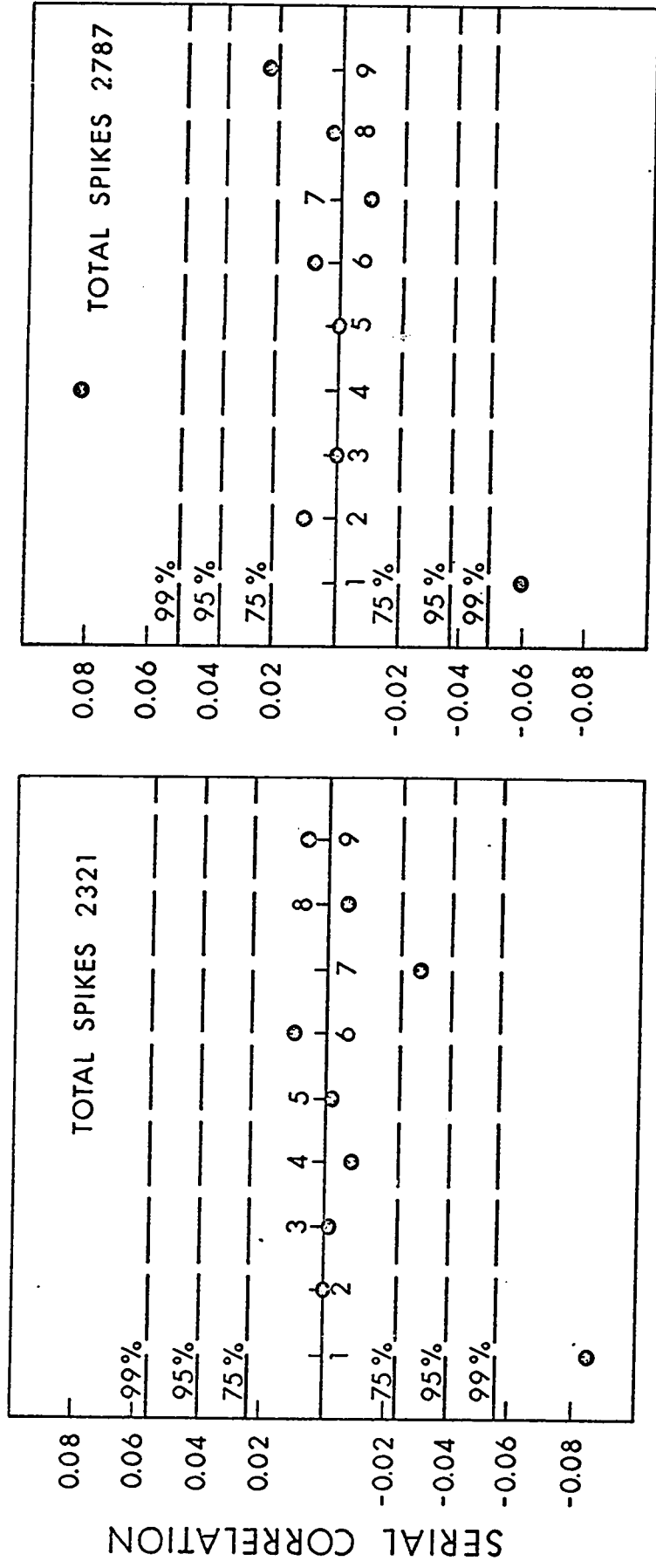Figure 6.6

THE GAUSSIAN AND GAMMA DENSITY FUNCTIONS.

Figure 6.7

THE THEORETICAL POWER SPECTRA OF POINT PROCESSES WITH INTERVALS

DESCRIBED BY THE DENSITY FUNCTIONS IN FIGURE 6.6.

LAG NUMBER

Figure 6.8

ESTIMATES OF THE SERIAL CORRELATION BETWEEN SPINDLE INTERSPIKE INTERVALS.

independent intervals were calculated from equation 5.24. In spite of the bias introduced by the detection technique, it is statistically 99% certain that adjacent intervals were negatively correlated. That is, an interval of less than the mean length tended to be followed by one that was greater than the mean and vice versa. This tendency to oscillate about the mean is apparently not of sufficient strength to result in significant contributions to the estimated power spectrum of the process. The large positive value of the fourth coefficient in the right side of figure 6.8 is likely due to statistical fluctuations in the estimator since it is not present in the left side of the figure. It is to be expected that for purely statistical reasons, about one in a hundred of the coefficients will be outside the 99% confidence region. The obvious weakness of the serial dependence between adjacent intervals coupled with much shorter data samples probably accounts for the earlier results concerning the independence of spindle interspike intervals (54,72). That neighbouring intervals are correlated might be expected from what is known about the initiation and conduction of action potentials in nerve fibers.

The power spectrum of a point process is apparently not exceptionally sensitive to serial correlation between the intervals. In a sense, use of the power spectrum to test for serial correlation between intervals is much like the test applied in figure 6.2. That is, both tests are rather qualitative in that any serial dependencies would probably become obvious only when a strong correlation exists. In addition, neither test would provide any information concerning the nature of any obvious correlation. But unlike the serial correlation coefficient, the power spectrum would probably maintain its sensitivity to serial dependence in the presence of trends that are long compared to the mean interval. These trends or nonstationarities appear as very low frequency components in the power spectrum. Since leakage between frequency bands during power spectrum estimation can be effectively controlled (see figure 5.2), the effects of the nonstationarities can be easily confined to the appropriate portions of the spectrum.

6.2 Dynamic Behavior

The effect upon the instantaneous frequency of spindle discharges of three different dynamic stimuli is shown in figures 6.1B, C,D. Each of the stimuli is a random signal and each has a different upper cutoff frequency. Estimates of the power spectrum of each of the signals, enclosed in 95% confidence intervals, are shown in figure 6.9. The signal described by figure 6.9A which shows a relatively flat spectrum up to about 2cps will be referred to as input A; the signal in figure 6.9B with a relatively flat spectrum to about 8 cps as input B and figure 6.9C with a flat spectrum to about 15 cps as input C. Figures 6.1, B,C,D which show the spindle responses to inputs A,B and C respectively, indicate that increasing the upper cutoff frequency of the dynamic stimulus resulted in discharges of higher instantaneous frequency.

Figure 6.10 shows estimates of the power spectrum of the spindle response to the three inputs at three different lengths. The steady state spectral estimates are included for comparison. All confidence intervals for this and succeeding figures are shown at the 95% level. The preparation in figure 6.10 is that described during static stimulation by table 6.1. The top row in figure 6.10 was obtained from the spindle at a static stimulus of $L_o-1.5$mm, the second row at $L_o+0.4$mm and the third row at $L_o+1.0$mm where L_o was about 23mm. The amplitude of all the inputs was about 45µm rms throughout. Columns 2,3 and 4 correspond to inputs A,B and C respectively.

Figure 6.10 indicates that the response of the receptor to the various inputs was largely an addition to the spectrum that existed before the dynamic stimulus was applied. This implies that the steady state spectrum was acting as the carrier for information concerning the dynamic state of the muscle length. In the band of frequencies studied, application of input power resulted in the addition to the output power of the receptor, power at only those frequencies at which an appreciable input existed. Interaction between the carrier spectrum and the input spectrum, apparently did not result in any sideband copies of the input. By comparing the responses of the spindle to the same

-71-
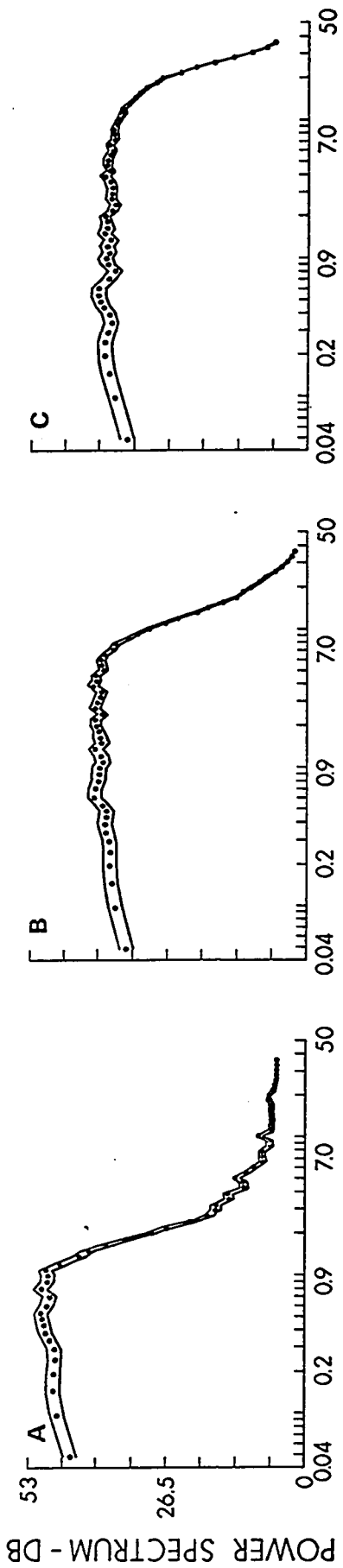
FREQUENCY - CPS

Figure 6.9

ESTIMATES OF THE POWER SPECTRA OF THE DYNAMIC STIMULI.
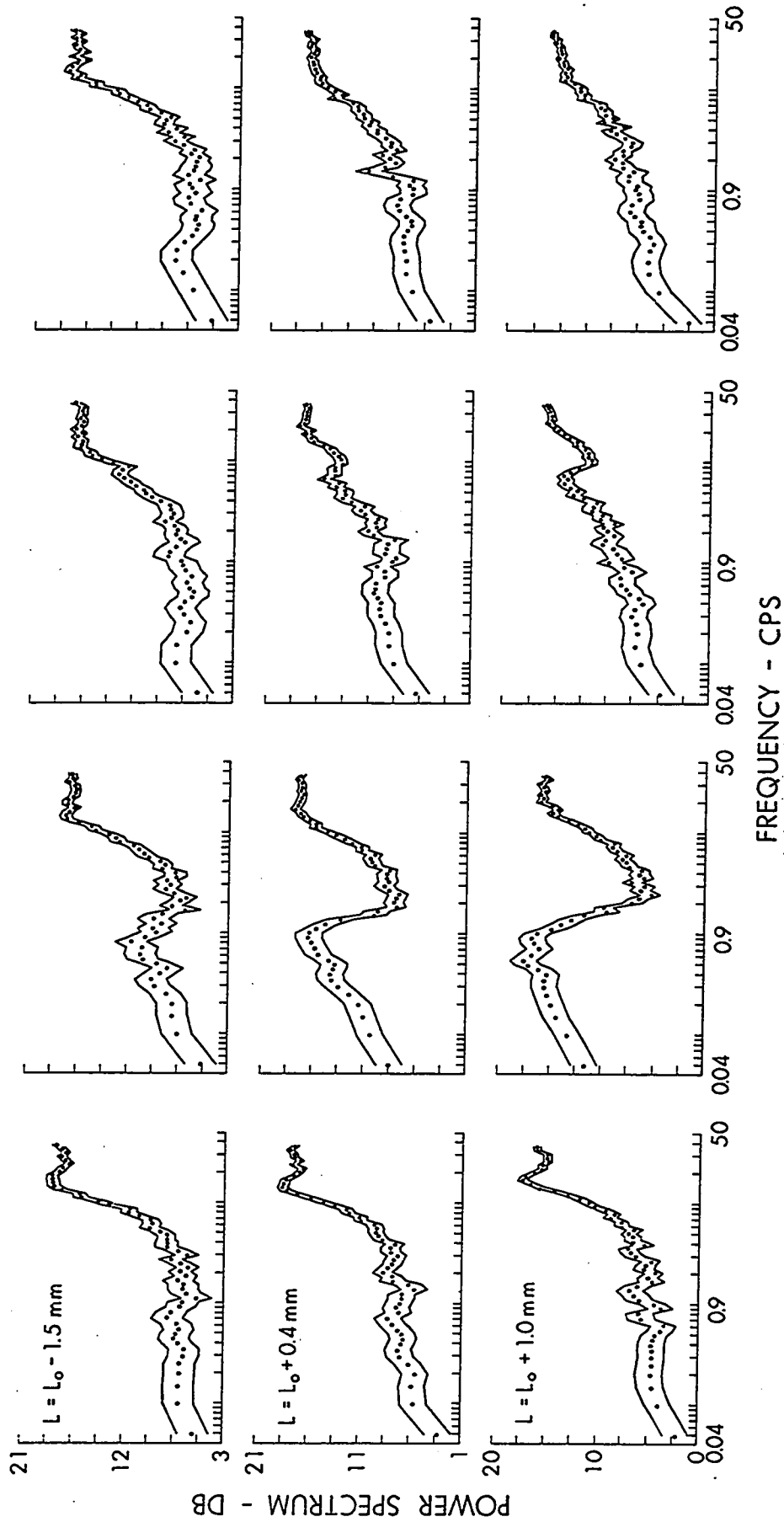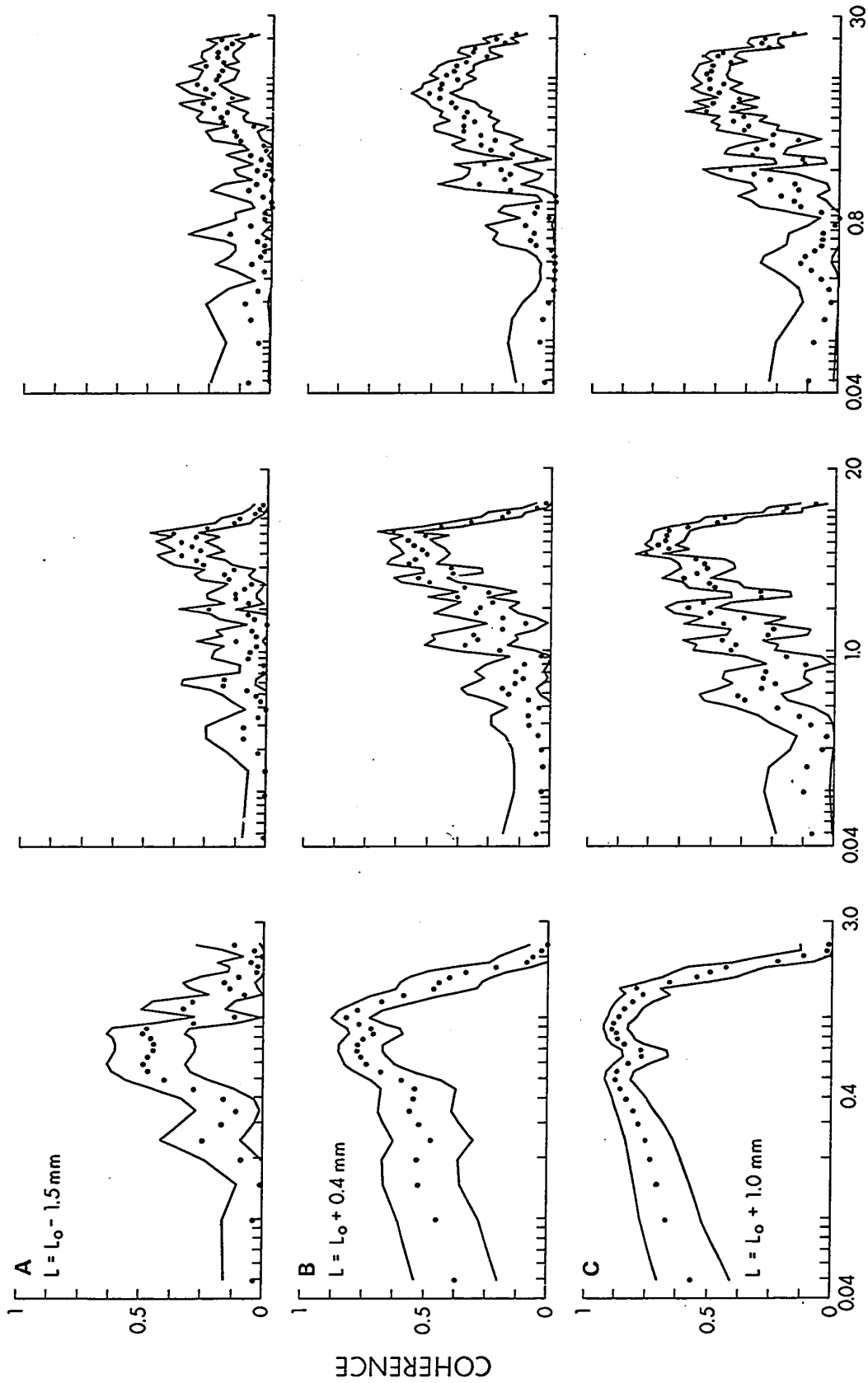
FREQUENCY – CPS

Figure 6.10

ESTIMATES OF THE POWER SPECTRA OF THE SPINDLE RESPONSE DURING STATIC AND RANDOM DYNAMIC LENGTH STIMULATION.

-73-

dynamic stimulus at different steady-state lengths, it is clear that the dynamic gain of the receptor depended strongly upon the length of the muscle. This is best demonstrated by input A. Here, the shape of the spindle response is almost identical at all three lengths with the exception that at the longest length the response was about 5 times greater (7db) than at the shortest length. The responses to inputs B and C are complicated by the fact that their spectra extended into the transition region of the carrier spectrum. Also, because their broader bandwidths resulted in relatively lower power densities, the power spectrum of the spindle response to inputs B and C was not as definitive as it was to input A, especially at the shorter muscle lengths. However, another feature of the spindle response is apparent from inputs B and C. These inputs have approximately equal power densities in the region below 7 cps. The flat portion of input C extends to somewhat higher frequencies. In the regions of the spectrum where inputs B and C have nearly equal power densities, it might be expected that the power density of the receptor response to these inputs would also be roughly the same. This was definitely not the case (cf figure 6.10 row 3 columns 3 and 4) and significantly less power existed in the response to input C especially in the region 1 to 7 cps. This then is an indication that the spindle gain was also dependent upon the bandwidth of the length variations applied to the muscle.

Estimates of the squared coherency spectrum between the spindle response and the impressed input are shown for the various cases of figure 6.10 in figure 6.11. Coherency between input and output was always greater with input A at all muscle lengths than with either input B or C. This might be expected since the power density of input A was so much greater in the region less than 2 cps than that of inputs B and C. However, inputs B and C had equal power densities to about 7 cps and yet the spindle response tended to be more coherent in that region with input B. All squared coherency curves attained a peak near the top end of the input spectrum. Input C consistently produced a smaller peak than input B.
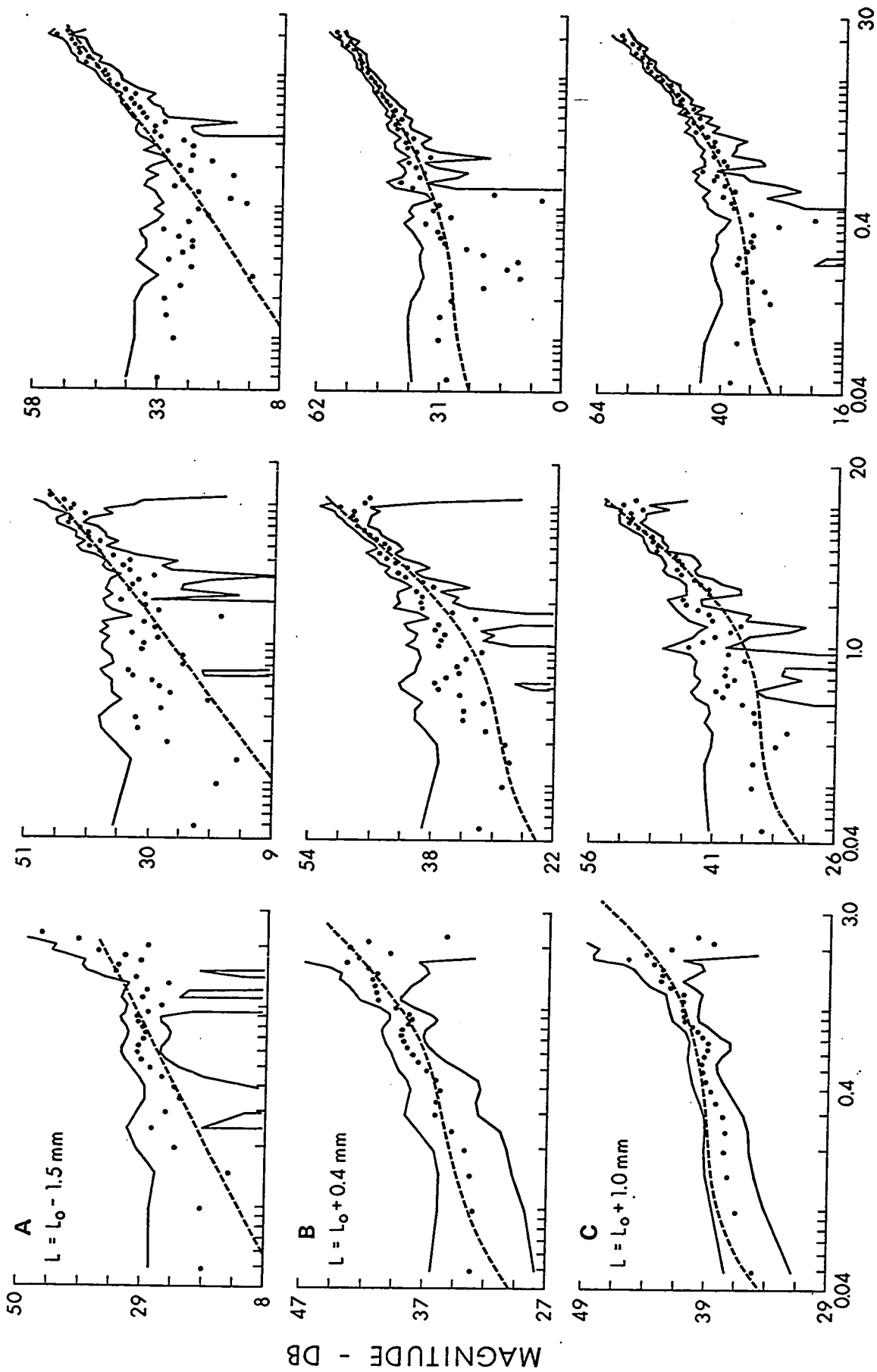
FREQUENCY - CPS

Figure 6.11

ESTIMATES OF THE SQUARED COHERENCY BETWEEN THE VARIOUS DYNAMIC STIMULI AND THE SPINDLE RESPONSE
AT DIFFERENT LEVELS OF STATIC STRETCH.

	Power Density of	Frequency—CPS				
		.07	.2	.7	2	7
1	Input A	46db	47db	49db	29db	8db
2	Input B	36	37	40	40	38
3	Input C	36	38	·38	38	38
4	Steady-State Response	4	5	6	5	9
5	Response to Input A	13	16	17		
6	Response to Input B	6	7	9	10	15
7	Response to Input C	4	7	8	10	12
8	Residue - Input A	9	11	10		
9	Residue - Input B	6	7	8	6	10
10	Residue - Input C	4	7	8	8	9

Table 6.3. Details of the Dynamic Response

Table 6.3, rows 8,9 and 10, contains estimates of the so-called noise residue of the spindle response to the three inputs. These numbers were calculated from the respective columns in rows 5,6 and 7 by substracting from these the quantities $1-\gamma_{xy}^2(f)$ obtained from figure 6.11 converted to decibels. The numbers in rows 8,9 and 10 are always greater than, or equal to, the numbers in the respective columns of row 4. This indicates that the portion of the spindle output that was totally incoherent with the input was always greater than, or equal to, the steady-state output. This is consistent with the earlier idea that the steady state spectrum was involved in the transmission of information concerning the dynamic activity of the muscle only to the extent that it acted as a carrier.

Figures 6.12 and 6.13 show estimates of the gain and phase functions corresponding to the squared coherency estimates of figure 6.11. In light of the inverse relationship between the width of the confidence interval for both gain and phase estimates and the squared coherency spectrum (see equations 3.51 and 3.52) the results of figure 6.11 predict that the most stable estimates for gain and phase would be obtained near the cut off frequency of each of the inputs. Examination of figure 6.12 reveals that increasing the muscle length resulted in an increase in the coherent gain of the system. Also, coherent gain in the region above

FREQUENCY - CPS

Figure 6.12

ESTIMATES OF THE GAIN FUNCTION BETWEEN THE VARIOUS DYNAMIC STIMULI AND THE SPINDLE RESPONSE AT DIFFERENT LEVELS OF STATIC STRETCH.

MAGNITUDE - DB
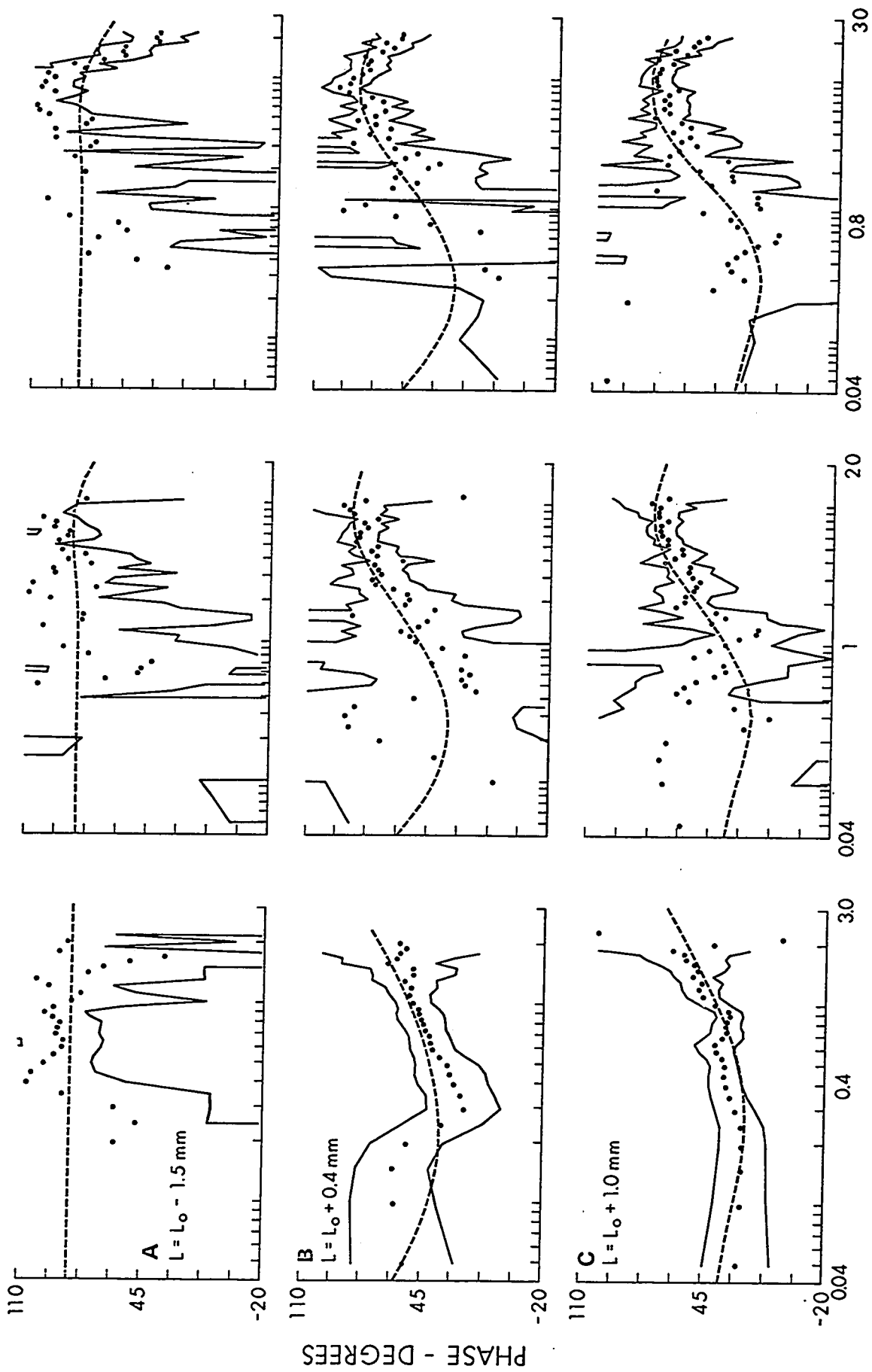
FREQUENCY - CPS

Figure 6.13

ESTIMATES OF THE PHASE FUNCTION BETWEEN THE VARIOUS DYNAMIC STIMULI AND THE SPINDLE RESPONSE
AT DIFFERENT LEVELS OF STATIC STRETCH.

PHASE - DEGREES

-78-

about 1 cps increased at the rate of about 20db per decade increase in frequency. Figure 6.13 indicates that increasing the muscle length produced a decrease in the relative phase lead of the receptor output over its input. At frequencies higher than about 10 cps the estimates of the phase function tended to return toward zero, predicting perhaps, that the gain function did not continue its upward trend indefinitely.

At each of the three lengths illustrated by figures 6.12 and 6.13, a transfer function was fitted by eye to the composite picture consisting of the three gain function estimates and the three phase function estimates corresponding to the three inputs. The transfer function was of the form

$$\frac{H(1 + \frac{s}{2\pi f_1}) \ (1 + \frac{s}{2\pi f_3})}{(1 + \frac{s}{2\pi f_2}) \ (1 + \frac{s}{2\pi f_4})} \tag{6.1}$$

f_3 was required to account for the +20db per decade slope of the magnitude characteristic in the region above 1 cps and f_4 was required so that the phase function would return to zero at high frequencies. f_1 amd f_2 produce the non-zero phase lead present in the system at the lowest frequencies. The dotted lines in figures 6.12 and 6.13 are the fitted functions. The four break frequencies are sufficient to account for the main features of all the estimates. By systematically changing f_1, f_2, f_3 and f_4, the required reduction in the phase advance produced by the spindle with increasing muscle length could be achieved. No difficulties were encountered in fitting the same four break frequencies to the estimates of gain and phase at a particular length with any of the three inputs. It was, however, impossible to maintain the same gain (H) and still obtain a satisfactory fit. The break frequencies and the gain at .35 cps for the dotted curves in figures 6.12 and 6.13 are shown in table 6.4.

Length	Break Frequency--CPS				Gain at .35 cps Input		
	f_1	f_2	f_3	f_4	A	B	C
$L_o-1.5mm$	<.004	.3	.4	80	22db	18db	17db
$L_o+0.4mm$	<.004	.067	.8	100	35	29	28
$L_o+1.0mm$	.01	.054	1.3	70	39	36	35

Table 6.4. Parameters of the Linear Model.

The coherent gain of the muscle spindle was about 8 times greater (17-18db) at the longest length than it was at the shortest length. To enable comparison, the curves fitted to the estimates of gain and phase in figures 6.12 and 6.13 input C, are consolidated in figure 6.14.

Figure 6.15 shows estimates of the squared coherency spectrum and the gain and phase functions of a muscle spindle (L_o=22mm) under two amplitudes of dynamic stimulus. Estimates in the left-hand column were obtained using input C at about 45μm rms, while those in the right-hand column were obtained using input C at 150 μm rms. Equation 6.1 was fitted by eye to the left-hand column and the same curve was drawn in the right-hand column for comparison with the estimates. Minor changes do occur in all three types of estimates. Both the coherency and the gain function are shifted upwards slightly by the increase in stimulus amplitude. The tendancy of the phase function to return toward zero at high frequencies and low stimulus amplitudes is no longer present under the increased input.

Figure 6.16 shows the response of the spindle described in table 6.4 at $L_o+1.0mm$ to a ramp increase in length. Using the parameters from table 6.4, the response to the ramp predicted by equation 6.1 can be shown to be proportional to

$$1 + 37.7\left(\frac{e^{t_1/3} - 1}{t_1}\right) e^{-t/3} + .0013 \left(\frac{e^{t_1/.002} - 1}{t_1}\right) e^{-t/.002} \quad t \geq t_1$$
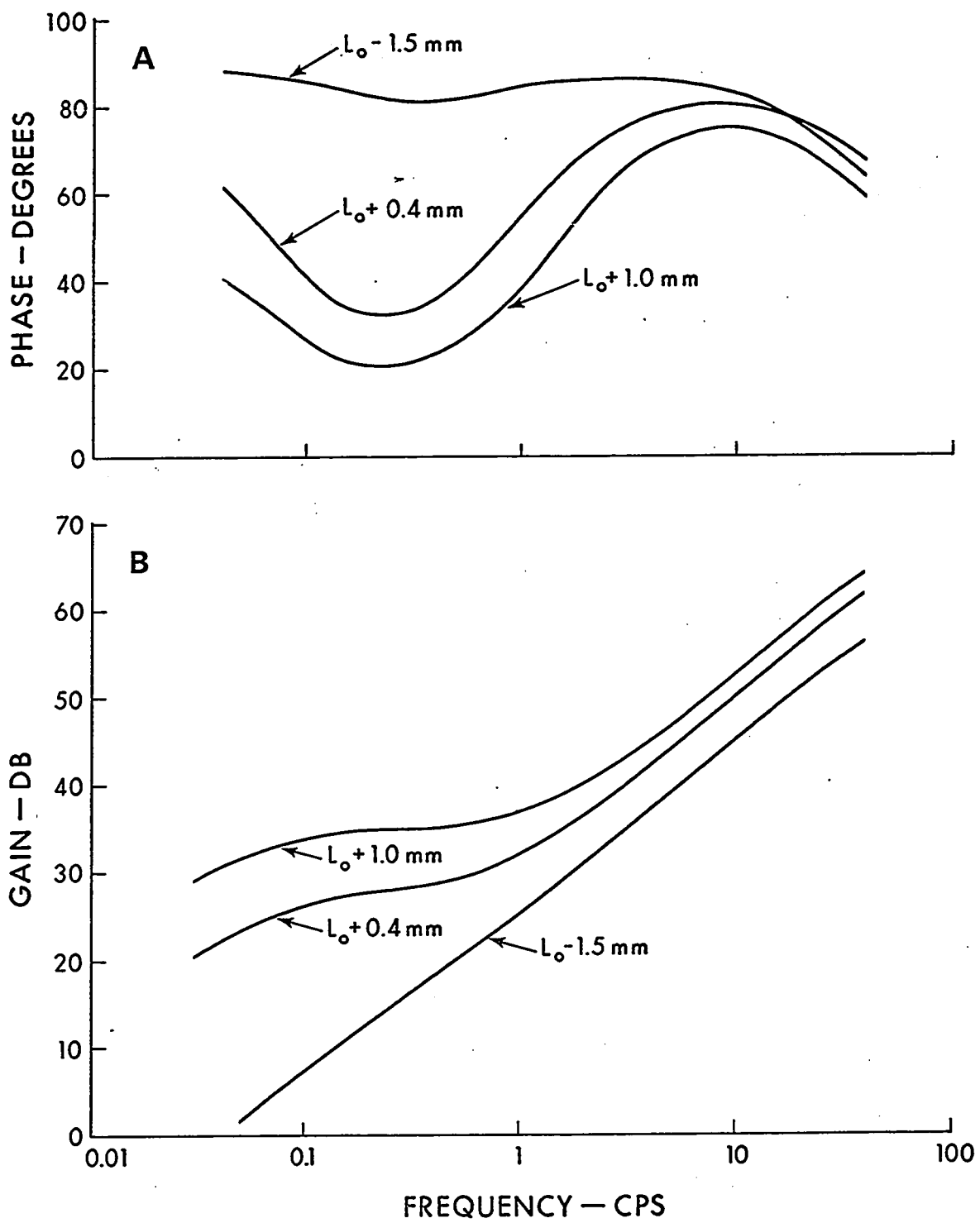
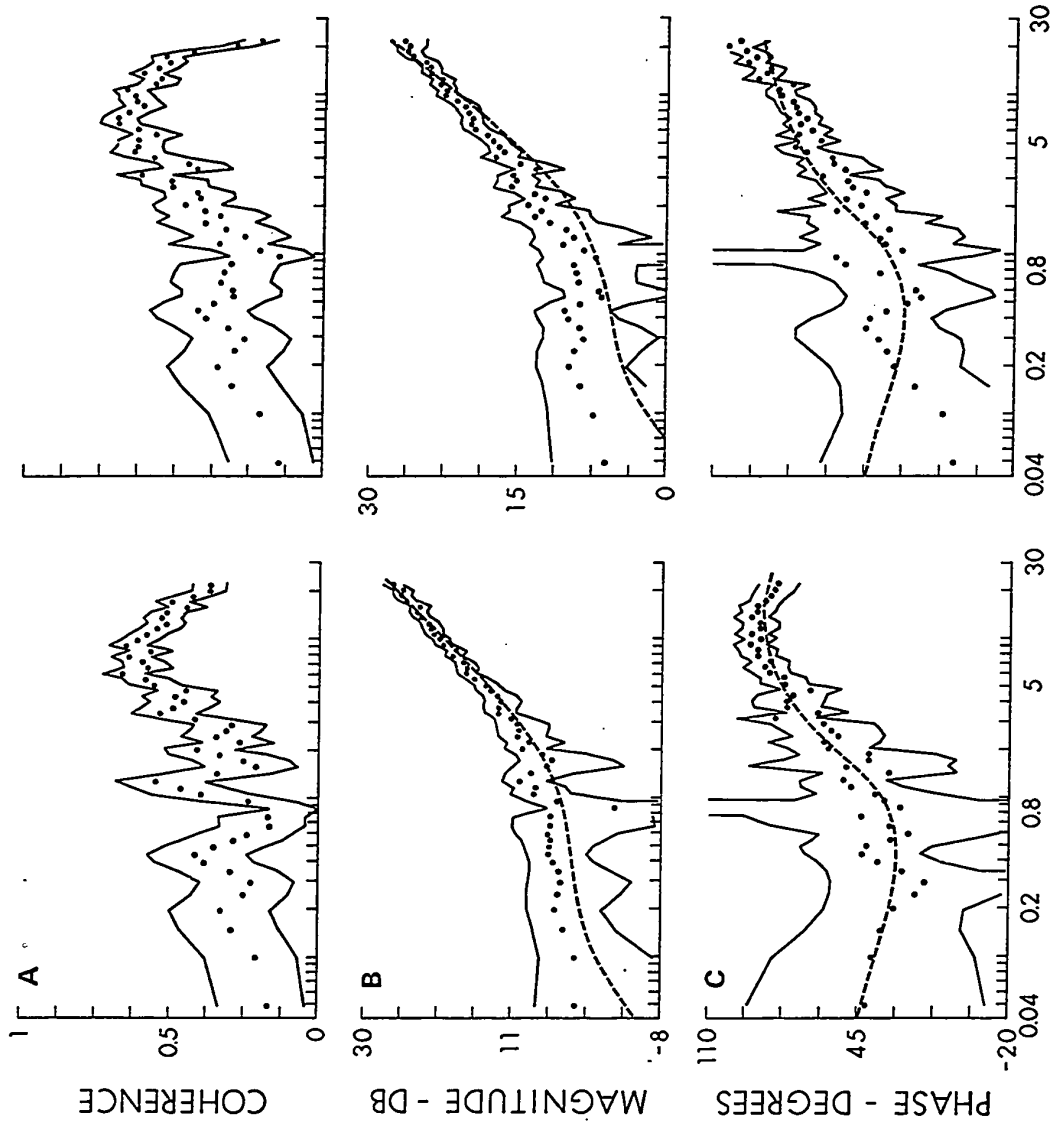$$(6.3)$$

Figure 6.14

LINEAR MODELS DESCRIBING MUSCLE SPINDLE DYNAMICS.

FREQUENCY - CPS

Figure 6.15

THE EFFECT ON THE COHERENT SPINDLE BEHAVIOR OF A 3-FOLD INCREASE IN THE STRENGTH OF THE DYNAMIC STIMULUS.

-82-

300 μm

60
40
20
0

1 sec / mm
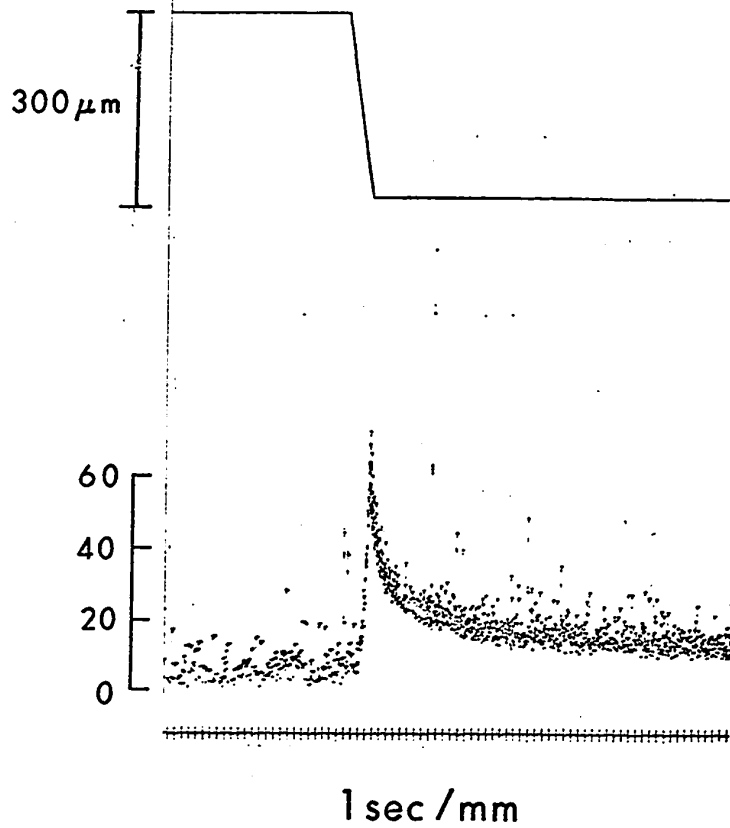
Figure 6.16

INSTANTANEOUS FREQUENCY OF THE SPINDLE RESPONSES TO A RAMP INCREASE IN

MUSCLE LENGTH.

-83-

where t_1 is the time during which the ramp is applied. If as in figure 6.16, $t_1=3$ seconds then equation 6.3 becomes approximately

$$1 + 21.4e^{-t/3} \qquad\qquad (6.4)$$

for all t slightly greater than t_1. Figure 6.16 definitely confirms the presence of a process with a time constant of about 3 seconds. However, another process with a much longer time constant is also indicated. Data segments for the spectral analysis were apparently too short to allow detection of this process. Equation 6.1 can be easily modified so that the additional feature of the ramp response made apparent by figure 6.16 is taken in account. Assuming that the additional time constant is about 50 seconds, the ramp response predicted by

$$\frac{H(1+52s)(1+16s)(1+.12s)}{(1+50s)(1+3s)(1+.002s)} \qquad\qquad (6.5)$$

will closely follow that in figure 6.16. The ramp response predicted by equation 6.5 with $t_1=3$ seconds is approximately

$$H(1 + 1.6e^{-t/50} + 23e^{-t/3}) \qquad\qquad (6.6)$$

for all t slightly greater than t_1. At $t=t_1$ equation 6.6 shows that the amplitude of the 3 second time constant process is about 5.7 times greater than that of the 50 second process consistent with figure 6.16. Equations 6.5 and 6.6 predict that the spindle will have a small static response at the muscle length at which they apply. This is consistent with table 6.1.

The power spectrum of a point process with nonindependent intervals can be calculated from equation 5.14 if the characteristic functions of all order intervals are known. If the density functions of all order intervals are bounded, then all of the characteristic functions will tend to zero as the frequency becomes large (96). Therefore, if the probability density functions of all order intervals are bounded

and the infinite summation in equation 5.14 is finite for some frequency f_o, then for $f > f_o$ equation 5.14 will tend to

$$S_{pp}(f) = \frac{A^2}{\bar{t}} \qquad\qquad (6.7)$$

Figure 6.2 implies that the density functions of all order intervals between muscle spindle discharges were bounded. Indications from figure 6.10 and from all muscle spindles examined under static stimulation were that the power spectrum of the sensory discharges was near its asymptotic value in the region above about 10 cps. If it is assumed that the convergence was to that predicted by equation 6.7, the absolute gain of the spindle receptor can be calculated.

According to equation 6.7 the power spectrum of the sensory discharges approaches a quantity which involves the area of a single nerve action potential. The shape of the action potential was calculated previously (99), and the results of this work were used to calculate A. For a 15 μm nerve in <u>Xenopus laevis</u> the area of a single action potential at 20°C is about 7×10^{-5} volt-seconds. In figure 6.10 row 3 column 1 (r3,c1), $\bar{t} = 60$ msec. Therefore, the power density of the spike train should approach about 8×10^{-8} volt^2-seconds. This is assumed to correspond to about 16db in figure 6.10. Hence, at 1 cps in figure 6.10 (r3,c1), the power density drops to about $.6 \times 10^{-8}$ volts^2-seconds. With the application of input A in figure 6.10 (r3,c2) the power density at 1 cps increases to about 9.5×10^{-8} volt^2-seconds. Therefore, input A at a muscle length of $L_o + 1.0$mm increased the power density in the spindle response at 1 cps by 8.9×10^{-8} volt^2-seconds. Input A was measured at about 45μm rms distributed as shown in figure 6.9A. Therefore, the power density of input A at 1 cps was about 1×10^{-9} m^2-seconds. Thus, the overall power gain of the receptor at 1 cps with input A was about 90 volts^2/m^2. Using figure 6.11 (r3,c1), the coherent gain of the spindle at the same frequency and with the same input was about 9 volts/m. This value was reduced somewhat for inputs B and C as indicated in table 6.4. Finally, using equation 6.5 and assuming input A, H was calculated to be about 1.3 volts/m.

CHAPTER 7

DISCUSSION

The results of the previous chapter indicate that methods of spectral estimation can be meaningfully applied to the analysis of a sensory receptor. By filtering, most problems associated with the detection of the point sensory discharges by continuous analog to digital conversion were eliminated. The transformation of the discrete sensory events into a continuous waveform enabled the analysis of both the stimulus and the receptor response with equal facility. Equi-spaced samples were obtained from both the stimulus and the response and spectral estimates were calculated using modern techniques (80).

Watanabe (100) has used techniques of spectral estimation to obtain estimates of transfer functions between simultaneous nerve impulse trains in the crayfish brain. Although it was claimed that the treatment of nerve discharges was analogous to the treatment of point processes by Bartlett (101), this was not the case. Watanabe sampled the spike trains by counting the number of discharges in the sampling interval. This procedure is equivalent to applying a digital difference filter to $N(t)$ the cumulative number of impulses up to time t. Mathematically, $N(t)$ is related to the point sensory process by integration. It can be shown that the gain and phase functions introduced by the integrate and difference operations are respectively

$$G(f) = \frac{\sin \pi f \Delta}{\pi f} \qquad f < \frac{1}{2\Delta} \qquad (7.1)$$

and

$$P(f) = -\pi f \Delta \qquad f < \frac{1}{2\Delta} \qquad (7.2)$$

where Δ is the sampling interval. Therefore, the power spectrum of a point process is apparently linearly related to the power spectrum of its

average frequency and exactly equivalent at $f=0$. All of Watanabe's spectral estimates were weighted by equations 7.1 and 7.2. In addition, since all the spectra were weighted by the same function, its effects would have cancelled in estimates of coherency, gain and phase. Therefore, it might seem that Watanabe's transfer functions did actually relate the power spectra of the point processes. However, consideration of the aliasing properties of $N(t)$ indicates that this is not always so. Suppose, as evidenced by discharges from the amphibian muscle spindle, that the point process from which $N(t)$ was derived had a flat power spectrum in the region around the folding frequency of 50 cps. Then, using arguments similar to those in chapter 5, the aliased power in the sampled version of $N(t)$ at 40 cps will be about 40%, at 25 cps about 15% and at 10 cps about 2%. In general, as stated in chapter 5, it is not possible to remove from a sampled signal that portion of the power which is aliased from higher frequencies. Therefore, it is impossible to relate Watanabe's transfer functions to those which relate the power spectra of the point processes except possibly at frequencies low compared to the folding frequency. At frequencies where aliasing is negligible the two transfer functions are identical.

If, as in this thesis, the point process is suitably low-pass filtered to control aliasing, then the methods of cross-spectral analysis described are extremely well suited for obtaining estimates of the transfer functions and the squared coherencies between two or more simultaneous nerve impulse trains. If all the spike processes involved are modified using filters with identical low-pass characteristics, then, as pointed out in the previous paragraph and by others (86), the effects of the filters cancel from estimates of the transfer functions and coherencies.

Sampling the average frequency of a spike train results in a loss of the fine details in the impulse pattern. That is, any information that is encoded in the impulse interval or in the relationship between adjacent or near adjacent intervals is lost. Also, relating the average frequency of the sensory spike train to the stimulus implies that the decoding mechanism responsible for the recovery of information from the

receptor is concerned with just the average frequency of the spike train. Evidence exists which indicates that sensory decoding more closely resembles low-pass filtering (13,16-20), a process which is strictly not equivalent to averaging. The results of this thesis show directly what information can be recovered from the receptor response by various filtering operations.

Comparison of the power spectra of the sensory discharges before and after the application of a dynamic stimulus has shown that although its spectral distribution was altered, the stimulus was present in the discrete discharges of the receptor output at the appropriate frequencies. The response to the dynamic stimulus was apparently an addition to the response to the static stimulus upon which the dynamic stimulus was superimposed. The power added to the receptor response by the dynamic stimulus was not entirely coherent with the input (see table 6.3). Transmission of dynamic information by the spindle was therefore a 'noisy' process. In the band of frequencies studied, the portion of the dynamic response that was linearly correlated with the dynamic input was related to both the amplitude and the velocity of the input. At short muscle lengths, the response was almost entirely proportional to the velocity of the stimulus. At longer lengths, the spindle became sensitive to the amplitude of the stimulus as well. The coherent dynamic characteristics of the receptor were only slightly altered by a three-fold increase in the strength of the stimulus. Therefore, in that sense, the receptor was studied in a linear range of its operation.

The response of the amphibian spindle to a ramp increase in length closely resembled that obtained by Poppele and Bowman (9) from the primary ending of the mammalian muscle spindle. In the de-efferented state, neither spindle showed much sensitivity to a static stretch and both showed a two-time constant decay from a ramp stimulus. The first of these was of the order of a few seconds, while the second was considerably longer. However, in the mammalian primary ending these time constants were not changed by different levels of static length stimulation. Changing the muscle length resulted only in gain changes in the mammalian spindle with no changes in the relative phase function between input

-88-

and output. These differences between the amphibian muscle spindle and the mammalian muscle spindle primary ending are apparently not the result of different analysis techniques. Although the mammalian spindle was examined by sampling the average frequency of the sensory discharges, the sampling rate was always adjusted to be much greater than the stimulus frequency (9). Changes in the time constant of the generator potential in the frog spindle from a ramp stimulus has also been reported by Ottoson et al. (102). Poppele and Bowman (9) report that the primary ending of the mammalian spindle tended to phase lock to sinusoidal stimuli. No related phenomenum was observed in the amphibian spindle response to random stimulation. The tendency of a neuron to phase lock to a sinusoidal stimulus is apparently related to the variability in the discharge before stimulation (103). The more variable the discharge the less the tendancy to phase lock. Stein and Matthews (104) report a coefficient of variation of about .05 from primary muscle spindle endings in the cat. This is almost 10 times less than the variability obtained for the frog spindle discharges. Therefore, although the use of a random stimulus probably reduced the tendency of the amphibian spindle to exhibit phase-locking properties, it cannot be considered the sole cause.

It is now evident that the estimates of the gain and phase functions of the amphibian muscle spindle could have been improved by shaping the input spectrum. In light of the form of the estimated gain function, application of a flat-spectrum stimulus resulted in the highest frequency components of the stimulus being the strongest in the receptor response. As a result, the coherency between the stimulus and response was greatest in that region of the spectrum. Therefore, estimates of gain and phase were most stable near the high frequency end of the stimulus. If on the other hand, the inputs were shaped to compliment the characteristics of the spindle, uniform stability of the gain and phase estimates could have been achieved. In this sense, a better stimulus would have been one which decreased at the rate of 20db per decade increase in frequency. Using the shaped input, an estimate of the best transfer function of the receptor could probably have been obtained from the single application of a single input. Also, shaping

the stimulus may eliminate or at least reduce the frequency dependent nonlinearity present in the receptor.

Stein and French (103) have shown that the effect of variability in their neural analog is to prevent noise-free recovery of encoded dynamic information by low-pass filtering no matter how widely the dynamic stimulus is separated from the mean discharge rate. This is because a random discharge contains power at all frequencies. If this random discharge is acting as a carrier of dynamic information, then the recovery of that information by low-pass filtering will at all frequencies be contaminated by the incoherent carrier. As the variability in the discharges of the neural analog was reduced it was shown that the power spectrum of the discharges contained less power at low frequencies permitting a more uncontaminated recovery of the information at those frequencies. Ultimately, for a completely regular carrier, Bayly (15) has shown that distortion-free recovery of the signal is theoretically possible by low-pass filtering if both the stimulus frequency to carrier frequency ratio and the depth of modulation produced by the stimulus are sufficiently restricted.

The low-noise recovery of the dynamic stimulus from the amphibian muscle spindle is facilitated by the fact that the power spectrum of the discharges is low at low frequencies. Therefore, information concerning the dynamic state of the muscle which exists at these low frequencies can be recovered with less contaminative noise than information of the same magnitude at higher frequencies. The reduction in low-frequency power can be predicted from the distribution of the interspike intervals and is not altered significantly by a weak serial correlation between adjacent intervals. Coherent information is recoverable from the spindle by low-pass filtering at frequencies well past the mean discharge rate of the carrier. However a larger percentage of the total signal recovered will be incoherent with the input as the frequency is increased. Bayly (15) suggests that parallel channels each with random carriers could result in an overall reduction of the noise distortion since the carriers will likely be mutually incoherent.

Estimates of the power spectrum suggest that the steady-state

discharges from the amphibian muscle spindle can be adequately described as a renewal process. That is, in the steady-state, the distribution of the first-order intervals constitutes a complete description of the point sensory process. Theoretical considerations of the power spectra of independent point processes have also shown that the exact form of the distribution chosen to describe the renewal process is not critical. However, the Gamma density must be preferred over the Gaussian density for the amphibian spindle. As shown by Buller et al. (54), extensive changes do occur in the distribution of the interspike intervals from the frog spindle at very low muscle lengths. At lengths which result in greater than 'critical depolarization' the distribution of intervals is nearly symmetrical. At lengths which result in less than 'critical depolarization' the distribution tends to be exponential. The Gamma density can be both exponential and highly symmetrical in form.

The overall dynamic characteristics of the amphibian muscle spindle are usually considered to be the result of the contributions from three functional subsystems. The first of these is referred to as the mechanical process. Any modification of the stimulus by this sub-system is due to the visco-elastic properties of the intrafusal muscle fibers upon which the sensory endings reside. The second is the trans-duction process. Here, the output of the mechanical process is converted to electrical energy as a generator current. Finally there is the encoding mechanism. Here, the resulting generator potential at the site of impulse initiation is encoded as a series of 'all-or-none' action potentials. Vallbo (105) has obtained evidence that in the frog, the region of the sensory axon in which the encoding mechanism resides has different properties from other portions of the axon. He noted that the frequency of discharge elicited by mechanical stimulation of muscle spindles was of longer duration and of a wider frequency range than the repetitive firing due to electrical stimulation of the sensory axon. The evidence suggests that the gross mechanical properties of the intra-fusal fibers in the frog spindles do not contribute to the dynamic characteristics of the receptor except possibly to attenuate the stimulus (22,23,25). Also, the frequency of the action potentials produced by the encoding mechanism is apparently linearly and instantaneously related

to the magnitude of the generator potential (41,56). Therefore, it would seem that the most likely origin for the dynamic characteristics of the spindle must be in the transduction process. On the other hand, the mechanical process could be involved if the dynamic response originates in the microscopic connections between the muscle fiber and the nerve terminals or in the mechanical properties of the nerve terminal membrane or even in the collective mechanical properties of the terminal nerve bulbs and interconnecting cylinders. Certainly, if the dynamic behavior is mechanical in origin then, for example, a nonlinear stress-strain relationship could account for the reduction in the relative phase advance produced by the receptor with increasing levels of static stretch.

The observation that the gross mechanical properties of the amphibian intrafusal muscle fibers do not contribute to the overall dynamic response of the spindle does not necessarily imply a similar behavior of the mammalian spindle. Indeed, there is some evidence that gross mechanical factors are involved in the mammalian spindle (24). Also, the finding that different levels of static stretch do not change the relative phase advance in the response of the de-efferented mammalian primary ending to dynamic stimulation (9) while increased static stretch does reduce phase advance in a similar frog preparation, suggests that the two receptors function by somewhat different mechanisms. Although the secondary ending of the mammalian spindles does show a changing phase advance with stretch, this ending is also sensitive to different levels of static stretch (9). When the changing time constants are scaled with respect to the mean discharge rate, they once again become invariant. A similar scaling is not possible with the amphibian spindle since there is very little change in the discharge rate with increasing static stretch. Invariance of the time constants would not be achieved by scaling with respect to muscle length since the time constants do not all change in the same direction (see table 6.4). Therefore, the mechanisms underlying amphibian spindle behavior must also be considered as being somehwat different from the mammalian secondary ending.

While stretching a de-efferented muscle it was observed (25) that the length of the reticular region of an intrafusal fiber increased

nonlinearly. At short overall muscle lengths, the strain in the 'reticular zone' was a very small percentage of the strain in the overall muscle. When the muscle was stretched past L_o, the length of the 'reticular zone' increased dramatically and then saturated. Further increase in muscle length produced no further strain in the 'reticular zone'. At lengths greater than L_o the overall sensitivity of the spindle to dynamic stimulation also increased suddenly. It was also noted (25), that when the intrafusal fiber was made to twitch under isometric conditions by electrical stimulation of the polar regions, the length of the 'reticular zone' increased during the twitch to its saturation length. Presumably, continuous fusimotor activity would therefore maintain the 'reticular zone' at the saturated length. This implies that by stretching the muscle well past L_o, the effect of motor nerve activity on the sensory ending was at least partially simulated. The adequancy of the simulation depends on whether the numerous nerve contacts on the 'compact zones' adjacent to the 'reticular zone' (45) serve simply to anchor the ending so that the length of the reticular region can be sensed. In this case, a good simulation of intact fusimotor activity would have been obtained. However, if the contacts on the 'compact zones' are sensitive to strain in that region, the simulation would have been only partially successful.

Verveen and Derksen (106) have been able to measure the noise fluctuations in the membrane potential of a frog nerve. For a 4µm nerve, the wide-band rms intensity of the noise was found to be about 200µV. This is almost an order of magnitude greater than that expected from theoretical considerations concerning thermal noise in the membrane. If the wide-band rms intensity maintains this relationship to the expected thermal noise then, in the fine .1µm nerve terminals of the frog muscle spindle, the noise intensity would be about 3mV (the figure for expected thermal noise obtained from (54)). This is a significant fraction of the 15-20mV required for threshold depolarization and could thus account for the variability seen in the discharges from the amphibian muscle spindle.

Presumably, muscle spindles are involved in an animal's ability to control and maintain its posture and in its ability to execute precise predetermined movements. Certainly, control of posture and movement by

simple activation of the motor nerves with no sensory feedback of the effects would be grossly inadequate. Such an 'open loop' system would not permit any compensation in effort for say muscle fatigue or for misjudgement of the magnitude of the load. In mammals, it is known that stretching a fully innervated muscle usually results in a reflex contraction which tends to resist the extension. In humans, this 'stretch-reflex' is easily demonstrated as the tendon jerk. The reflex is mediated by a sensory volley, initiated by the stretch, from the muscle spindles. The 'stretch-reflex' therefore has the properties of a length servomechanism, that is, of a closed-loop system in which negative feedback is used to maintain a constant length in the midst of external disturbances. It has been suggested (107) that in the mammal, precise movements are initiated by central activation of the small motor nerves which innervate the intrafusal muscle fibers (γ motoneurons). Activity of the γ motoneurons excites the sensory endings of the muscle spindles which in turn monosynaptically excite the large motor nerves which innervate the extrafusal fibers (α motoneurons). This scheme of control is known as the 'follow-up servo' hypothesis (107). The control inputs to the system are the γ motoneurons. Error between the desired and actual limb position for example, is measured by the muscle spindles and the error signal is fed to the central nervous system along the sensory nerves. The errors are continuously processed by the central nervous system and corrective signals are sent peripherally along the α motoneurons. The extrafusal muscle fibers act as the actuators which correct the error. The 'follow-up servo' hypothesis is a very attractive idea since any conflict between the voluntary systems and the postural or reflex systems which resist the change is simply and elegantly resolved. However as has been pointed out (8) there are difficulties with this idea. First of all, large modulations in the discharge frequency of the γ motor nerve produce relatively modest changes in the sensory discharge from the spindle. Second, it is not always true that the activity in the γ fibers leads the activity in the α motor fibers. In fact, rapid movements are sometimes implemented exclusively by α motoneurons. In light of these difficulties, the current idea is that both α and γ motoneurons are intimately involved in the control of movement. It is postulated that

three distinct controlling signals from higher centers are involved in voluntary control (108). The centers separately control the α moto-neurons and the γ motoneurons. A third signal controls the sensitivity of the monosynaptic reflex within the spinal cord. The sensitivity of the agonistic muscle system is turned on during voluntary movement while the antagonistic system is desensitized. Deliberate movements are controlled by parallel γ and α activation and a sensitized reflex loop. Activation of the γ nerves constitutes a control input and is available if compensation against unexpected loading conditions is required. This scheme is considered a 'servo-assisted' method of producing movement (8).

The 'stretch-reflex' which is apparently of prime importance in mammals can only be weakly elicited in amphibia (109). The postural activity in the frog appears to depend much more on afferent impulses of cutaneous origin. However, a weak stretch reflex does not necessarily imply that muscle spindles in the frog do not play a part in the precise control of movement. Assuming that the current thinking on the control of movement in mammals is correct, then it is not unreasonable to assume that the control of movement in amphibia is a simplified version of the same thing. Intrafusal muscle fibers in the frog are co-innervated with extrafusal fibers. Separate control of the sensitivity of the frog muscle spindle is therefore not possible. However, as mentioned earlier, it was observed (25) that any fusimotor activity seems to stretch the 'reticular zone' of the spindle into saturation. Hence, it may be that the amphibian muscle spindle operates as a two-state device. If this were so, then sensitivity of the sensory ending would not depend on the magnitude of the activity in the motor nerves but only on whether or not there was any activity at all. Instead of three central controlling pathways as in the mammal, it seems that the frog would require only one. Activation of the agonistic motor system would fully sensitize the 'servo-assist' loop as well as initiating the movement. Inhibition of the antagonistic motor system would densensitize any reflex loop which might resist stretch in the antagonistic muscles.

BIBLIOGRAPHY

1. G.P. Moore, D.H. Perkel, and J.P. Segundo. 1966. Statistical analysis and functional interpretation of neuronal spike data. Ann. Rev. Physiol., 28, 493.

2. D.H. Perkel, G.L. Gerstein, and G.P. Moore. 1967. Neuronal spike trains and stochastic point processes. I. The single spike train. Biophys. J., 7, 391.

3. D.H. Perkel, G.L. Gerstein, and G.P. Moore. 1967. Neuronal spike trains and stochastic point processes. II. Simultaneous spike trains. Biophys. J., 7, 419.

4. J.W.S. Pringle, and V.J. Wilson. 1952. The response of a sense organ to a harmonic stimulus. J. Exptl. Biol., 29, 220.

5. K.M. Chapman, and R.S. Smith. 1963. A linear transfer function underlying impulse frequency modulation in a cockroach mechanoreceptor. Nature, 197, 699.

6. M.C. Brown, and R.B. Stein. 1966. Quantitative studies on the slowly adapting stretch receptor of the crayfish. Kybernetik, 3, 175.

7. L. Maffei, and G. Rizzolatti. 1967. Transfer properties of the lateral geniculate body. J. Neurophysiol., 30, 333.

8. P.B.C. Matthews, and R.B. Stein. 1968. The sensitivity of muscle spindle afferents to small sinusoidal changes of length. J. Physiol., 200, 723.

9. R.E. Poppele, and R.J. Bowman. 1970. Quantitative description of linear behavior of mammalian muscle spindles. J. Neurophysiol., 33, 59.

10. R. Gesell, C.S. Magee, and J.W. Bricker. 1940. Activity patterns of the respiratory neurons and muscles. Am. J. Physiol., 128, 615.

11. H.K. Hartline, and C.H. Graham. 1932. Nerve impulses from single receptors in the eye. J. Cell. Comp. Physiol., 1, 277.

12. C. Enroth-Cugell, and J.G. Robson. 1966. The contrast sensitivity of retinal ganglion cells of the cat. J. Physiol., 187, 517.

13. T.A. McKean, R.E. Poppele, N.P. Rosenthal, and C.A. Terzuolo. 1970. The biologically relevant parameter in nerve impulse trains. Kybernetik, 6, 168.

14. J.J. Groen, O. Lowenstein, and A.J.H. Vendrik. 1952. The mechanical analysis of the responses from the end-organs of the horizontal semicircular canal in the isolated elasmobranch labyrinth. J. Physiol., 117, 329.

15. E.J. Bayly. 1968. Spectral analysis of pulse frequency modulation in the nervous systems. IEEE Trans. Bio-Medical Engr., BME-15, 257.

16. L.D. Partridge. 1965. Modifications of neural output signals by muscles: A frequency response study. J. Appl. Physiol., 20, 150.

17. C.A. Terzuolo, and E.J. Bayly. 1968. Data transmission between neurons. Kybernetik, 5, 83.

18. P. Fatt, and B. Katz. 1951. An analysis of the end-plate potential recorded with an intra-cellular electrode. J. Physiol., 115, 320.

19. C.F. Stevens. 1968. Synaptic physiology. Proc. IEEE, 56, 916.

20. B. Katz. 1966. Nerve, muscle, and synapse. McGraw-Hill, New York.

21. B.H.C. Matthews. 1931. The response of a single end organ. J. Physiol., 71, 64.

22. D. Ottoson, and G.M. Shepherd. 1968. Changes of length within the frog muscle spindle during stretch as shown by stroboscopic photomicroscopy. Nature, 220, 912.

23. D. Ottoson, and G.M. Shepherd. 1970. Length changes within isolated frog muscle spindle during and after stretching. J. Physiol., 207, 747.

24. R.S. Smith. 1966. Properties of intrafusal muscle fibers. In: R. Granit (ed.), Nobel Symposium I. Muscular afferents and motor control. Stockholm: Almqvist and Wiksell.

25. Z.J. Koles, and R.S. Smith. 1971. Mechanical properties of intrafusal muscle fibers in Xenopus laevis. Submitted for publication.

26. J.W. Cooley, and J.W. Tukey. 1965. An algorithm for the machine calculation of complex Fourier series. Math. of Comput., 19, 297.

27. I. Tasaki, and K. Mizutani. 1944. Comparative studies on the activities of the muscle evoked by two kinds of motor nerve fibres. Jap. J. Med. Sci. Biophys., 10, 237.

28. R.K. Orkand. 1963. A further study of electrical responses in slow and twitch fibres of the frog. J. Physiol., 167, 181.

29. L.D. Peachey, and A.F. Huxley. 1962. Structural identification of twitch and slow striated muscle fibres of the frog. J. Cell. Biol., 13, 177.

30. S.G. Page. 1965. A comparison of the fine structures of frog slow and twitch muscle fibres. J. Cell. Biol., 26, 477.

31. J. Lannergren, and R.S. Smith. 1966. Types of muscle fibres in toad skeletal muscle. Acta. Physiol. Scand. 68, 263.

32. R.S. Smith, and J. Lannergren. 1968. Types of motor units in the skeletal muscle of Xenopus laevis. Nature, 217, 281.

33. J.C. Eccles, B. Katz, and S.W. Kuffler. 1941. Nature of the 'end-plate potential' in curarized muscle. J. Neurophysiol., 4, 362.

34. W. Burke, and B.L. Ginsborg. 1956. The action of the neuro-muscular transmitter on the slow fibre membrane. J. Physiol., 132, 599.

35. E.G. Gray. 1957. The spindle and extrafusal innervation of a frog muscle. Proc. Roy. Soc. London, B 146, 416.

36. P.B.C. Matthews. 1964. Muscle spindles and their motor control. Physiol. Rev., 44, 219.

37. S.W. Kuffler, and E.M. Vaughan Williams. 1953. Small-nerve junctional potentials. The distribution of small motor nerves to frog skeletal muscle, and the membrane characteristics of the fibres they innervate. J. Physiol., 121, 289.

38. C.C. Hunt, and S.W. Kuffler. 1951. Further study of efferent small-nerve fibres to mammalian muscle spindles. Multiple spindle innervation and activity during contraction. J. Physiol., 113, 283.

39. C.C. Hunt, and S.W. Kuffler. 1951. Stretch receptor discharges during muscle contraction. J. Physiol., 113, 298.

40. M. Hines. 1927. Nerve and muscle. Quart. Rev. Biol., 2, 149.

41. B. Katz. 1950. Depolarization of sensory terminals and the initiation of impulses in the muscle spindle. J. Physiol., 111, 261.

42. C. Eyzaguirre. 1957. Functional organization of neuromuscular spindle in the toad. J. Neurophysiol., 20, 523.

43. F. Ito, K. Toyama, and R. Ito. 1964. A comparative study on structure and function between the extrafusal receptor and the spindle receptor in the frog. Jap. J. Physiol., 14, 12.

44. J.K.S. Jansen. 1967. On the functional properties of stretch receptors of mammalian skeletal muscles. In: A.V.S. de Reuck and J. Knight (ed.), Ciba foundation symposium on myotatic and vestibular mechanisms. London: J.E.A. Churchill Ltd.

45. B. Katz. 1961. The terminations of the afferent nerve fiber in the muscle spindle of the frog. Phil. Trans. Roy. Soc. (London), 243B, 221.

46. B. Katz. 1949. The efferent regulation of the muscle spindle in the frog. J. Exptl. Biol., 26, 201.

47. C. Eyzaguirre. 1958. Modulation of sensory discharges by efferent spindle excitation. J. Neurophysiol., 21, 465.

48. R.S. Smith. 1964. Activity of intrafusal muscle fibres in muscle spindles of Xenopus laevis. Acta. Physiol. Scand., 60, 223.

49. R.S. Smith. 1964. Contraction in intrafusal muscle fibres of Xenopus laevis following stimulation of their motor nerves. Acta. Physiol. Scand., 62, 195.

50. S.W. Kuffler, C.C. Hunt, and J.P. Quilliam. 1961. Function of medullated small-nerve fibres in mammalian ventral roots: efferent muscle spindle innervation. J. Neurophysiol., 14, 29.

51. I.A. Boyd. 1962 The structure and innervation of the nuclear bag muscle fibre system and the nuclear chain muscle fibre system in mammalian muscle spindles. Phil. Trans. Roy. Soc. London, B 245, 81.

52. B.H.C. Matthews. 1931. The response of a muscle spindle during active contraction of a muscle. J. Physiol., 72, 153.

53. G.M. Shepherd, and D. Ottoson. 1965. Response of the isolated muscle spindle to different rates of stretching. Presented at the 1965 Symp. on Quantitative Biology, 30, Sensory Receptors, Cold Spring Harbor Lab. of Quantitative Biology.

54. A.J. Buller, J.G. Nicholls, and G. Strom. 1953. Spontaneous
       fluctuations of excitability in the muscle spindle of
       the frog. J. Physiol., 122, 409.

55. P.B.C. Matthews, and D.R. Westbury. 1965. Some effects of fast
       and slow motor fibres on muscle spindles of the frog.
       J. Physiol., 178, 178.

56. C. Edwards. 1955. Changes in the discharge from a muscle spindle
       produced by electrotonus in the sensory nerve. J.
       Physiol., 127, 636.

57. D. Ottoson, and G.M. Shepherd. 1965. Receptor potentials and
       impulse generation in the isolated spindle during controlled
       extension. Presented at the 1965 Symp. on Quantitative
       Biology, 30, Sensory receptors, Cold Spring Harbour Lab.
       of Quantitative Biology.

58. O.C.J. Lippold, J.G. Nicholls, and J.W.T. Redfearn. 1960.
       Electrical and mechanical factors in the adaptation of a
       mammalian muscle spindle. J. Physiol., 153, 209.

59. B. Katz. 1950. Action potentials from a sensory nerve ending.
       J. Physiol., 111, 248.

60. F. Ito. 1969. Abortive spikes of the frog muscle spindle. Jap.
       J. Physiol., 19, 373.

61. S.J. Hubbard. 1958. A study of rapid mechanical events in a
       . mechano-receptor. J. Physiol., 141, 198.

62. W.R. Loewenstein. 1956. Excitation and changes in adaptation
       by stretch of mechano-receptors. J. Physiol., 133, 588.

63. J.C. Houk, Jr., V. Sanchez, and P. Wells. 1962. Frequency response
       of a spindle receptor. M.I.T. Research Lab. of Electronics,
       Cambridge, Mass., QPR #67, 223.

64. K. Toyama. 1966. An analysis of impulse discharges from the spindle
       receptor. Jap. J. Physiol., 16, 113.

65. J.C. Houk, R.W. Cornew, and L. Stark. 1966. A model of adaptation
       in amphibian spindle receptors. J. Theoret. Biol., 12, 196.

66. G.L. Gottlieb, G.C. Agarwal, and L. Stark. 1969. Stretch receptor
       models. I-Single-efferent single-afferent innervation.
       IEEE Trans. Man-Machine Systems, MMS-10, 17.

67. A. Crowe. 1968. A mechanical model of the mammalian muscle spindle. J. Theoret. Biol., 21, 21.

68. J.C. Houk, Jr., and L. Stark. 1962. An analytical model of a muscle spindle receptor for simulation of motor coordination. M.I.T. Research Lab. of Electronics, Cambridge, Mass., QPR#66, 384.

69. T. Rudjord. 1969. A second order mechanical model of muscle spindle primary endings. Kybernetik, 6, 205.

70. A.J. Buller. 1965. A model illustrating some aspects of muscle spindle physiology. J. Physiol., 179, 402.

71. R.B. Stein. 1965. A theoretical analysis of neuronal variability. Biophys. J., 5, 173.

72. S. Hagiwara. 1954. Analysis of interval fluctuation of sensory nerve impulse. Jap. J. Physiol., 4, 234.

73. S.W. Kuffler, R. Fitzhugh, and H.B. Barlow. 1957. Maintained activity in the cat's retina in light and darkness. J. Gen. Physiol., 40, 683.

74. W.M. Siebert. 1965. Some implications of the stochastic behavior of primary auditory neurons. Kybernetik, 2, 206.

75. V.V. Solodovnikov. 1965. Statistical dynamics of linear automatic control systems. Van Nostrand, London.

76. J.S. Bendat, and A.G. Piersol. 1966. Measurement and analysis of random data. Wiley, New York.

77. N.R. Goodman. 1965. Measurement of matrix frequency response functions and multiple coherence functions. AFFDL TR 65-56, Research and Technology Division, AFSC, Wright-Patterson, AFB, Ohio.

78. R.B. Blackman, and J.M. Tukey. 1958. The measurement of power spectra from the point of view of communications engineering. Dover, New York.

79. G.M. Jenkins, and D.G. Watts. 1968. Spectral analysis and its applications. Holden-Day, San Francisco.

80. C. Bingham, M.D. Godfrey, and J.W. Tukey. 1967. Modern techniques of power spectrum estimation. IEEE Trans. Audio and Electroacoustics, AU-15, 56.

81. E.A. Sloane. 1969. Comparison of linearly and quadratically modified spectral estimates of Gaussian signals. IEEE Trans. Audio and Electroacoustics, AU-17, 133.

82. M.J. Hinich, and C.S. Clay. 1968. The application of the discrete Fourier Transform in the estimation of power spectra, coherence, and bispectra of geophysical data. Geophys. Rev., 6, 347.

83. P.D. Welch. 1967. The use of the Fast Fourier Transform for the estimation of power spectra: a method based on time averaging over short, modified periodograms. IEEE Trans. Audio and Electroacoustics, AU-15, 70.

84. G. Dumermuth, and H. Fluhler. 1967. Some modern aspects in numerical spectrum analysis of multichannel electro-encephalographic data. Med. and Biol. Engng., 5, 319.

85. G.D. Bergland. 1969. A guided tour of the Fast Fourier Transform. IEEE Spectrum, July, 41.

86. M.R. Foster, and N.J. Guinzy. 1967. The coefficient of coherence: its estimation and use in geophysical data processing. Geophys., 32, 602.

87. V.A. Benigus. 1969. Estimation of the coherence spectrum and its confidence interval using the Fast Fourier Transform. IEEE Trans. Audio and Electroacoustics, AU-17, 145.

88. V.A. Benigus. 1969. Estimation of the coherence spectrum of non-Gaussian time series populations. IEEE Trans. Audio and Electroacoustics, AU-17, 198.

89. N.R. Goodman. 1957. On the joint estimation of the spectra, co-spectrum, and quadrature spectrum of a two-dimensional stationary Gaussian process. University of Princeton Thesis.

90. W.T. Cochran, J.W. Cooley, D.L. Favin, H.D. Helms, R.A. Kaenel, W.W. Lang, G.C. Maling Jr., D.E. Nelson, C.M. Rader, and P.D. Welch. 1967. What is the Fast Fourier Transform? IEEE Trans. Audio and Electroacoustics, AU-15, 45.

91. P. Buttuls. 1968. Adaptation of Sande's Fast Fourier Transform subroutine to IBM/360 Model 67. University of Alberta, Department of Computing Science Program Library, PS301A.

92. Z.J. Koles, E.M. Edwards, and R.S. Smith. 1969. A method for the measurement of instantaneous pulse frequency. J. Scientific Instruments, 2, 597.

93. A. Papoulis. 1965. Probability, random variables and stochastic processes. McGraw-Hill, New York.

94. D.R. Cox, and P.A.W. Lewis. 1966. The statistical analysis of series of events. Wiley, New York.

95. Modern Computing Methods. 1961. Notes on Applied Science No. 16, Department of Scientific and Industrial Research, National Physical Laboratory, London.

96. D.E. Nelsen. 1964. Calculation of power density spectra for a class of randomly jittered waveforms. M.I.T. Research Lab. of Electronics, Cambridge, Mass., QPR#76, 168.

97. C.K. Knox. 1969. The power spectral density of random spike trains. In: Systems Approach to Neurophysiological Problems. Minneapolis: Univ. of Minnesota Press, 73.

98. P.I. Richards. 1967. Computing reliable power spectra. IEEE Spectrum, Jan., 83.

99. N.A. Hutchinson, Z.J. Koles, and R.S. Smith. 1970. Conduction velocity in myelinated nerve fibres of Xenopus laevis. J. Physiol., 208, 279.

100. Y. Watanabe. 1969. Statistical measurement of signal transmission in the central nervous system of the crayfish. Kybernetik, 6, 124.

101. M.S. Bartlett. 1963. The spectral analysis of point processes. J. Roy. Statist. Soc. B, 25, 264.

102. D. Ottoson, J.S. McReynolds, and G.M. Shepherd. 1969. Sensitivity of isolated frog muscle spindle during and after stretching. J. Neurophysiol., 32, 24.

103. R.B. Stein, and A.S. French. 1969. Models for the transmission of information by nerve cells. Presented at the 5th international meeting of neurobiologists. Oslo, Norway.

104. R.B. Stein, and P.B.C. Matthews. 1965. Differences in variability of discharge frequency between primary and secondary muscle spindle afferent endings of the cat. Nature, 208, 1217.

105. A.B. Vallbo. 1964. Accommodation of single myelinated nerve
            fibres from Xenopus laevis related to type of end organ.
            Acta. Physiol. Scand., 61, 413.

106. A.A. Verveen, and H.E. Derksen. 1968. Fluctuation phenomena in
            nerve membrane. Proc. IEEE, 56, 906.

107. P.H. Hammond, P.A. Merton, G.G. Sutton. 1956. Nervous gradation of
            muscular contraction. Brit. Med. Bull., 12, 214.

108. G.L. Gottlieb, G.C. Agarwal, and L. Stark. 1970. Interactions
            between voluntary and postural mechanisms of the human
            motor system. J. Neurophysiol., 33, 365.

109. R.M. Chambers, and J.P. Simcock. 1960. Postural reflexes in fore-
            limb of toad, Bufo marinus. J. Neurophysiol., 23, 54.
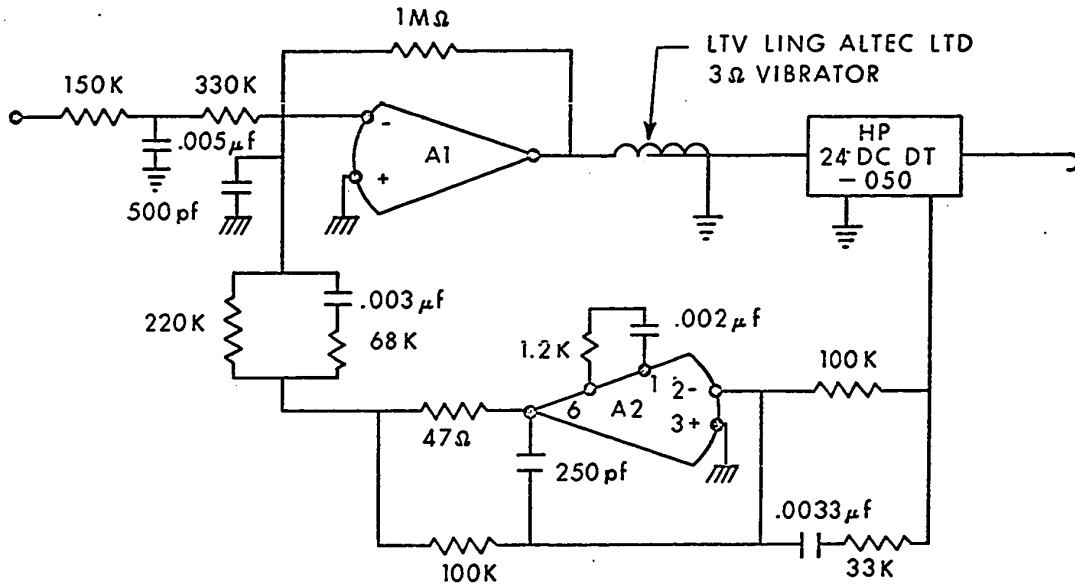
APPENDIX 1

THE DIFFERENTIAL PULLER

Figure A1.1

CIRCUIT DIAGRAM OF ONE SIDE OF THE DIFFERENTIAL PULLER

Component List—Figure A1.1

A1 50 watt Operational Amplifier
A2 Motorola MC1439G Operational Amplifier
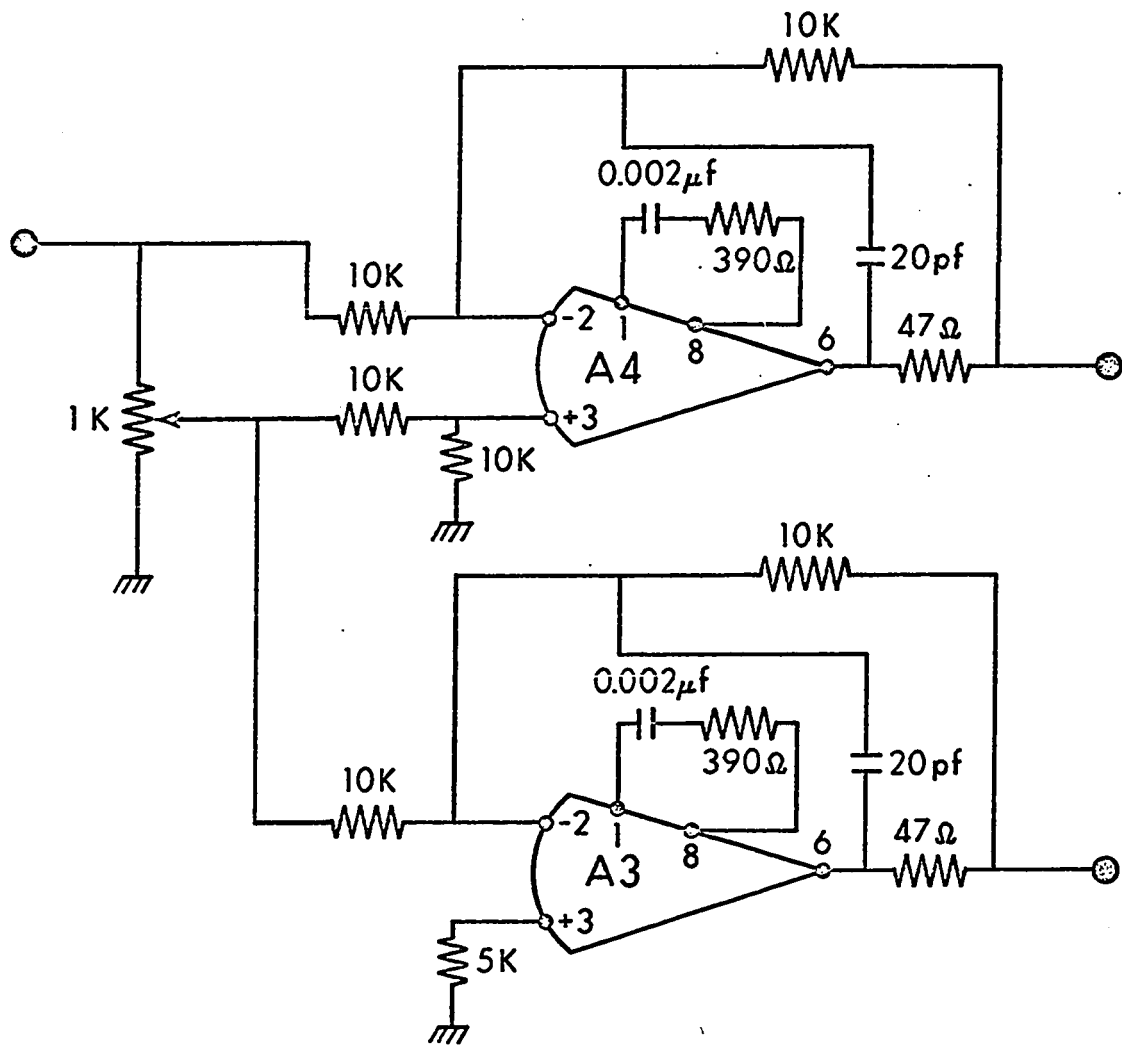   HP24DCDT-050 Hewlett-Packard Length Transducer.
   Maximum Displacement ±.1 inch

Figure A1.2

CIRCUIT DIAGRAM OF THE SIGNAL SPLITTER.

Component List--Figure A1.2

A3 ⎤
    ⎦ - Motorola MC1439G Operational Amplifiers.
A4 ⎦

Figure A1.3 shows the gain and phase performance of the
differential puller. The gain and phase relations are shown between the
control input and the output of the HP24DCDT-050. The dotted curves show
the predicted relations between the control input and the actual dis-
placement produced by the puller. These curves were obtained from the
solid curves by applying the correction formulas for the HP24DCDT-050
supplied by Hewlett-Parkard.
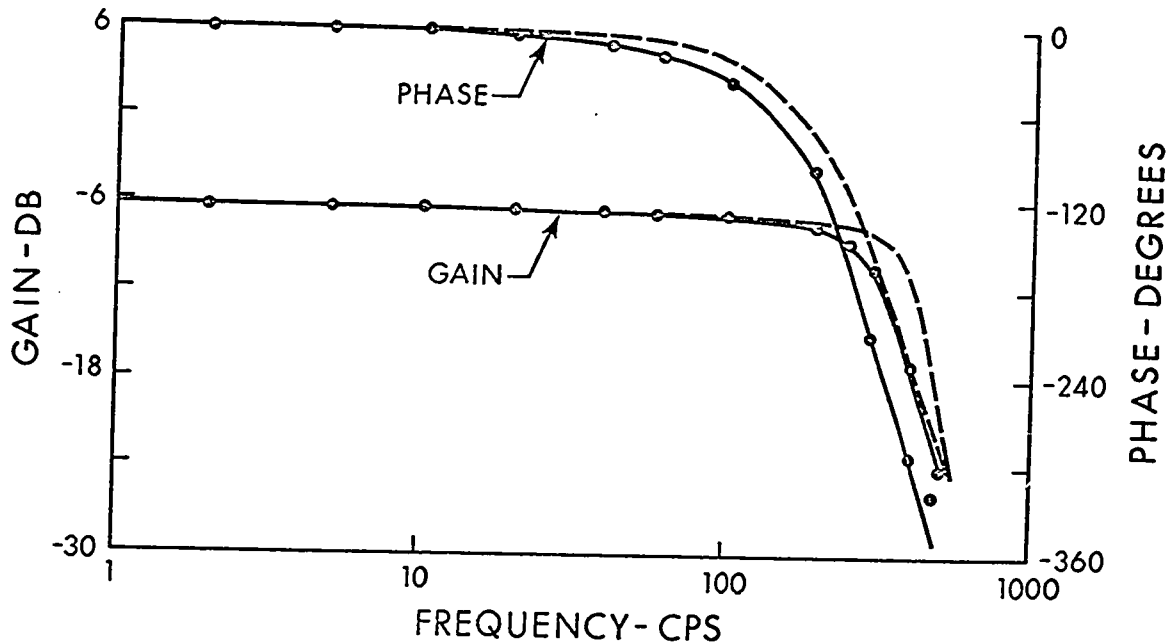
Figure A1.3

FREQUENCY RESPONSE OF THE DIFFERENTIAL PULLER.

APPENDIX 2 .

THE PULSE-HEIGHT DISCRIMINATOR

Component List--Figure A2.1

A5 Motorola MC1439G Operational Amplifier
A6 Minimum pulse amplitude ⎫
⎬ Fairchild µA710C Comparators
A7 Maximum pulse amplitude ⎭
G1-G10 Motorola MC724P Nor Gates
FF1-FF2 Motorola MC790P j-k Flip-Flops
B1   Motorola MC799P Buffer

     The output of B1 falls from the 1 state to the 0 state
coincident with the fall of the input pulse if and only if comparator A6
was set by the rising phase of the input pulse and A7 was not.
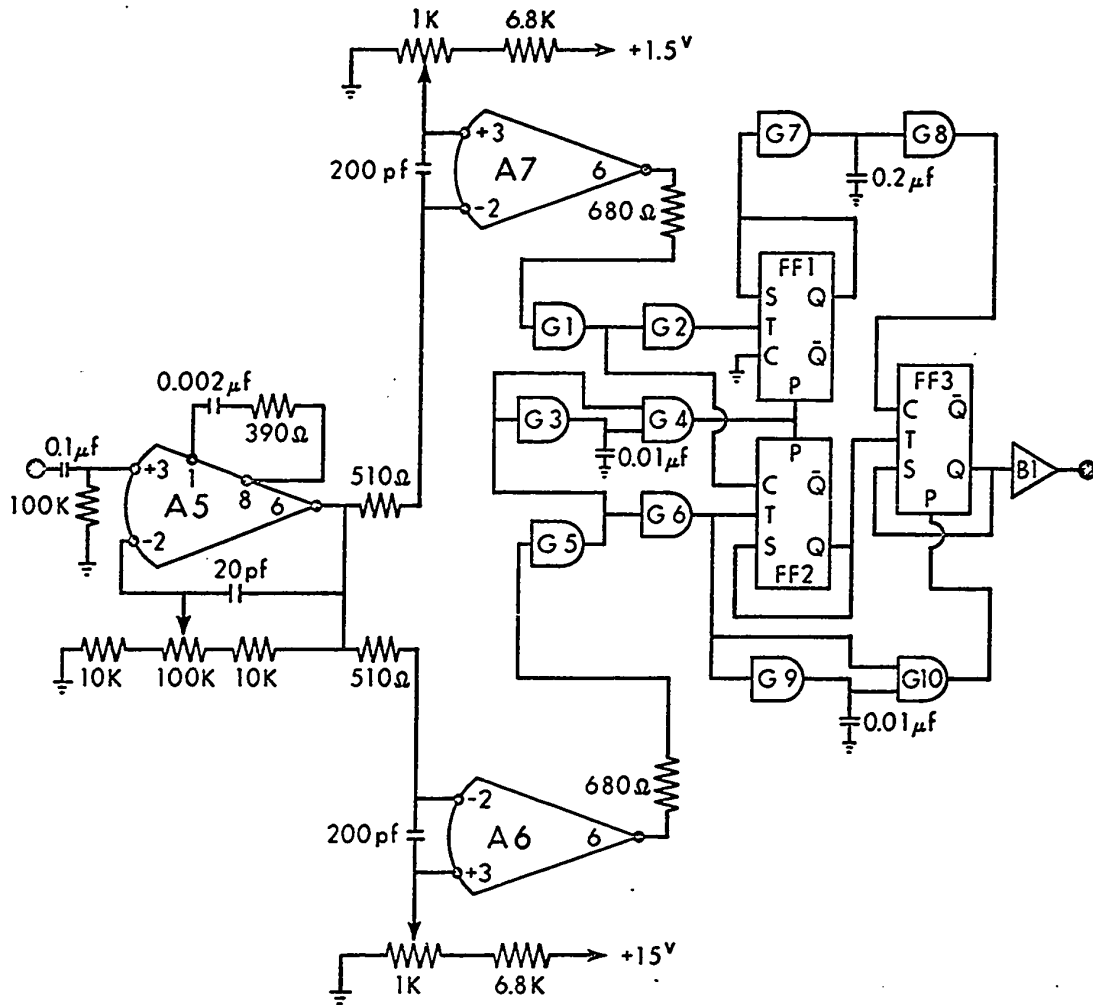
Figure A2.1

CIRCUIT DIAGRAM OF THE PULSE-HEIGHT DISCRIMINATOR.
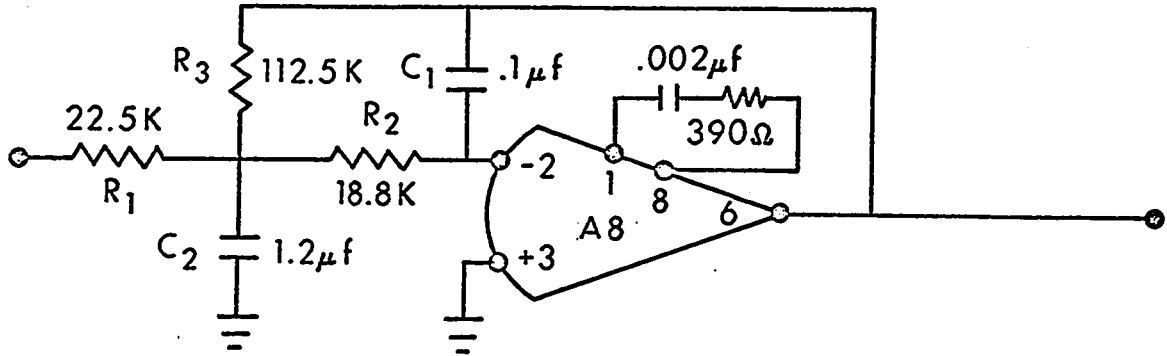
THE SPIKE FILTER

Figure A3.1

CIRCUIT DIAGRAM OF ONE SECTION OF THE SPIKE FILTER.

The transfer function of the circuit in figure A3.1 is

$$\frac{-R_3}{R_1} \quad \frac{1}{1 + [C_1 R_2 R_3 (\frac{1}{R_1} + \frac{1}{R_2} + \frac{1}{R_3})]s + R_2 R_3 C_1 C_2 s^2} \qquad (A3.1)$$

If the components are chosen as shown in figure A3.1 equation A3.1 becomes

$$\frac{-5}{1 + \frac{\sqrt{2}s}{21} + \frac{s^2}{442}} \qquad (A4.1)$$

The characteristics given by equations 5.27 and 5.28 were obtained by cascading two stages of the circuit shown in figure A3.1.

APPENDIX 4

THE CROSS-SPECTRAL ANALYSIS--FORTRAN IV SOURCE PROGRAM

```
      DIMENSION X(2048),Y(2048),Z( 802,4),F( 802),FAX(36),BATA(2048),
     .LABEL(32),A( 802),B( 802),JS(1024,2),AVG(2),TITLES(5,3),NT(3),
     .T(512,2),VAR(2),DED(265)
      DATA XDIM,YDIM,DPTS,FREQM/6.0,4.0,0.07,23.0/
      DATA TITLES/'COHERENCE               PHASE - DEGREES       MAGNITUDE - D
     .B        '/
      DATA            NT/9,15,14/
      CALL PLOTS(BATA(1),8192)
      NRECS=4
      PI=6.283185307
      DO 25 I=1,802
      F(I)=FLOAT(I-1)*100./2043.
   25 CONTINUE
      DO 30 I=1,4
      DO 31 J=1,802
      Z(J,I)=0.
   31 CONTINUE
   30 CONTINUE
      CALL PTAPE(0)
      DO 600 L=1,NRECS
      READ(1,200)(LABEL(I),I=1,32)
      WRITE(6,250)(LABEL(I),I=1,32)
      READ(1,100)(JS(I,1),JS(I,2),I=1, 512)
      WRITE(6,351)(JS(I,1),JS(I,2),I=1,10)
      DO 11 J=1,2
      DO 12 I=1,512
      T(I,J)=FLOAT(JS(I,J))/512.
   13 CONTINUE
   11 CONTINUE
      DO 601 K=1,7
      READ(1,100)(JS(I,1),JS(I,2),I=1, 512)
      DO 550 J=1,2
      AVG(J)=0.
      VAR(J)=0.
      DO 12 I=1,512
      X(I)=T(I,J)
      T(I,J)=FLOAT(JS(I,J))/512.
      X(I+512)=T(I,J)
   12 CONTINUE
      DO 10 I=1,1024
      IF(J.EQ.1)X(I)=-X(I)
      AVG(J)=AVG(J)+X(I)
      Y(I)=0.
   10 CONTINUE
      DO 20 I=1025,2048
      X(I)=0.
      Y(I)=0.
   20 CONTINUE
```

```fortran
      AVG(J)=AVG(J)/1024.
      DO 40 I=1,1024
      Y(I)=X(I)-AVG(J)
      VAR(J)=VAR(J)+X(I)**2
      DA=0.5*(1.-COS(PI*FLOAT(I-1)/1023.))
      X(I)=Y(I)*DA
   40 CONTINUE
      VAR(J)=VAR(J)/1023.
      CALL PS301A(11,X,Y,1)
      IF(J.EQ.2)GO TO 550
      DO 60 I=1,802
      A(I)=X(I)
      B(I)=Y(I)
   60 CONTINUE
  550 CONTINUE
      WRITE(6,30)(AVG(I),I=1,2)
      WRITE(6,31)(VAR(I),I=1,2)
      DO 63 I=1,802
      Z(I,1)=Z(I,1)+A(I)**2+B(I)**2
      Z(I,2)=Z(I,2)+A(I)*X(I)+B(I)*Y(I)
      Z(I,3)=Z(I,3)+A(I)*Y(I)-B(I)*X(I)
      Z(I,4)=Z(I,4)+X(I)**2+Y(I)**2
   63 CONTINUE
  601 CONTINUE
  600 CONTINUE
      DO 2 I=1,4
      DO 3 JJ=1,9
      FAX(9*(I-1)+JJ)=FLOAT(JJ)*10.0**(I-3)
    3 CONTINUE
    2 CONTINUE
      KK=4
    5 KK=KK+1
      IF(FAX(KK).LE.FREQM)GO TO 5
      FC=FAX(KK)
      FS1=ALOG10(0.04)
      FS2=(ALOG10(FC)-FS1)/XDIM
      I=2
      II=0
   32 J=I+1
      FSI=(ALOG10(F(I))-FS1)/FS2
      FST=FSI
   34 FSF=(ALOG10(F(J))-FS1)/FS2
      IF(FSF-FSI.GT.DPTS)GO TO 33
      FST=FSF
      J=J+1
      IF(F(J).GT.FREQM)GO TO 35
      GO TO 34
   33 II=II+1
      IF(II.GT.265)GO TO 35
      DEP(II)=(J-I)/4+1
      F(II)=(FST+FSI)/2.
      J=J-1
      DO 26 M=1,4
```

```
      Z1=0.
      DO 27 L=I,J
      Z1=Z1+Z(L,M)
   27 CONTINUE
      Z(II,M)=Z1/FLOAT(J+1-I)
   26 CONTINUE
      I=J+1
      GO TO 32
   35 DO 65 I=1,II
      FST=10.**(F(I)*FS2+FS1)
      CR=1.-( FST/21.)**2
      CI= FST*SQRT(2.)/21.
      SXX=Z(I,1)
      SXY=SQRT(Z(I,2)**2+Z(I,3)**2)
      Z(I,1)=SXY**2/(SXX*Z(I,4))
      Z(I,2)=ATAN2(Z(I,3),Z(I,2))+2.*ATAN2(CI,CR)
      IF(Z(I,2).GT.5.)Z(I,2)=Z(I,2)-PI
      Z(I,2)=Z(I,2)*360./PI
      Z(I,3)=SXY/SXX*(CR**2+CI**2)
   65 CONTINUE
      CALL PLOT(0.0,-40.0,-3)
      CALL PLOT(0.0,2.0,-3)
      YL=2.0
      F(II+1)=0.
      F(II+2)=1.
      I=KK-4
      KA=3
   47 KA=KA+1
      IF(I.NE.I/KA*KA)GO TO 47
      KB=KA-4
      EDF=14.*NRECS*18./19.
      Z(II+1,1)=0.
      Z(II+2,1)=1./YDIM
      Z(II+268,1)=0.
      Z(II+269,1)=Z(II+2,1)
      Z(II+535,1)=0.
      Z(II+536,1)=Z(II+2,1)
      Z(II+1,2)=-20
      Z(II+2,2)=130./YDIM
      FSI=Z(1,3)
      FSF=FSI
      DO 14 L=1,II
      FSI=AMIN1(FSI,Z(L,3))
      FSF=AMAX1(FSF,Z(L,3))
   14 CONTINUE
      FSI=0.5*FSI
      FSF=1.5*FSF
      Z(II+1,3)=0.
      Z(II+2,3)=20.0*ALOG10(FSF/FSI)/YDIM
      DO 42 M=1,3
    8 CALL AXIS(0.0,0.0,TITLES(1,M),       NT(M),YDIM,90.0,Z(II+1, M),
     .Z(II+2, M),20.0)
      CALL PLOT(0.0,0.0,3)
```
                                  -113-

```
      K=2
      DO 4 I=4,KK
      FS=(ALOG10(FAX(I))-FS1)/FS2
      CALL PLOT(FS,0.0,2)
      IF(KA.EQ.KK-4.AND.I.EQ.(4+KK)/2+1)GO TO 53
      IF(I+KB.EQ.(I+KB)/KA*KA)GO TO 53
      CALL SYMBOL(FS,   0.0,0.1,13,0.0,-1)
      GO TO 43
   53 CALL SYMBOL(FS,   0.0,0.2,13,0.0,-1)
      IF(I.GT.9)K=1
      CALL NUMBER(FS-0.10,-.25,0.10,FAX(I),0.0,K)
   43 CALL PLOT(FS,0.0,3)
    4 CONTINUE
      IF(M-2)44,45,46
   44 DO 71 I=1,II
      FST=EDF*DFD(I)
      DA=SQRT(Z(I,1))
      IF(DA.GE.1.)DA=0.99999
      DA=0.5*ALOG((1.+DA)/(1.-DA))
      Z(I+267,1)=TANH(DA-1.65/SQRT(FST))
      IF(Z(I+267,1).LT.0.)Z(I+267,1)=0.
      Z(I+267,1)=Z(I+267,1)**2
      Z(I+534,1)=TANH(DA+1.65/SQRT(FST))
      IF(Z(I+534,1).GT.1.)Z(I+534,1)=1.
      Z(I+534,1)=Z(I+534,1)**2
   71 CONTINUE
      CALL LINE(F,Z(1,1),II,1,-1,132)
      CALL LINE(F,Z(268,1),II,1,0,0)
      CALL LINE(F,Z(535,1),II,1,0,0)
      GO TO 56
   45 DO 72 I=1,II
      FST=EDF*DFD(I)
      IF(Z(I,1).LE.0.)Z(I,1)=0.000001
      X(I)=SQRT(2./(FST-2.)*3.15*(1.-Z(I,1))/Z(I,1))
      Y(I)=X(I)
      IF(X(I).GE.1.)X(I)=0.99999
      DA  =ARSIN(X(I))*360./PI
      Z(I+267,2)=Z(I,2)-   DA
      Z(I+534,2)=Z(I,2)+   DA
      IF(Z(I,2).LE.-20..OR.Z(I,2).GE.110.)GO TO 72
      CALL SYMBOL(F(I),(Z(I,2)-Z(II+1,2))/Z(II+2,2),0.05,4,0.0,-1)
   72 CONTINUE
      K=3
      DO 73 I=1,II
      IF(Z(I+267,2).LE.-20..OR.Z(I+267,2).GE.110.)GO TO 74
      CALL PLOT(F(I),(Z(I+267,2)-Z(II+1,2))/Z(II+2,2),K)
      K=2
      GO TO 73
   74 K=3
   73 CONTINUE
      K=3
      DO 76 I=1,II
      IF(Z(I+534,2).LE.-20..OR.Z(I+534,2).GE.110.)GO TO 75
```

-114-

```
      CALL PLOT(F(I),(Z(I+534,2)-Z(II+1,2))/Z(II+2,2),K)
      K=2
      GO TO 76
   75 K=3
   76 CONTINUE
      GO TO 56
   46 DO 37 L=1,II
      Z(L+267,3)=Z(L     ,3)*(1.-X(L))
      Z(L+534,3)=Z(L     ,3)*(1.+Y(L))
   37 CONTINUE
      DO 38 L=1,II
      Z(L,3)=20.0*ALOG10(Z(L,3)/FSI)
      Z(L+267,3)=20.0*ALOG10(Z(L+267,3)/FSI)
      Z(L+534,3)=20.0*ALOG10(Z(L+534,3)/FSI)
   38 CONTINUE
      CALL LINE(F,Z(1,3),II,1,-1,132)
      K=3
      DO 82 I=1,II
      IF(Z(I+267,3).LE.0..OR.Z(I+267,3).GE.Z(II+2,3)*YDIM)GO TO 83
      CALL PLOT(F(I),(Z(I+267,3)-Z(II+1,3))/Z(II+2,3),K)
      K=2
      GO TO 82
   83 K=3
   82 CONTINUE
      K=3
      DO 85 I=1,II
      IF(Z(I+534,3).LE.0..OR.Z(I+534,3).GE.Z(II+2,3)*YDIM)GO TO 34
      CALL PLOT(F(I),(Z(I+534,3)-Z(II+1,3))/Z(II+2,3),K)
      K=2
      GO TO 85
   34 K=3
   85 CONTINUE
   56 IF(M.EQ.3)GO TO 42
      YL=YL+YDIM+2.
      IF(YL+YDIM.GT.29.)GO TO 55
      CALL PLOT(0.0,YDIM+2.,-3)
      GO TO 42
   55 YL=YL-YDIM-2.
      CALL PLOT(XDIM+4.,(-YL)+2.,-3).
   42 CONTINUE
      CALL PLOT(0.0,0.0,999)
  300 FORMAT(16(A4,A2))
  350 FORMAT(1H1//5X,16(A4,A2))
  100 FORMAT(16I6)
  351 FORMAT(///////2016)
   70 FORMAT(///////////(1X,F10.4,3F20.7))
   80 FORMAT(//////5X,'AVERAGE INPUT LEVEL',E20.3,5X,'AVERAGE OUTPUT LEVE
     .L',F20.3)
   81 FORMAT(/5X,'INPUT VARIANCE',E20.3,5X,'OUTPUT VARIANCE',E20.3)
      STOP
      END
```

-115-